

ARGONNE NATIONAL LABORATORY
PHYSICS DIVISION

PHY-9039-ME-98

September 1998

**Laser Trapping and Cooling of
Noble Gas Atoms**

David J. Lim

Physics Division, Argonne National Laboratory, Argonne, IL 60439



9700 South Cass Ave
Argonne, Illinois 60439

COPIES AVAILABLE FROM:

PHYSICS DIVISION
BUILDING 203
ARGONNE NATIONAL LABORATORY
ARGONNE, IL. 60439

DISCLAIMER

This report was prepared as an account of work sponsored by an agency of the United States Government. Neither the United States Government nor any agency thereof, nor any of their employees, makes any warranty, expressed or implied, or assumes any legal liability or responsibility for the accuracy, completeness, or usefulness of any information, apparatus, product, or process disclosed, or represents that its use would not infringe privately owned rights. Reference herein to any specific commercial product, process, or service by trade name, trademark, manufacturer, or otherwise, does not necessarily constitute or imply its endorsement, recommendation, or favoring by the United States Government or any agency thereof. The views and opinions of authors expressed herein do not necessarily state or reflect those of the United States Government or any agency thereof.

ARGONNE NATIONAL LABORATORY, ARGONNE ILLINOIS

Operated by THE UNIVERSITY OF CHICAGO
for the U.S. DEPARTMENT OF ENERGY
under Contract W-31-109-Eng-38

ARGONNE NATIONAL LABORATORY

**LASER TRAPPING AND COOLING
OF NOBLE GAS ATOMS**

**PHYSICS DIVISION
BUILDING 203**

BY

DAVID J. LIN

ARGONNE, ILLINOIS

DECEMBER 1998

TABLE OF CONTENTS

	Page
ABSTRACT	ii
LIST OF TABLES	iii
LIST OF FIGURES	iii
LIST OF APPENDICES	iv
ACKNOWLEDGEMENTS	v
CHAPTER	
1. INTRODUCTION	1
A Brief History	1
Applications	2
Tests of Fundamental Physical Theories	3
Antimatter Trapping and Containment	4
Improving Time Standards	5
Optical Tweezers and Scissors	6
Bose Einstein Condensate	7
Noble Gas Isotope Trace Analyzer	8
2. THE PRINCIPLES OF LASER COOLING AND TRAPPING	11
Slowing	13
Velocity Dependent Damping Forces	15
Position Dependent Damping Forces	17
Zeeman Effect	17
The Need for the Metastable Level	20
Summary	21
3. EXPERIMENTAL SET-UP	22
Optical System	22
Lasers	22
Laser Beams	22
Polarization	24
Vacuum System	24
Saturated Absorption Cell	24
Atomic Beam Line	24
Detection Systems	31
Visual Detectors	31
Electronic Detectors	32
Structural Support	33
Laboratory Infrastructure	34
4. EXPERIMENTAL PROCEDURES AND PARAMETERS	35
Building and Optimizing the System	35
Metastable Atom Source	35
Skimmer Centering	37

Collimator Centering	38
Laser Beams Alignment	38
Proper Quarter-Wave Plate Setting	43
5. Operating the System to Trap Atoms	43
General Thoughts and Words of Wisdom	47
6. THE ZEEMAN TUNED SLOWER	49
Basic Theory	49
Mathematical Treatment	50
Cutoff Velocity	51
Deceleration Factor	54
Limits of Acceleration	55
Update: New Zeeman-tuned Slower Design	62
6. CALCULATIONS	63
Metastable Flux using the Faraday-Cup	63
Metastable Flux using Fluorescence Spectroscopy	63
Multiplicative Factor	64
Second Op-Amp Stage in Photodetector (Summer)	64
First Op-Amp Stage in Photodetector (Current	
Converter)	64
Total Power of Photons	64
Number of Photons	65
Actual Number of Photons Emitted	65
Number of Atoms Present	66
Metastable Flux	66
Atomic Transition Rate	66
Converting Photodetector Signal Strength to	
Number of Atoms	67
7. THE RESULTS	70
Isotope Abundance	70
Isotope Frequency Shifts	70
Trap Loading Time	73
Conclusion	73
REFERENCES	75
APPENDIX I: ANALYSIS OF A 3.8 kHz FREQUENCY NOISE IN NEW FOCUS VORTEX DIODE LASERS	80
Abstract	80
Introduction	81
A Primer on Saturated Absorption	
Spectroscopy	81
A Little Bit About Noise	88
Discovery of the 3.8 kHz Frequency Noise	90
Breakthrough	95
Post Script	99
APPENDIX 2: EXHAUSTIVE EQUIPMENT LIST	100

ABSTRACT

This paper describes Phase I of a project at Argonne National Laboratory using laser trapping and cooling techniques to measure concentrations of ^{81}Kr and ^{85}Kr in a variety of samples. With a half-life of 2×10^5 years, ^{81}Kr is ideal for dating polar ice and other geological specimens. Measuring ^{85}Kr with optical techniques also has important applications, including monitoring the global activity of nuclear fuel reprocessing. In Phase I of this project, we have successfully built and characterized a metastable atom source (flux $\sim 10^{13} \text{ s}^{-1} \text{ sr}^{-1}$), necessary to excite atoms to energy levels accessible to laser transition frequencies ($\sim 811.7 \text{ nm}$). We have also finished building the entire trapping apparatus, including a Zeeman slower, Magneto-Optical Trap (MOT), as well as the saturated absorption reference cavity for laser frequency locking. We proceeded to successfully trap Ar and Kr isotopes and measured their frequency shifts. Short term goals including improving the detection system, demonstrating single atom counting, and improving the efficiency of producing meta-stable atoms.

LIST OF TABLES

Table		Page
4-1.	Optimum System Parameters for Trapping	48
7-1	Summary of Ar and Kr Isotope Abundance	70
7-2	Relative Frequencies of Argon and Krypton Isotopes	73
A1-1	Process of Characterizing the Problem	98

LIST OF FIGURES

Figure		Page
2-1	Momentum Transfer Between Photon and Atom	11
2-2	Doppler Shift due to Atom's Velocity	12
2-3	Effect of Doppler Shift	13
2-4	The Scattering Force	14
2-5	Optical Molasses	15
2-6	Velocity Dependent Forces	16
2-7	Classical Analogies	17
2-8	Position Dependent B Field Causes Corresponding Zeeman Shift	18
2-9	Zero Net Force at Trap's Center	19
2-10	Net Force Toward Center Points At Points Away from Center	19
2-11	Atomic Excitation Scheme	20
3-1	Optics Table Layout	23
3-2	Atomic Beam Line	26
5-1	Simplified Apparatus Schematic	50
5-2	Velocity vs. Position	52
5-3	Doppler Shift vs. Position	52
5-4	B vs. Position	53
5-5	Demonstrating Cut-off Velocity	53
5-6	Poor Zeeman Slower Design (B vs. Position)	57
5-7	Poor Zeeman Design (Acceleration vs. Position)	57
5-8	Improved Solenoid Design (B vs. Position)	58
5-9	Improved Solenoid Design (Acceleration vs. Position)	58
5-10	Actual Measurements from Final Zeeman Slower	59
5-11	Actual Measurements of Transition Area	60
7-1	Atomic Fluorescence Intensity vs. Relative Laser Frequency	71
7-2	Argon Isotope Frequency Shifts	72
7-3	Krypton Isotope Frequency Shifts	73

Figure		Page
7.4	Trap Loading Time	74
A1-1	Laser Absorption Spectroscopy Basic Set-Up	81
A1-2a	Absorption Spectrum of Metastable Argon Gas	82
A1-2b	Absorption Spectrum of Metastable Argon Gas	83
A1-3	The Boltzmann Distribution	84
A1-4	Laser Saturated Absorption spectroscopy Set-Up	85
A1-5	Ideal Saturated Absorption Signal	87
A1-6	Amplitude Noise	89
A1-7	Frequency Noise	89
A1-8	Fabry-Perot Cavity	91
A1-9	Absorption Signal with Fabry-Perot Signal	92
A1-10	Oscilloscope Scan of Fabry-Perot Signal	94
A1-11	FFT Output of Noise	94
A1-12	Saturated Absorption Signal - FM Input at High Gain	96
A1-13	Saturated Absorption Signal - FM Input at Low Gain	96
A1-14	Response of Noise Range to Increasing Resistance	97
A1-15	Final Saturated Absorption Signal	98

LIST OF APPENDICIES

Appendix		Page
1.	Analysis of a 3.8 kHz Frequency Noise in New Focus Vortex Diode Lasers	80
2.	Exhaustive Equipment List	100

ACKNOWLEDGEMENTS

First to my parents, who's given me the life and the means to explore this great big universe. We may have different methods, but we have the same goal ... to appreciate truth and beauty wherever we can find it. Thanks for giving me that chance.

Next to my mentor and friend, Dr. Zheng-Tian Lu, who helped transform physics from something very dry into something very lush to me. I will always appreciate you as THE Master Trapper and the Source of Puzzles, without whom this project would have taken thrice as long and a third as fun.

Then, to my predecessor, Dr. Chun-yen Chen, for your example of hard work and taking the baton. Good luck on Phase II of the project! I wish I were here to help, but I'm positive you'll do just fine. (Maybe I'll drop by the lab on Sunday's to check on ya!)

Also, to my summer students, Ms. Kim Lewis and Ms. Lisa Tung, for keeping me at Argonne longer than I probably should have stayed. But thanks for that ... this thesis is that much more rich because of you gals.

Finally, to all the host of help and encouragement I received along the way, without whom this project would have been much less colorful ... Dr. Linda Young, Dr. Shuichi Hasegawa, Mr. Kevin Bailey, Mr. Henning Back, and the great people of the machine, electrical, and glass shops at Argonne National Laboratory.

CHAPTER 1

INTRODUCTION

Using lasers to trap atoms is a timely and fascinating subject. Just last year (1997), Steven Chu, Claude Cohen-Tannoudji, and William Phillips, the three physicists most influential in developing the field, received the Nobel Prize in physics [Levy, 1997, p.17]. Applying these methods, scientists have accomplished extraordinary things, including building better time keeping devices, manipulating fragile DNA strands, and producing the Bose-Einstein condensate from gas, to name just a few. Moreover, with this new tool, researchers are in a position to more carefully probe fundamental theories by making more accurate physical measurements.

A Brief History

Ever since the last century, leading figures in physics have examined the mechanical interactions between light and matter. In late nineteenth century, James Clerk Maxwell applied electromagnetic theory to study radiation pressure, stating that "in a medium in which waves are propagated there is a pressure normal to the waves and numerically equal to the energy in unit volume" [Maxwell, 1892, pp.790-791]. Shortly afterwards, in 1901, Nichols and Hull at Dartmouth College quantitatively confirmed the radiation pressure using a delicate torsion balance [Nichols, 1901, p.307]. In 1917, Albert Einstein applied quantum theory to show how the Plank radiation field of light can cause thermal equilibrium in molecules, a calculation which helped establish the quantum nature of light. Otto Frisch in 1933 performed the first experiment demonstrating momentum transfer between a photon and atom, observed when a beam of sodium atoms was deflected by light from a sodium lamp. Then in 1950, Alfred Kastler wrote a paper on optical pumping and suggested ways of cooling or heating atoms using light [Wineland, 1987, p.35].

The advent of lasers greatly increased the intensities of light available to researchers. One of the first to propose using lasers to manipulate atoms was Arthur Ashkin of Bell Telephone Laboratories in Holmdel, New Jersey. In his 1970 article in *Physical Review Letters*, he reported the first use of continuous wave laser light to accelerate and trap micron-sized particles in liquid and gas. He hypothesized that atoms and molecules could similarly be manipulated, and specifically mentioned the separation of isotopes as an application [Ashkin, 1970, p.156-159]. In another article that same year, Ashkin proposed using the laser scattering force to "separate, velocity analyze, or trap neutral atoms of specific isotopic species or hyperfine level" [Ashkin, 1970, p.1321]. Several scientists in the (then) Soviet Union proposed similar ideas, notably Vladilen S. Letokhov, who in 1968 first suggested that dipole forces from light beams could be used to trap atoms [Chu, 1992, p.72, Wineland, 1987, p.35].

Thoughts on how to use lasers to cool a low-density gas to improve laser spectroscopy began in 1975 with two independent groups. One group, Theodor Hansch and Arthur Schawlow (1981 Nobel laureate) of Stanford, pointed out that if the laser beams were slightly detuned below the atomic resonance transition, a moving atom

would be Doppler shifted into resonance and feel a force opposing its motion. Thus, the average velocity of all the atoms in such a light field would decrease, and hence its temperature. Interestingly, they surmised that radiation cooling might happen naturally in volumes of gas in space [Hansch, 1975, p.68].

In the same year, David J. Wineland and Hans G. Dehmelt (1989 Nobel laureate) of the University of Washington presented a similar cooling method to improve laser fluorescence spectroscopy on thallium ions [Wineland, 1975, p.637]. The velocity distribution of atoms produces an effect called Doppler broadening, which obscures laser spectroscopy results. First cooling the atoms substantially reduces the Doppler broadening, and advances the precision of laser spectroscopy closer to the natural linewidth of the atoms.

Wineland and his team at the National Bureau of Standards went on in 1978 to successfully cool Mg^+ ions in a Penning trap down to 40 K [Wineland, 1978, p.1639]. That same year, another group in Heidelberg, Germany, also demonstrated cooling of Ba^+ ions in a Paul trap down to less than 36 mK [Neuhauser, 1978, p.233, Neuhauser, 1980, p.1137]. New ideas and techniques would soon reduce the temperature even lower.

In 1985, Steven Chu and his colleagues at AT&T Bell Laboratories at Holmdel utilized six counterpropagating laser beams to confine and cool neutral sodium atoms down to 240 μK , the limit predicted by the theory of Doppler cooling [Chu, 1985, p. 48]. With the addition of an inhomogeneous magnetic field, the scattering forces were given positional dependence, and the first magneto-optical trap was revealed in 1987 by E. L. Raab, et al., also at AT&T Bell Labs [Raab, 1987, p.2631]. In 1988, atoms were laser cooled to around 40 μK , lower than the Doppler limit, thus testing physicists' understanding of what was actually going on [Lett, 1988, p.169]. Later that year, Alain Aspect (of Bell's Inequality fame), Claude Cohen-Tannoudji, and other researchers at the Ecole Normale Supérieure (ENS) in Paris brought down the temperature to 2 μK , lower than the single photon recoil limit [Aspect, 1988, p.826]. By 1990, temperatures of 1 μK were measured at the University of Colorado [Monroe, 1990, p.1571]. More recently, ENS reported cooling a cloud of metastable helium atoms down to 180 nK in three-dimensions [Lawall, 1995, p.4194], and cesium atoms to below 3 nK in one-dimension [Reichel, 1995, p.4575].

Another important development in laser cooling techniques occurred in 1982, when William Phillips and Harold Metcalf demonstrated for the first time laser deceleration of an atomic beam of sodium. A critical part of the slowing method was their Zeeman-Tuned Slower, which relied on the Zeeman effect to compensate for the changing Doppler shifts as the atom slowed.

Applications

The methods developed to trap and cool atoms using lasers have given scientists powerful, yet simple tools to explore fundamental questions as well as solve long standing problems. Significant experiments can be performed at modest cost and laboratory space. In fact, most undergraduate institutions have the resources to build a laser trapping lab, and with dedicated individuals, are able to perform experiments that are both interesting and important.

Tests of Fundamental Physical Theories

Recently, Lu for his doctoral thesis at the University of California, Berkley, trapped radioactive atoms for the first time [Lu, 1994, p. 3791]. This opens new avenues for testing fundamental physical theories, such as the Standard Model, CPT violations, supersymmetry, and in the process, hopefully reveal new physics.

Parity Non-Conservation

Most physical laws are invariant (do not change) if the coordinate system is reflected. The physics describing the interaction of a system of particles is the same, even if the spatial coordinates are changed from positive to negative. Another way to say it is, "Parity is conserved." One way to picture this is by considering normal, everyday screws and springs. The thread on a screw or the coil of a spring may twist in a right or left-handed way. However, a bicycle built with right-handed screws and springs should ride as well as one built with left-handed ones. The two bicycles form a symmetric pair; both are allowed by physics, and both obey the same physics.

However, such symmetry does not seem to exist at a more fundamental level. In the 1950's, the Chinese-American physicists Tsung Dao Lee, Chen Ning Yang (1957 Nobel laureates) [Lee, 1956, p.254], and Chien Shiung Wu [Wu, 1957, p.1413] discovered that parity is not conserved for radioactively emitted particles, that is, in weak interactions. They found that neutrinos, a fundamental particle, always spins in a left-handed manner. There are no right-handed neutrinos, and a mysterious, fundamental asymmetry exists in nature.

Since then, parity non-conservation (PNC) effects have been measured in many stable and radioactive atoms. In experiments involving radioactive atoms, researchers have difficulty keeping enough atoms together to study them effectively. Laser trapping would help conserve the number of radioactive atoms in a PNC experiment. Moreover, it would allow detailed study of a PNC effect due to the nuclear spin, the anapole moment [Apenko, 1982, p.L57]. Using trapped ^{21}Na as a beta source also makes possible very precise measurements of the beta-asymmetry parameter, A, which would provide a sensitive test of how the Standard Model accounts for PNC [Lu, 1994, p.6-21].

Time-Reversal-Asymmetry

Just as the principle of parity conservation says the laws of nature should not change upon spatial reflection, the principle of time-reversal-symmetry says that physics should remain the same if time were reversed. Run a movie backwards, and everything should still consistently follow the laws of physics. However, in 1964, the American physicists James W. Cronin, Val L. Fitch (1980 Nobel laureates) and their Princeton team discovered evidence in the decay of a neutral kaon into two pions which suggested time-reversal-symmetry did not hold in weak interactions [Christenson, 1964, p.138]. Later, time-reversal-asymmetry was directly deduced from data in a neutral kaon decay [Casella, 1968, p.1128]. Theories based on supersymmetry explain this effect, but

predict the neutron and electron have permanent electric-dipole-moments (EDM) [Barr, 1993, p.302]. Performing high precision spectroscopy on trapped, heavy atoms would substantially improve EDM measurements, and provide a test for supersymmetry.

Antimatter Trapping and Containment

The CPT Theorem

In addition to space and time, another conservation principle seems to appear in nature: charge conjugation. This principle says that a reaction involving matter is symmetrical to its antimatter counterpart. For instance, let a, b, c, and d be normal matter particles, and a reaction between them is $a + b = c + d$. The conservation of charge conjugation says that the corresponding antiparticle reaction $A + B = C + D$, where A is the antiparticle of a, B of b, etc., will also occur. The symmetry of charge conjugation (C), parity (space) (P), and time (T) are brought together in the CPT theorem

Based on a fundamental theory of physics, relativistic quantum field theory, the CPT theorem predicts natural symmetries between charge conjugation, parity, and time. When violations of CPT occur, as we began to consider above, our current knowledge is tested, and new theories must be considered to account for them. One of the things the CPT theorem predicts is that every particle has an antiparticle of the same mass, spin, and lifetime, but different charge and magnetic moment. The proton has an antiproton; the electron, a positron. The normal hydrogen atom consists of a proton and an electron. Thus, the antihydrogen atom has an antiproton and positron. One way to test CPT is to study antiparticles, and much effort today is going into producing, trapping, and studying antihydrogen, the simplest antimatter atom.

Antihydrogen

Since antimatter annihilates matter, special consideration must be made to handle and store it. Using a Penning trap, which involves radio-frequency fields, Gabrielse and his colleagues first trapped antiprotons produced at CERN, the high energy accelerator in Geneva, Switzerland [Gabrielse, 1986, p.2504]. At the time, only 300 antiprotons were trapped for around 100 seconds. Refining their techniques, the team went on to trap 2×10^5 antiprotons for 2 months, allowing for a thousandfold improvement in the measurement of the mass of antiproton [Gabrielse, 1990, p.1317]. As a result, the mass of the proton and antiproton are now known to agree to an accuracy of 10^{-9} , in outstanding agreement with the CPT theorem. Again with a Penning trap, the researchers at CERN proceeded to trap 3.5×10^4 positrons [Haarsma, 1995, p.806]. To produce antihydrogen, the trapped antiprotons and positrons must be brought together and allowed to combine. A combined Penning trap of ions and electrons was recently demonstrated, and work towards applying the technique to synthesize antihydrogen proceeds [Walz, 1995, p.3257].

Using a different method, researchers at CERN produced antihydrogen for the first time [Baur, 1996, p.251]. Xenon atoms were shot across the path of antiprotons. An electron-positron pair may be produced when an antiproton passes through the electric field of a xenon nucleus, and sometimes, the positron will be captured by the antiproton

to form antihydrogen. Eleven antihydrogen atoms were counted, although they existed only 37 nanoseconds. More recently, antihydrogen was produced by similar methods (using hydrogen instead of xenon) at Fermilab in northern Illinois [Blanford, 1998, p.3037]. The goal now is to produce 500 – 5000 antihydrogen atoms, and perform laser spectroscopy on them.

Laser trapping and cooling of antimatter atoms such as antihydrogen should be as straightforward as for normal atoms [Lett, 1988, p.335]. Laser trapping and cooling methods are capable of capturing significant amounts of antihydrogen, and may be the best way to hold it sufficiently well to study it. To work, a continuous wave laser capable of producing intense 121.6 nm light is needed, and such technology is still being developed. Currently, pulsed lasers of that wavelength can be used, but a pulsed laser source makes trapping and cooling difficult. Thus, this application will hopefully be realized in the near future.

Improving Time Standards

What is time? Philosophers, professional and otherwise, have pondered this question ... over time. Time is completely mysterious, yet it forms the basis of our reality. Einstein added to the mystery by pointing out that time is actually relative, appearing to pass faster or slower depending on one's relative motion to the instrument measuring time. Whatever time is, we can for practical purposes define a unit of time as being how long it takes something to happen. To be very consistent and accurate, we want to choose this event to be free from the effects of any physical factors, such as location or environment. The time a pendulum swings would be a poor choice, since that could be affected by gravity, friction, air currents, orientation, location, etc.

A much better clock is actually an atom. Starting in 1927, when the physicist Charles Darwin, grandson of the eminent biologist, theoretically considered the nature of the atom's angular momentum, much work has been done to base time on a physical characteristic unaffected by external forces [Ramsey, 1972, p.90]. Today, the basic unit of time in the International System of Units is based on the energy difference between two hyperfine levels in ^{133}Cs atoms. Microwave radiation is applied to the atoms, and the frequency of the radiation is tuned to the resonance frequency of the transition between the two levels. When this happens, ^{133}Cs atoms are excited into the higher level. From the microwave frequency, the period of each wave is found. The second is defined to be 9,192,631.770 periods of the radiation (1967 Conference Generale des Poids et Mesures).

Laser trapping combined with the atomic fountain invented by Jerold R. Zacharias in 1953 can provide the best possible measurements of an atom's energy levels [Hall, 1989, 2194; Wineland, 1987, p.34]. After atoms are laser trapped, another laser beam launches them upward with a small velocity. They are excited by two pulses of microwave radiation at the top of their path, according to Ramsey's method [Ramsey, 1949, p.996; 1950, p.695; 1951, p.506]. Sources of perturbations in the atoms' energy levels are minimized and easily shielded as the atoms are in free fall, and the measurement time (the time between the two pulses) can be as long as one second. The uncertainty principle states that the uncertainty in measuring the energy level is inversely proportional to the measurement time. Thus, increasing the measurement time

substantially improves the accuracy of the energy measurement, which in turn, increases the accuracy of the atom clock [Chu, 1991, 864; Chu, 1992, p.75].

Recent work on the atomic fountain clock suggests that the energy frequency can be measured to an accuracy of one part in 10^{16} . Compare this to the finest optical frequency measurements to date using cold hydrogen atoms and an sophisticated optical frequency internal divider: 3.4 parts in 10^{13} [Udem, 1997, p.2646]. Led by Theodore Hansch (who was also one of the first to conceive laser cooling in 1975), the research group at the Max-Planck Institute accomplished this feat using a system of lasers so complicated that Daniel Kleppner, an MIT physicist, commented, "... I don't know of any American lab that could reproduce it in the present funding climate" [Schwarzchild, 1997, p.21]. While work continues on perfecting the atomic fountain clock, it can potentially be much more accurate and much more simpler than other methods .

Optical Tweezers and Scissors

Laser trapping has even developed into a sophisticated and sensitive tool in biological studies. Laser light can exert scattering and dipole forces, which together can move or hold objects so small and delicate that no other mechanical method can [Ashkin, 1987, p.1517].

The scattering force, to be considered in detail in Chapter 2, arises since photons from a laser beam are coming from a particular direction, whereas atoms re-emit photons in all directions. The net effect is that the laser beam pushes atoms in the direction of the beam.

To understand the dipole force, consider the common experience of combing one's hair. The comb acquires a net positive charge, as electrons are rubbed off and transferred to the hair. If the comb is then held over a tiny piece of paper, the paper flies upwards off the table, defying gravity, and sticks onto the comb. Of course, the magic is easily explained. What happens is the positively charged comb attracts the negative charges in the paper and pushes away the positive charges, so that the paper, even though it remains electrically neutral over all, acquires a definite charge polarity. To describe this, we say the comb has induced an electric *dipole moment* on the paper. The paper's negative charges are now physically closer to the comb than the paper's positive charges. Since the comb is itself positively charged, the attractive force is greater than the repulsive force, and the net effect is that the paper will want to move toward the comb. We could say that a *dipole force* is acting. If this dipole force is greater than the gravitational force, the paper will fly up and stick to the comb.

Since laser light can be considered an oscillating electric field, if we focus a laser beam at a point, the electric field is greatest at that point and a field gradient is established around it. Just as the comb induced a dipole moment in the paper, the focused laser beam can induce dipole moments in nearby particles, with the resulting effect that the particles will move toward the focal point. However, the scattering force wants to push the particles away. The point where the scattering and dipole forces cancel is where the particles will finally come to rest and be trapped. Moreover, the particles will move where the focal point is moved, allowing researchers to precisely manipulate objects normally too small to handle [Ashkin, 1992, p.569].

Microscope optics have developed to such a high level of precision that they are easily adapted to focus laser light on specimens on the microscope stage. Since cells are virtually transparent to light, the laser beam can even be focused *inside* a cell, and sub-cellular objects (organelles), can be manipulated without puncturing the cell's membrane. Of course, if the laser beam is too intense, it will damage or kill the specimen. At just the right intensity, optical tweezers do not harm the specimen and provide a non-invasive tool for exploring biological and medical questions.

With the optical tweezers technique, researchers have trapped and manipulated viruses and bacteria [Ashkin, 1987, p.1517], single cells and organelles [Ashkin, 1987, p.769], and even single DNA molecules [Perkins, 1994, p.822]. Not only is the mechanical nature of DNA vital for understanding its role in cellular functions, it is a good model in polymer physics. Recently, Princeton biophysicists used optical tweezers to stretch DNA molecules to study its elastic properties. The results fit well with an elasticity theory which considered enthalpic and entropic factors to stiffness [Wang, 1997, p.1335].

Optical tweezers has also been used to measure the forces caused by sub-cellular, molecular motors, such as kinesin [Block, 1990, p.348] and dynein [Ashkin, 1990, p.346]; closely examine events in mitosis (cellular reproduction); demonstrate position-dependence of B and T cells in human immunity; study the swimming forces of sperm; and even guide sperm into eggs to facilitate fertilization [Berns, 1998, p.65-66]. Using both techniques of laser trapping and laser scissors (in which laser beams are used to make precision cuts), human cancer cells have been fused into one hybrid cell containing genetic material of both [Berns, 1998, p.66]. Then, researchers can take advantage of genetic features of both cells. For instance, one might code for a desirable enzyme, while another can continue reproducing itself indefinitely. The hybrid, then, would become an undying source of the desirable enzyme.

The use of laser trapping and scissors in biology and medicine is rapidly increasing. Laser workstations are even being marketed to fertility clinics to improve fertilization techniques. The National Institutes of Health has a Laser Microbeam and Medical Program Biotechnology Resource, which has set up a confocal laser fluorescence microscope incorporating two optical tweezers and one laser scissor beam. It also has a confocal ablation trapping system (CATS), used in cellular, subcellular, and DNA sequencing experiments [Berns, 1998, p.67]

Bose Einstein Condensate

In 1924, Albert Einstein (1921 Nobel laureate) and Satyendra Nath Bose proposed that below a certain temperature, a gas of non-interacting bosonic atoms (atoms with integer spin) will lose their distinct identities and condense into a single entity, the Bose-Einstein condensate (BEC). The atoms' individual wavefunctions become one. They all share the same space, move with the same speed and direction, and act as one big, indistinguishable atom. While similar behavior has been observed in superfluidity and superconductivity, none had ever been demonstrated in a gas. Finally in 1995, Carl Wieman, Eric Cornell, and colleagues realized BEC as Einstein and Bose first envisioned it. Using laser cooling and trapping, the University of Colorado team cooled 2,000

rubidium atoms to around 100 nK, and BEC formed for more than 15 seconds [Anderson, 1995, p.198].

More than just demonstrating an interesting aspect of quantum mechanics, achieving BEC gives researchers precision control over matter. Just as a laser is a beam of identical, coherent photons, BEC can be focused into a beam of identical, coherent atoms. Already, "atom-lasers" have been developed, and applications in improved time-keeping and atomic-level lithography are being explored [Cornell, 1998, p.40].

Noble-Gas Isotope Trace Analyzer

At Argonne National Laboratory, laser trapping and cooling is being applied in a new way: to analyze trace amounts of certain noble gas isotopes. This remainder of this thesis describes Phase I of the project, the building of the trapping system, and selective trapping of argon and krypton isotopes.

Why Trap Noble Gas Isotopes?

Trace analysis of noble gas isotopes is important for many reasons. In environmental research, certain noble gas isotopes have been found to be ideal tracers, because their chemical inertness makes their formation and transportation easier to understand.

⁸¹Kr. Take ⁸¹Kr for example. It is formed when cosmic rays induce reactions which activate neutrons of stable krypton in the upper atmosphere. When a sample of water or ice is on the surface of the earth, Kr freely diffuses into the sample, and the ratio of ⁸¹Kr to stable Kr is representative of that found in the air. However, if the water goes underground or other ice layers form over the original ice, the gaseous exchange ceases, the ⁸¹Kr /Kr ratio decreases over time due to the radioactive nature of ⁸¹Kr (half-life 2×10^5 years). Thus, measuring ⁸¹Kr is a way to date ancient groundwater and deep ice samples. In fact, on the time scale of 10^5 to 10^6 years, ⁸¹Kr may be the only suitable tracer [Aseyev, 1991, p.2755].

The easiest method to date polar ice is simply counting the layers, much like counting tree rings [Alley, 1998, p.80]. Snow crystals in summer are larger (and more acidic) than those formed in winter, and the resulting layering is noticeable visually (and chemically). Each season, a fresh layer of snow falls and freezes over existing layers, and the result is an ice chronology. Deeper layers are thus older. However, very deep layers deform due to gravity, and it becomes impossible to distinguish annual layers beyond around 100,000 years. Another radioactive tracer, ¹⁴C has a half-life of only 5715 years, so using it to date ice is reliable only to around 50,000 years.

The ability to measure ⁸¹Kr can greatly extend our ability to date ice layers to millions of years, which, in turn, is vital to understanding the earth's long term climate. Furthermore, since the formation of ⁸¹Kr involves cosmic rays, ancient ice cores provide a natural, historical record of cosmic ray activity, important in better understanding this important astrophysical phenomenon. Similarly, ⁸¹Kr dating of groundwater around potential radioactive waste burial sites will help planners determine the long-term impact on the environment of such sites.

⁸⁵Kr. Another isotope of krypton, ⁸⁵Kr, is the product of uranium and plutonium fission. The advent of the nuclear age substantially increased the concentration of ⁸⁵Kr in the atmosphere (⁸⁵Kr/Kr = 1x10⁻¹¹). Monitoring ⁸⁵Kr concentrations gives an indication of how much nuclear-fuel reprocessing is occurring on a global scale, which in turn reveals nuclear weapons production activity. Vital to the success of the nuclear disarmament effort is a way to assure compliance to disarmament agreements. Thus, a simple method of measuring ⁸⁵Kr would provide a practical tool to help take us a step further away from the threat of nuclear annihilation [Grossman, 1985, p.1128].

Somewhat less dramatically, ⁸⁵Kr can also be used to detect leaks in nuclear reactors, specifically, from nuclear fuel claddings [Murgatroyd, 1972, p.41; Waldschmidt, 1973, p.435]. Being a noble gas, ⁸⁵Kr diffuses through any cracks, no matter how small. By measuring the ⁸⁵Kr concentration around a nuclear facility, safety officials can constantly monitor the plant's structural integrity, thus minimizing health risks for workers at the plants and residents in surrounding neighborhoods. In fact, the radioactive nature of ⁸⁵Kr aroused concern that it is an environmental hazard. Toxicological studies of ⁸⁵Kr on rats found that doses less than 1000 rad is sufficient to induce cancer, while doses over the range from 1000 to 4750 rad increases the incidence of skin tumors [Ballou, 1985, p.453]. Reassuringly, a recent report of ⁸⁵Kr concentrations in air at Clonskeagh, Dublin, between two major reprocessing plants in Europe, affirmed that no present radiological hazard exists there [Howlett, 1998, p.15].

Currently, measuring ⁸⁵Kr involves low-level decay counting, which is conducted at a deep, underground site, expensive to build and not easily accessible [Goles, 1981, p.740; Fernandez, 1985, p.682]. Moreover, samples require much time to properly prepare. To make constant monitoring of ⁸⁵Kr feasible, a much less expensive and faster method is necessary.

³⁹Ar. As a final example, ³⁹Ar, with a half-life of 269 years, can be used to map ocean currents on an important time scale. Currently, researchers use ³H ($t_{1/2}=12$ years), ¹⁴C ($t_{1/2}=5715$ years), and ¹²⁹I ($t_{1/2}=15$ million years). Thus, ³⁹Ar would fill the gap, by providing a tracer, which would be reliable on the order of 10²-10³ years. This time scale is important in studying such things as vertical mixing rates of ocean waters [Cannon, 1985, 57-64].

Current Methods of Measuring Noble Gas Isotopes

Applying trace analysis of noble gas isotopes in such ways has been considered important for a long time. However, current methods of counting the isotopes all have serious disadvantages. Low-level decay counting, mentioned above to measure ⁸⁵Kr, was once used to measure ⁸¹Kr as well. However, so much ⁸⁵Kr has been produced as a result of nuclear activity in the last few decades that the background levels of ⁸⁵Kr mask the signal of the lighter isotope. Moreover, the cost of building and maintaining suitable facilities deep underground, and the length of time and exacting standards required to prepare samples have prompted researchers to develop other counting methods. Three have been explored, but each is limited.

Accelerator Mass Spectrometry (AMS). Accelerator Mass Spectrometry (AMS), separates isotopes based on mass (m). A particle of charge (q) moving perpendicular to a magnetic field (B) experiences a force perpendicular to both the velocity (v) of the

particle and the magnetic field. As a result, the particle's path becomes circular, with a radius $r = mv / qB$, as derived by equating the Lorentz and centripetal forces. Heavier (or lighter) particles have larger (or smaller) radii, and detectors can record how many particles impinge at a certain radius. Hence, isotopes, which differ in mass by multiples of the neutron mass, can be effectively separated and measured using AMS. The problem is, *isobars* are not so easily separated. Isobars have the same mass number (total number of nucleons, that is, protons and neutrons), but different atomic numbers (total number of protons). Because the difference in mass between protons and neutrons is tiny, AMS is barely able to separate isobars. Requiring an accuracy of 1×10^{-12} , the pairs ^{81}Kr - ^{81}Br and ^{85}Kr - ^{85}Rb are very difficult to distinguish by AMS. In addition, the large accelerator facility necessary to perform AMS is expensive to build, run, and maintain [Ludin, 1995, p.461].

Resonance-Ionization Spectrometry (RIS). Another method, Resonance-Ionization Spectrometry (RIS), uses pumped lasers to excite atoms above their ionization potential to form ions. The individual ions are counted. Pulsed lasers are used instead of continuous wave lasers, to insure sufficient intensity that all atoms become ionized. The drawback, however, is that the large frequency range of such laser pumping ionizes several isotopes of the atom, not just one. The frequency of the laser is not specific enough to ionize only the desired isotope. Thus, RIS can not effectively separate isotopes [Ludin, 1995, p.461].

Photon-Burst Mass Spectrometry. Finally, Photon-Burst Mass Spectrometry shows promise in measuring trace levels of isotopes. This method involves shining a continuous laser beam into an atomic beam, so that the beams are colinear but counterpropagating [Cannon, 1985, p.57]. The laser excites the desired isotope, and the "burst" fluorescence is detected and measured. However, the time in which the laser and isotope interact is very small, and spectroscopic observations are thus limited. It would be like trying to examine a baseball flying past at high speed.

Our proposal to trap noble gas isotopes using laser cooling and trapping techniques solves all these problems. It is simple to build and maintain, requiring only a modest laboratory, readily obtainable parts, and few personnel. It is relatively inexpensive. Samples are easily prepared and loaded into the apparatus. It can easily separate the desired isotopes and provide a long interrogation time. In sum, it would be an ideal solution to analyze trace amounts of noble gas isotopes.

CHAPTER 2

THE PRINCIPLES OF LASER COOLING AND TRAPPING

To understand how lasers slow and trap atoms, we first consider the photon model of light, which pictures light as being made up of individual packets of energy called photons. In a way, a photon of light can be considered a "particle" of light. The laser beam, then, is made up of a huge number of these photon particles all travelling together with the same frequency in the same direction. As Einstein described, the energy of each photon is simply,

$$E = hv \quad (2.1)$$

where h is Plank's constant ($6.626 \times 10^{-34} \text{ J s}$), and v is the frequency of the light. In terms of momentum,

$$p = E / c \quad (2.2)$$

$$= hv / c \quad (2.3)$$

$$= h / \lambda \quad (2.4)$$

where c is the speed of light ($3 \times 10^8 \text{ m/s}$). Thus, a photon has a certain momentum determined by its frequency (or wavelength), much like a rolling marble has a momentum due to its mass and velocity. In fact, viewing the photon like a rolling marble is helpful.

Just like a rolling marble can transfer its momentum to a second marble if the two collide, a photon can transfer its momentum to an atom if the two "collide" (Figure 2-1). However, in order for the collision of a photon and atom to occur, a condition must be met: the frequency of the photon must equal the atom's resonance frequency. This, of course, is due to the quantized nature of the atom's energy levels. In the ideal case, if the photon does not have just the right amount of energy (i.e. the right frequency), it won't excite the atom (i.e. no collision occurs.) But if the photon's frequency is correct, the atom will absorb the photon, and the momentum of the photon will be transferred to the atom.

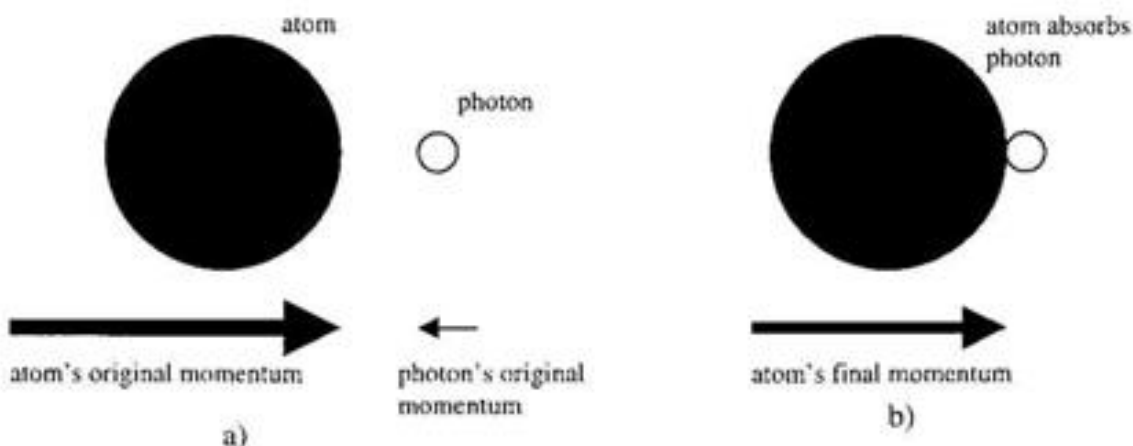


Figure 2-1. Momentum Transfer Between Photon and Atom.
a) A photon approaches a moving atom with opposing momentum. b) After the photon is absorbed, its momentum is transferred to the atom, and the atom's resulting momentum decreases accordingly.

An additional consideration must be made if the atom is moving. The Doppler effect, commonly experienced by us when emergency vehicles' sirens sound higher pitched when approaching and lower pitched when speeding away, changes the relative frequency of the incoming photon. Because the atom is moving toward the photon, the frequency of the photon appears greater to the atom than what we measure it to be in the rest frame. Specifically, if the photon's frequency is f_p in the rest frame, the atom moving at velocity v towards the photon will actually see the frequency to be $f_p + (v/c) f_p$, where c is the speed of light (Figure 2-2).

If the moving atom's resonance frequency is f_r , and we provide it with a photon of frequency $f_p = f_r$, the atom will *not* interact with a photon since the actual frequency the atom sees is shifted up by $+(v/c) f_r$. Instead, we need to provide the atom with a photon of slightly less frequency, $f_p = f_r - (v/c) f_r$, so that the Doppler effect will make up the difference, and the atom ends up seeing a photon of frequency f_r , exactly what it wants. In practice, this technique is called "de-tuning" the laser under the resonance frequency (Figure 2-3). In the chapter describing the Zeeman tuned slower, we re-consider the Doppler effect, because as the atom slows down, the Doppler shift decreases, and somehow, the laser must always be in resonance with the atom.

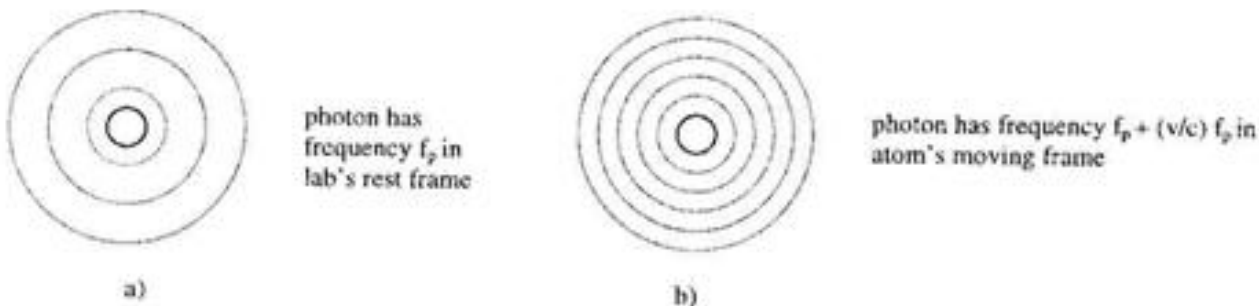


Figure 2-2. Doppler Shift due to Atom's Velocity

a) If the atom were at rest, it would see the frequency of the photon to be the same as that measured in the rest frame, f_p . b) A moving atom sees a higher frequency, because its velocity causes a Doppler shift, $(v/c) f_p$.

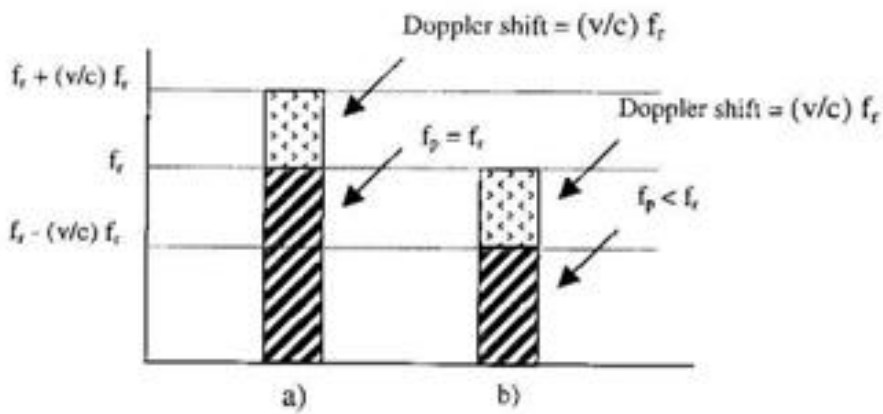


Figure 2-3. Effect of Doppler Shift.

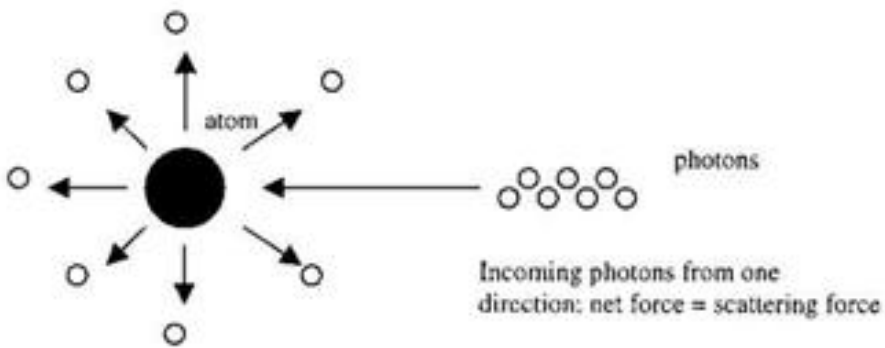
- a) If photon has frequency $f_p = f_r$, the additional Doppler shift due to the atom's velocity increases the frequency that the atom sees beyond the resonance frequency, and no interaction between atom and photon will occur. b) By providing lower frequency photons in the first place, the additional Doppler shift will increase the effective frequency up to the atom's resonance frequency, and the atom will interact with the photon.

Slowing

Suppose an atom is travelling in the positive x direction and a photon of the proper frequency is travelling in the negative x direction, so that they are headed directly for each other, like two marbles about to have a head-on collision. When they meet, the atom will absorb the photon, momentum from the photon will be transferred to the atom, and the atom will experience a tiny "kick" in the negative x direction due to the momentum transfer. Instead of picturing marbles of comparable size, a more accurate perspective would be to consider a bowling ball (the atom) plowing in the positive x direction toward a ping pong ball (the photon) flying in the opposite, negative x direction. The effect of one elastic collision between the bowling ball and ping pong ball is insignificant, but the summed effect of trillions of ping pong ball collisions could conceivably stop the bowling ball, and even begin accelerating the bowling ball in the other (negative x) direction! That's basically what also happens to the atom, as it absorbs a constant stream of photons from a laser beam.

Unlike a simple collision between balls, the interaction between an atom and a photon is somewhat more involved, even though the net effect is similar. The atom absorbs the energy of the photon, whereby the atom is excited to a higher energy level. But then, the atom de-excites, and re-emits a photon of the same frequency as the incoming photon. This results in another momentum kick due to the law of action and reaction, so that if the atom re-emits a photon in the positive y direction, say, the atom will experience a kick in the negative y-direction. But the particular direction in which the atom re-emits a photon is completely random, so that a photon can be re-emitted in any direction. One may be in the positive z direction, but then another will be in the negative z direction, and so on equally for all directions. Thus, the momentum kicks due to the isotropic re-emission of many photons all cancel each other out. On the other

hand, the momentum kicks due to the absorbed photons are coming only in one direction, namely, against the direction of the atom's motion. Thus, the net effect of all the absorptions and re-emissions is that the atom experiences a force, called the "scattering force", which slows it down. Figure 2-4 pictures this.



Re-emitted photons in random directions: net force = 0.

Figure 2-4. The Scattering Force

Momentum coming from incident photons are in only one direction. These photons are absorbed and re-emitted isotropically, and so the momentum kicks due to re-emission all cancel each other out. Thus, the net effect is a scattering force against the direction of motion of the atom.

To be more quantitative about the effect of one photon on a moving krypton atom, consider the following. By momentum conservation, the change in momentum (Δp) of the atom's original momentum (P) must simply be the momentum (p) of the incoming photon.

$$P_f = P_i \quad (2.5)$$

$$P + \Delta p = P - p \quad (2.6)$$

$$\Delta p = -p \quad (2.7)$$

Then from equation 2.4,

$$\Delta p = -h/\lambda \quad (2.8)$$

Now, since

$$\Delta p = \Delta m v \quad (2.9)$$

$$\Delta v = -\Delta p / m \quad (2.10)$$

$$= -\frac{h}{\lambda m} \quad (2.11)$$

For ${}^{81}\text{Kr}$, $m = 83.3 \text{ amu} \times 1.661 \times 10^{-27} \text{ kg/amu}$, and $\lambda = 811.7 \text{ nm}$ (resonance wavelength of $5s[3/2]_2 - 5p[5/2]_3$ levels), Δv is found to be -0.006 m/s . Thus, one photon can change the velocity of an atom by -6 mm/s . In one second, a krypton atom can scatter (absorb and re-emit) 10^7 photons. Another way to express this is to say that the photon scattering rate is 10^7 s^{-1} . Thus, if one photon can change the velocity of an atom by -0.006 m/s , 10^7 photons can change it by $60,000 \text{ m/s}$. This occurs every second, so the deceleration caused by a continuous laser beam on an atom is $6 \times 10^4 \text{ m/s}^2$, or 6000 times greater than the gravitational acceleration! With this large force, an atom travelling at 500 m/s can come to a stop in only 2 m.

Velocity Dependent Damping Forces

After an atom is slowed down to nearly zero velocity, it can be loaded into the actual trap, a three-dimensional extension of the cooling method, called "optical molasses" (Figure 2-5). Here, six laser beams quench every component of an atom's velocity. For instance, a vector of three orthogonal (perpendicular) components (x , y , and z) can describe any velocity an atom might have. So, if we shine three laser beams in each direction (x , y , z), and then reflect each of those beams in the negative of each direction ($-x$, $-y$, $-z$), all positive and negative components of the atom's velocity can be affected. (Notice that as long as the three beams are orthogonal to each other, the particular orientation of the beams is not important, since the atom's velocity can always be completely described by a basis set of three orthogonal components.)

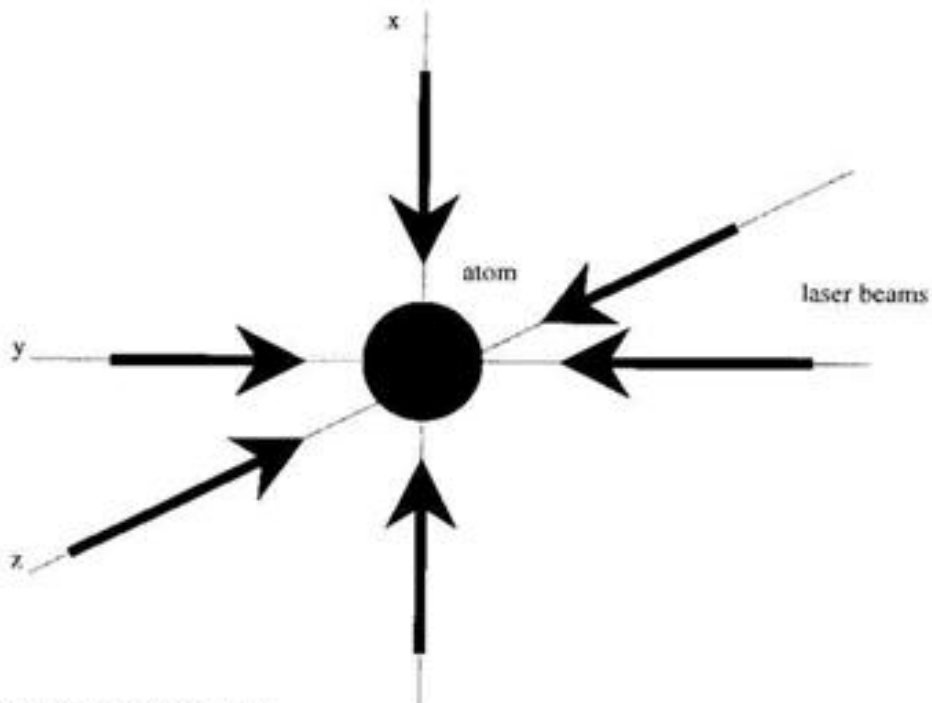


Figure 2-5. Optical Molasses.

Three pairs of orthogonal laser beams quench the atom's motion in all directions.

Suppose an atom is at rest in the center of the six beams, which are slightly detuned under resonance frequency. First, because it is at rest, its velocity is zero and no Doppler shift occurs. In the simplified, ideal picture, which we assume for the sake of easing understanding, the atom is basically unaware of the beams, does not interact with the photons, and feels no effect by them. (In actuality, the atom does interact with photons which are not exactly at the specific resonance frequency; it just does so at a lesser rate than it would at resonance. As long as the atom is still, it interacts with all the beams equally, so any existing forces cancel.) If the atom begins to drift in one direction (Figure 2-6), say the positive-x direction, it starts to have a velocity in that direction and moves *into* the beam pointing in the negative-x direction. The resulting Doppler effect shifts the frequency of this beam towards resonance, and the atom begins to interact with these photons, as described above. On the other hand, because it is moving *away* from the beam in the positive-x direction, the Doppler shift is *further* away from resonance. The atom remains unaffected by this beam, as well as the other beams. The only beam it sees is the one in the negative-x direction. Thus, it feels a scattering force in the negative-x direction, thus slowing it down. Because the atom's motion is damped, as if it were in a thick fluid, this arrangement of laser beams produces what is called "optical molasses".

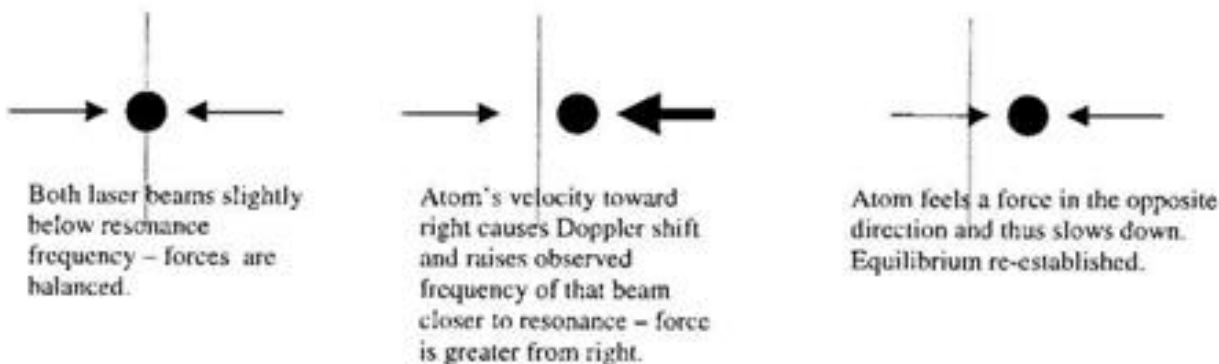


Figure 2-6. Velocity Dependent Forces

Notice that in this arrangement, the forces are velocity dependent: $F = -\alpha v$. The atom acts as if it were in a container of viscous fluid, molasses, if you like (Figure 2-7 a). When the atom moves, it feels an opposing force due to its motion. The force's direction is always against the direction of motion, but not towards any specific point in space. The atom could be sitting anywhere on the bottom of the container and feel no force if it was not moving. Everywhere the atom experiences stable equilibrium, and forces arise only if it moves. Because a real "trap" is a singular point of stable equilibrium (like the bottom of a well), we need position dependent forces, all pointing in to one spot in space (Figure 2-7 b). Thus, optical molasses is insufficient to actually trap atoms.

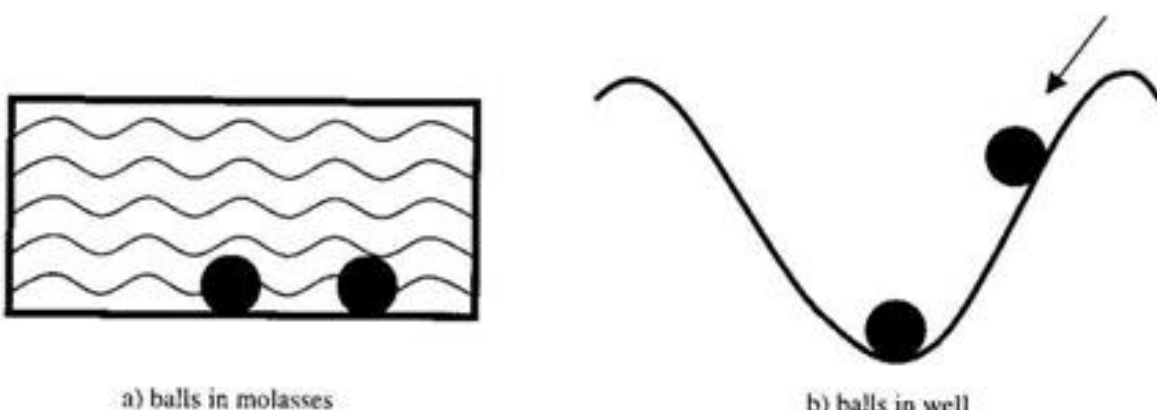


Figure 2-7. Classical Analogies. a) *Velocity-dependent forces*. Balls in an aquarium filled with viscous fluid, like molasses. Forces arise only if the ball moves. $F = -\alpha v$. If both balls are stationary, they will stay where they are. b) *Position-dependent forces*. Ball at the bottom of a well is in stable equilibrium, but the ball placed motionless on the wall of the well will experience a force toward the bottom. $F = -kx$. Both balls will wind up only at the bottom.

Position Dependent Trapping Forces

The way to produce position-dependent forces is by applying a magnetic field gradient around the trapping region and using circularly polarized laser beams. Together, these make up the Magneto-Optical Trap, or MOT. The magnetic field is zero where the trap is, and increases in magnitude linearly away from the trap. That is, how much magnetic field an atom experiences depends on its position relative to the center of the trap. Close to the center, the magnetic field is small. Farther away, it is larger. Thus, the magnetic field is position-dependent.

Zeeman Effect

When an atom is in a region where a magnetic field exists, the degeneracy of the n^{th} state is broken. The energy levels are split according to the angular momentum in the "z" direction of the electrons, chosen for convenience to be the direction of the magnetic field. Two Zeeman effects have been observed. The "normal" Zeeman effect was predicted classically and depends entirely on the direction of the electrons' angular momentum. The "anomalous" Zeeman effect was not predicted classically, and results from the inherent spin of an electron interacting with the magnetic field.

To examine the source of the normal Zeeman effect, consider a free electron in a magnetic field. The Hamiltonian for this system (in Gaussian units) is

$$H = (1/2m) [\mathbf{p} - (e/c) \mathbf{A}]^2 \quad (2-12)$$

where \mathbf{p} is the momentum operator, and \mathbf{A} is the vector potential. This Hamiltonian can be solved exactly for a uniform, constant magnetic field. The solution resembles that of the harmonic oscillator. The energy levels are quantized, where

$$E = (h/2\pi) \Omega (n + \frac{1}{2}) \quad (2-13)$$

$$\text{and} \quad \Omega = \frac{eB}{mc} \quad (2-14)$$

Solving, we find the energy levels to be split into three:

$$\Delta\lambda = 0, \pm \frac{B\lambda^2 c}{4\pi mc} \quad (2-15)$$

Thus, the amount of splitting of the energy levels depends on how large B is. In the MOT, the B field increases linearly away from the center of the trap. Thus, an atom will experience a corresponding linear increase in Zeeman shift, the farther it is from the trap's center. Graphically, we can represent the 1-dimensional situation as shown in Figure 2-8.

At the center of the trap, the B field is zero. No Zeeman shift is present. We shine oppositely polarized, counterpropagating laser beams on the atom. The laser beam from the right is negatively polarized (σ^-), and due to the conservation of angular momentum, will excite transitions from the ground state to the $m = -1$ state. The left beam is positively polarized (σ^+), and the transitions occur between ground and the $m = +1$ state. Both beams are at slightly lower than resonance frequency. With no Zeeman shift, the magnitude of the transitions between the ground state and the $m = -1$ and $m = +1$ states are equal. Thus, the atom will interact with both beams equally, and no net force results, as illustrated in Figure 2-9.

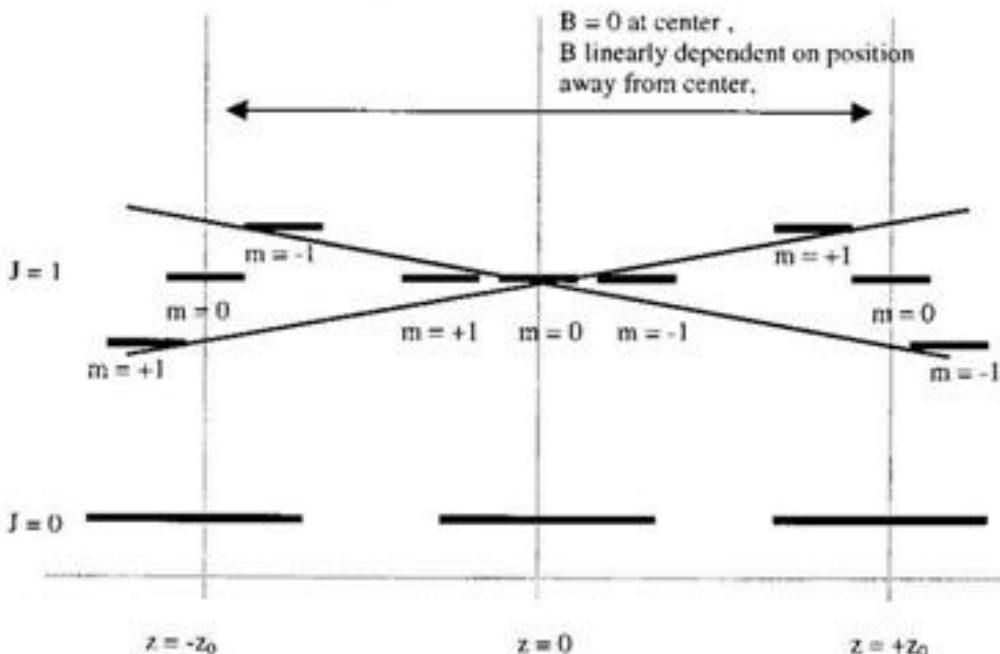


Figure 2-8. Position Dependent B Field Causes Corresponding Zeeman Shift.
Note the polarity of the B field causes an asymmetrical splitting of energy levels about the center.

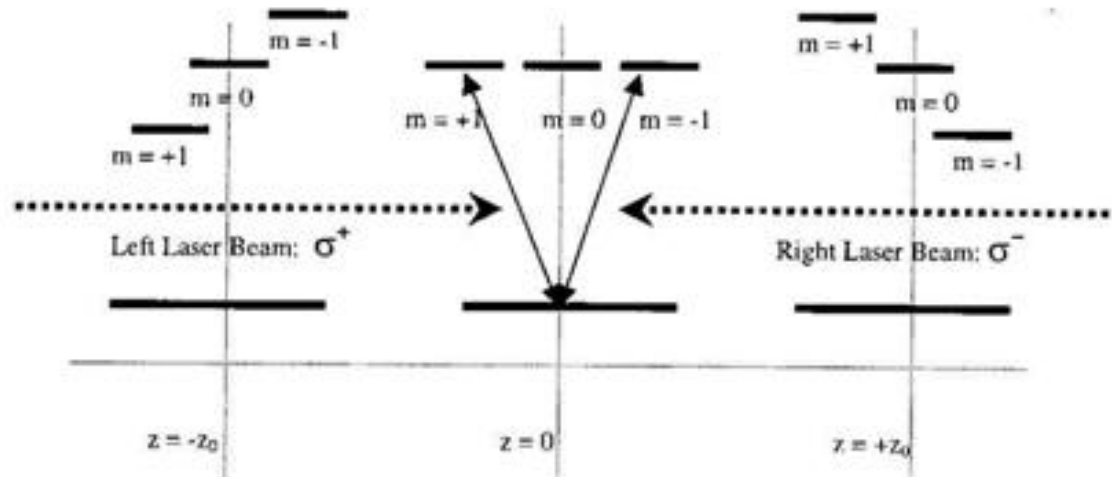


Figure 2-9. Zero Net Force at Trap's Center.

Since no B-field is present at the trap's center, no Zeeman shift occurs, and the right and left beams excite the atoms equally. The two beam's effect cancels, and the net force is zero.

Consider what happens when the atom drifts right of center, to $z = z_0$. Now, a B-field does exist, resulting in a Zeeman shift. The polarity of the B-field is such that it lowers the $m = -1$ level closer towards resonance, while raising the $m = +1$ level further away. Again, the beam from the right has a σ^- polarization and excites transitions from the ground state to the $m = -1$ state. Since now the magnitude of the transition between ground and the $m = -1$ state is lower, the atom will interact more with the beam from the right. The energy difference between the ground and $m = +1$ states is greater, and so the atom interacts less with the beam from the left. Thus, a net force from the right toward the trap center results (Figure 2-10). The opposite occurs when the atom drifts toward the left.

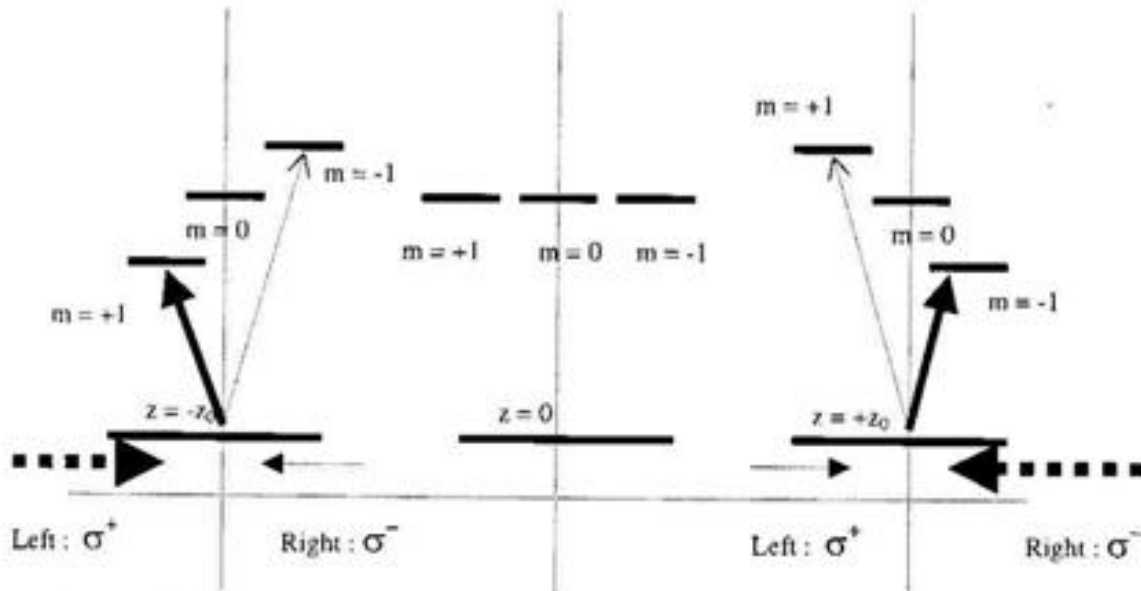


Figure 2-10. Net Force Toward Center At Points Away from Center.

If the atom moves to $z = +z_0$, the polarity of the B field there causes a corresponding Zeeman shift, which will lower the $m = -1$ level closer to resonance and raise the $m = +1$ further away. Since the right beam's polarization is σ^- , the right beam will more easily excite the atom than the left beam, resulting in a net force towards the trap's center. The opposite occurs at $z = -z_0$.

As a result, depending on where an atom is, it will be affected more by a particular beam than another. That is, the forces caused by the laser beams now depend on where the atom is, or $F = -kx$. All forces point toward the center, just like the forces on a ball in a well (Figure 2-7 b), where we expect to trap atoms. Thus, unlike the velocity dependent forces in the case of optical molasses, the positional dependent forces caused by the MOT actually pushes the atoms back towards the center of the trap.

The Need for the Metastable Level

To excite the krypton or argon atoms from their ground levels, we need a laser capable of producing a constant beam of light of wavelength 120 nm, in the vacuum ultra-violet (VUV) region. Such a laser is currently not available, although considering the intense research and development in VUV technology, it may soon be. On the other hand, infrared lasers are common, and fortunately, we can take advantage of this.

Instead of exciting the atom directly from the ground level, we first excite it to a metastable level using a direct current (DC) discharge. (A metastable level is an excited level that does not immediately decay back to the ground level. In the case of krypton, the lifetime of the $5S[3/2]_2$ metastable state is 39 seconds, that is, after being excited to the metastable level, it will stay excited for 39 seconds before spontaneously decaying back to the ground level. So, it is "somewhat" stable, hence, "meta"-stable.) The energy required to excite the atom from the ground level to the metastable level is only 10 eV. As will be discussed in the chapter describing the metastable atom source, we produce metastable atoms from a DC discharge between a tungsten rod and grounded skimmer.

Once the atom is excited to the metastable state, the transition to the $5P[5/2]_3$ excited level requires light at 811 nm, in the infrared. So, the laser cycles the transition between the $5S[3/2]_2$ and $5P[5/2]_3$ states, and the cooling and trapping phenomenon can occur. A readily available Ti:Sapphire ring laser or a GaAlAs diode laser outputs a continuous laser beam at the desired wavelength.

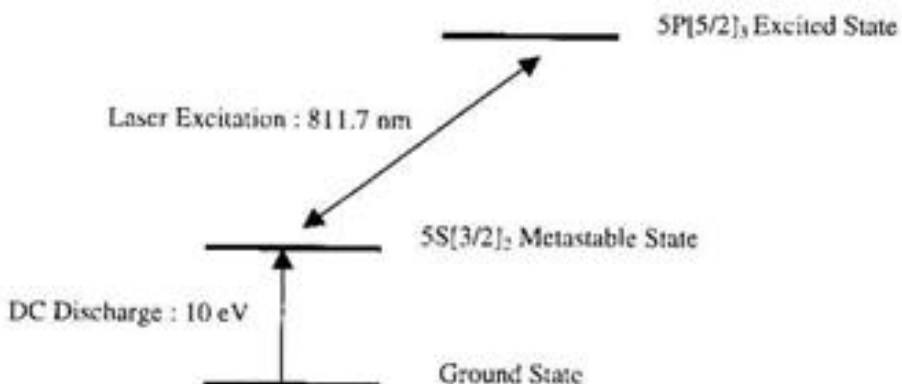


Figure 2-11. Atomic Excitation Scheme.

Summary

Putting this all together, a moving atom is first slowed down by shining one laser beam against its direction of motion. After it is slowed to nearly zero velocity, it enters a region of inhomogeneous magnetic fields and six circularly polarized beams. All forces point toward the center of the trap, and atoms are trapped. With this general understanding of the principles behind laser slowing and trapping, we are in a position to appreciate the details of getting it all to work.

CHAPTER 3

EXPERIMENTAL SET-UP

Being the first member of Dr. Lu's team, I had the privilege of helping build the laboratory from the ground up. When we first started, we had just been given a room, F-118, which had been a machine shop. We invested a few weeks cleaning out left-over equipment and supplies; arranging for the walls to be painted a pretty sky-blue and the windows to be boarded up and darkened; choosing furniture from storage and laying out the floor plan; and a myriad of other details, like putting in phone and computer lines. After building some of the apparatus, another, better-equipped room, H-126, became available. Moving into the new room, we finished building the system without significant interruption.

Here, then, is a detailed consideration of our trapping apparatus.

Optical System

Figure 3-1 lays out the main optical elements of our experiment schematically.

Lasers

The main laser is a newly purchased, Coherent Sabre Innova Argon-Ion Laser. It produces a laser beam in the visible region with wavelengths around 500 nm. The output power is variable, and when running the experiment, is set at 15 W. The argon-ion laser pumps a Coherent 899 Ti:Sapphire Ring Laser, which converts the laser beam to 811 nm and roughly 1 W of power. The controller for the ring laser is based on a system of etalons, which allows for precise laser frequency control and scanning.

Laser Beams

Beam splitters separate the main beam into four. One beam enters a Burleigh Wavemeter, basically a Michelson interferometer, which displays the approximate wavelength of the laser beam. Another beam goes through the setup for saturated absorption spectroscopy, needed to precisely tune the laser to the atomic resonance frequency. Saturated absorption spectroscopy will be examined in detail in Appendix 1.

The third beam is enlarged through a beam expander (a mini telescope of two lenses) from 1 mm to 3 cm diameter and becomes the slowing beam, directed against the atom beam. The beam expander is adjusted such that the slowing beam is focused to a point near the atomic source. The focusing helps to push atoms toward the center of the atomic beamline, by providing components of force toward the center. Focusing also helps to optically pump the atoms into the proper quantum state, whereby the laser can most efficiently excite the atoms. The slowing beam's intensity is attenuated to 5 mW/cm².

The fourth and final beam is also expanded through a beam expander but is not focused (the focus is at infinity). It is then split into three beams, each one directed into the trapping chamber orthogonal to the others. These form the trapping beams, two in the horizontal plane, and one vertical. Mirrors on the opposite sides of the trapping chamber

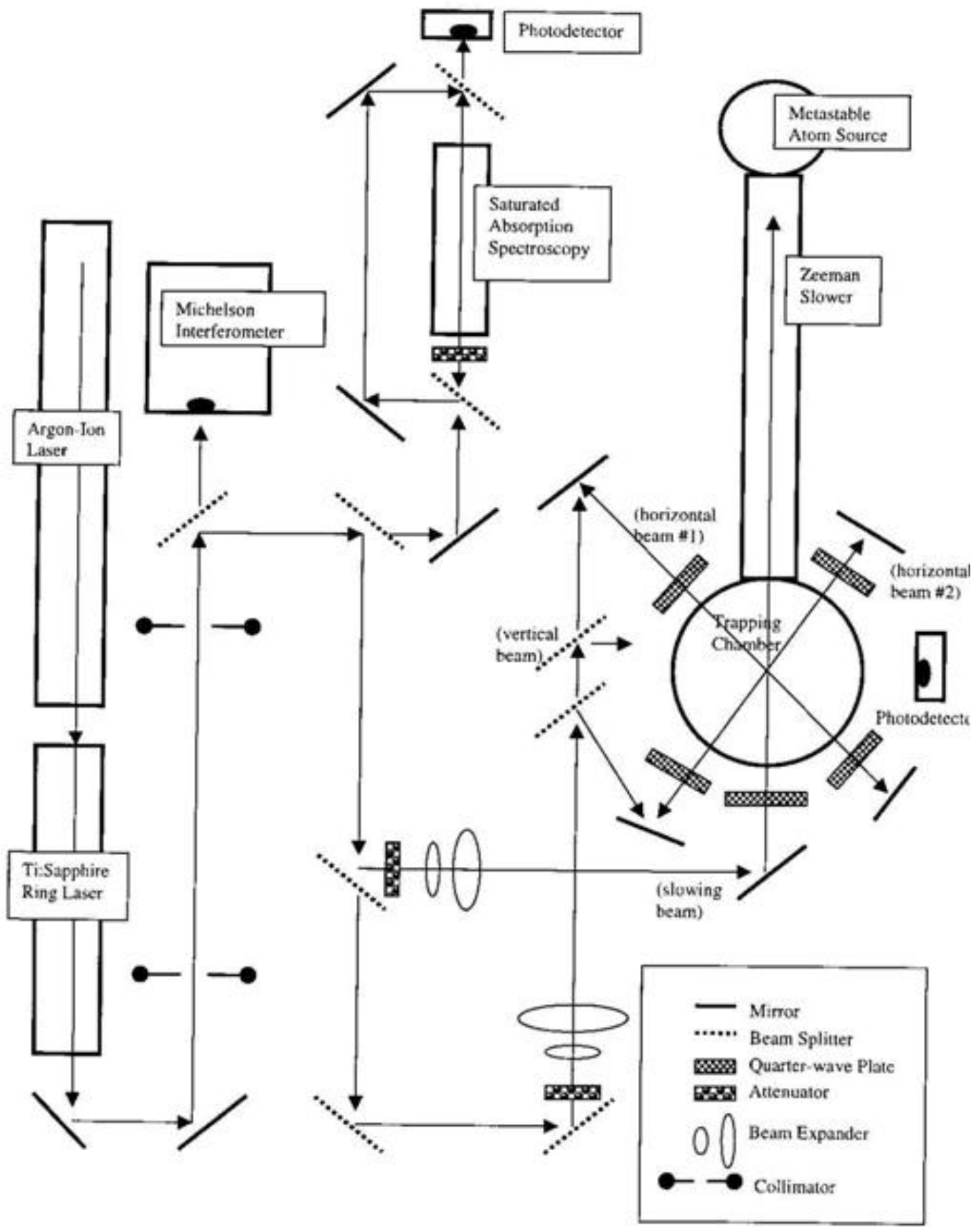


Figure 3-1. Optics Table Layout.

reflect these beams back on themselves, so the result is six counterpropagating beams. The intensities of the slowing beams do not have to equal, but should be close. Specifically, the first pair of horizontal beams was 19 mW/cm^2 ; the second pair, 13 mW/cm^2 , and the pair of vertical beams was 20 mW/cm^2 .

Polarization

When the beam comes out of the laser, it is linearly polarized. In order to trap atoms, the beams need to be circularly polarized, as was explained in Chapter 2. Thus, before each of the trapping beams enters the trapping chamber, it passes through a quarter-wave plate, set with its fast-axis of polarization 45 degrees clockwise to the vertical. Then, as it exits the chamber and is reflected back into the chamber, it passes through another quarter-wave plate, the axis-orientation of which can be arbitrary. The reflected beam is thus also circularly polarized but in the opposite sense as the entering beam. The sense of the polarization depends upon the direction of the magnetic field. In the case of the vertical beam, the quarter-wave plate before the top beam enters the chamber is set with the fast-axis of polarization 45 degrees counter-clockwise to the vertical. This is because the nature of the magnetic field is such that it points inward toward the center in the horizontal plane but outward from the center in the vertical.

The above references to "clockwise" and "counterclockwise" is relative to the direction of the magnetic field from the MOT. In this case, the MOT field along the vertical direction is away from the center of the trap. Along the horizontal direction, the field is pointing in towards the trap. Of course, the direction of the field is determined by the direction of current flowing through the anti-Helmholtz coils. By determining the proper direction of the field and correctly setting the corresponding polarizations of the quarter-wave plates, a potential source of error can be avoided.

Vacuum System

Gas Supply and Control

Compressed gas cylinders (supplier: AGA) store the neutral, noble gas atoms. A home-made, branching, valve system enables easy switching between argon and krypton gasses. Stainless steel tubing connects the gas source to the saturated absorption cell (SAC) and copper tubing to the discharge source chamber (DSC), the first stage of the atomic beam line. Both the SAC and DSC are under vacuum. Fine control of gas flow into the SAC is achieved using a variable leak valve, while a servo-driven valve assembly and electronic flow controller is used in the DSC.

Saturated Absorption Cell

The SAC is simply a glass cell around which a radio-frequency (RF) coil is positioned. An RF frequency generator and amplifier powers the coil, which ionizes the noble gas. Collisions between free electrons and ions produce neutral metastable atoms, and as will be explained in detail, saturated absorption spectroscopy performed on these

atoms will serve as a precise reference of the atomic resonance frequency. The cell is connected to a Varian mechanical, scroll pump, and the vacuum is maintained around 100 mT.

Atomic Beam Line

Figure 3-2 displays the schematic diagram for the atomic beam line.

Discharge Source Chamber

The DSC is the first stage of the atomic beam line in the main vacuum chamber system, which eventually leads to the trapping chamber. The DSC is effectively a 2 ¾" 4-way cross vacuum chamber. The four ends are connected to: 1) gas inlet valve, 2) electrical feedthrough, 3) skimmer chamber, and 4) Convectron gauge chamber (which houses a Convectron pressure gauge to measure the source chamber's pressure). An exhaust valve is found at the other end of the Convectron gauge chamber, which is connected to the same scroll pump that evacuates the SAC. The valve allows us to reduce the pressure in the source chamber, if desired. Under normal operating conditions, the pressure in the supply chamber is 2 – 3 T.

Electrical Supply. The discharge source is based on a sustained direct-current (DC) discharge between a 7" long tungsten rod and a grounded, metal skimmer. An electrical feedthrough connects the tungsten rod (0.5 cm diameter) to an external, variable DC voltage supply via a high voltage cable. Under experimental conditions, the DC supply is set at -2000 to -3000 V. Two 250-kΩ, 50-W resistors are attached in series between the voltage supply and tungsten rod.

The purpose of the series resistors is two-fold. First, it helps to reduce the voltage across the discharge after it starts. Before the discharge starts, all the applied voltage exists across the rod tip and skimmer. Once a current forms, though, a voltage drop exists across the resistor, lessening the voltage across the discharge itself. Thus the voltage is maximized when we want to start the discharge (making it easier to accomplish), and then lessened after the discharge has started.

Another purpose for the resistors is to help stabilize the current. If for whatever reason, the current increases, the voltage drop across the resistor increases, thus decreasing the voltage drop across the discharge. The diminished voltage will thus act to decrease the current across the discharge and counter the initial current increase. Likewise, if the current decreases, the voltage drop across the discharge will increase and help increase the current. Thus, by introducing resistors into the circuit effectively puts a feedback control into the system, helping to stabilize the current.

Quartz Tube. The tungsten rod sits inside a quartz tube, custom made at Argonne's glass shop by a master glass-blower. A tiny capillary tube 4 mils (0.1 mm) diameter was fused to a glass tube of 1.5 cm diameter, so the final product is a quartz tube with a large entrance and a small exit openings. The length of the tube is approximately 14 cm. A compression port adapter is welded into the DSC, and the adapter holds the quartz tube securely. The half of the tube with the entrance opening is in the DSC, and the exit opening half is in the next chamber, the skimmer chamber. The

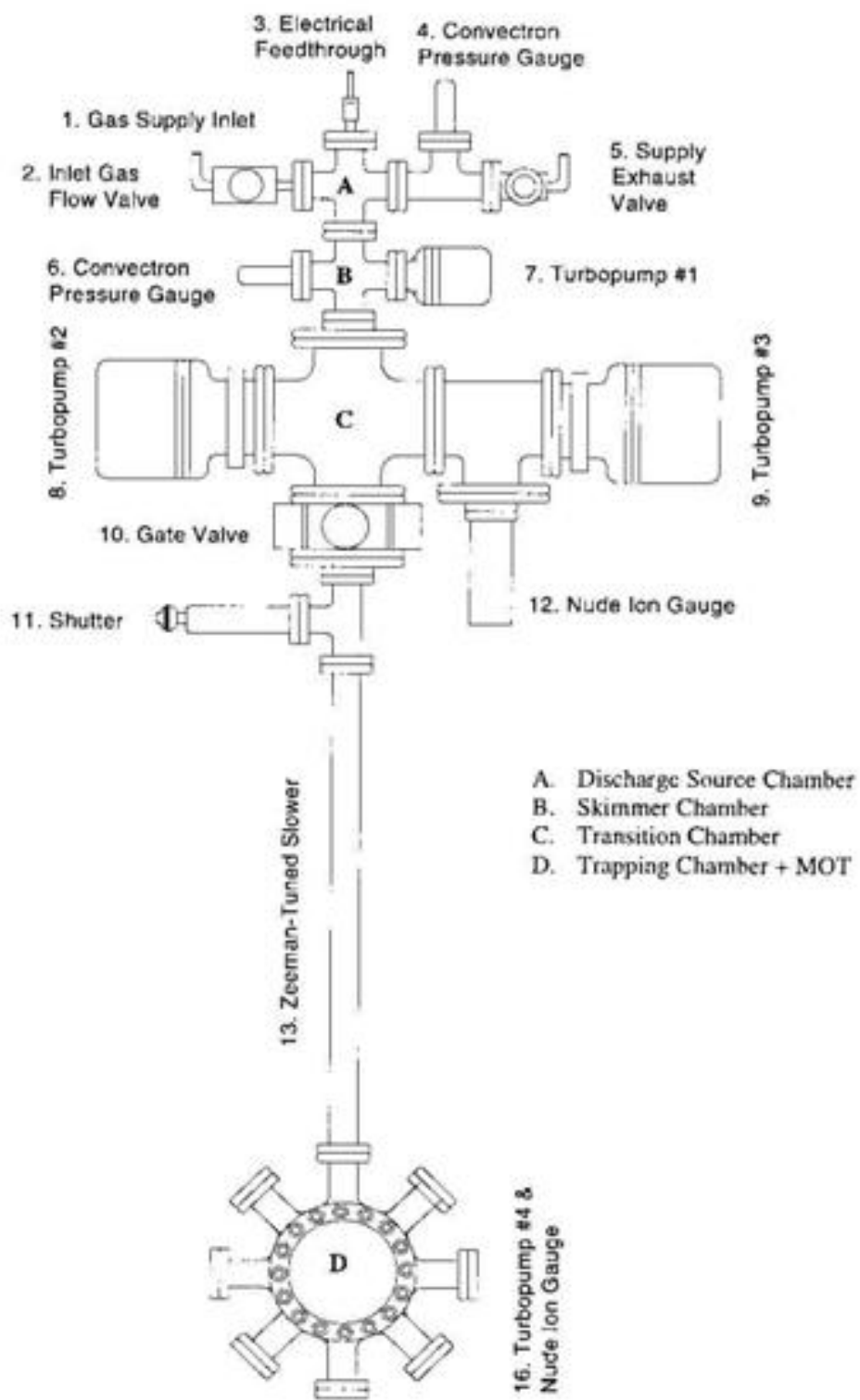


Figure 3-2. Atomic Beam Line

compression port adapter allows differential pressures to exist between the DSC and the skimmer chamber, with the quartz tube bridging the two chambers.

The purpose of the quartz tube is two-fold. First, it insulates the tungsten rod from the inside metal walls of the vacuum chamber. This effectively intercepts the electric field lines from the rod (at high voltage) to the walls (at ground), and encourages the discharge to occur only in a forward direction, from the tip of the rod to the skimmer. The other purpose of the tube is to facilitate creation of metastable atoms by forcing neutral gas atoms through a small region of space where the density of energetic electrons is high. The gas actually ionizes, and glows a light violet color, although whether the ionized gas plays any role in producing metastable atoms is unclear. Atomic interactions between the free electrons and gas atoms form the desired, neutral metastable atoms.

Skimmer Chamber

The next step down in the atomic beam line is the skimmer chamber. It is a $2\frac{3}{4}$ " five-way cross, and the five connections are 1) the DSC, 2) a small turbopump (50 L/s), 3) a window port, 4) a Convectron gauge, and 5) the next step down the atomic beam line, the transition chamber.

Inside the skimmer chamber is positioned a metal skimmer. The skimmer is a delicate, cone-shaped piece of aluminum. The base is about 2 cm in diameter, while the tip of the cone has a 1.5 mm diameter opening. The base is fashioned into a flattened lip, which can be clamped between two other aluminum rings to hold it in place. One of the rings is secured to the vacuum chamber using Torr-Seal®. (Torr-Seal® is applied as a paste and allowed to dry into a solid ceramic. It does not out-gas, so it can be used to "glue" things inside vacuum chambers without affecting the pressure.) The other ring is screwed into the first ring with three 2-56 screws, and the base of the skimmer is sandwiched in between the two rings. Thus, the exact position of the skimmer can be adjusted, which is vital to properly center the skimmer opening with the tip of the glass tube.

When the gas flow is on, the pressure in the skimmer chamber is around 0.7 mT, thanks to a small turbopump. The turbopump is connected with 1" plastic tubing to a mechanical, "roughing" pump, which assists in reducing the pressure. The same mechanical pump is connected to all four turbopumps in the system, and cut-off valves are attached to each connection, so that the turbopumps can be isolated from the roughing pump when necessary.

Transition Chamber

Next is the transition chamber, which is a 6" six-way cross. On two sides are two large turbopumps (250 and 360 L/s), both attached to the same mechanical pump as the first turbopump in the skimmer chamber. Two other sides are windows, to be used for transverse cooling beams in the future. (Laser beams will be shone in from the sides to confine the atomic beam into a narrower path, thus increasing the flux.) One side of the chamber came from the skimmer chamber, and the final side leads to the gate valve. Also, attached to one of the turbopumps is a 6" three-way tee, making room to attach a

nude ion gauge, which monitors the pressure to be 10^{-6} T, when the gas flow is on. This chamber is vital to help improve the pressure in the trap chamber. Pumping out much of the gas at this stage helps the turbopump in the trapping chamber to improve the vacuum by two more orders of magnitude, enough to trap atoms.

Gate Valve

Next is a gate valve operating on compressed air. The air is supplied by a cylinder of compressed nitrogen, regulated to a pressure of 60 lbs/in². When shut, the gate valve allows complete isolation of the first half of the vacuum system (higher pressure) from the trap side (lower pressure). Sometimes, maintenance or improvements on the first half of the system needs to be done. By shutting the gate valve and closing the valves between the first three turbopumps and the shared roughing pump (so that the trapping chamber's turbopump will not be affected) we can isolate the trapping chamber, maintain its high vacuum, and open up the rest of the system to perform the necessary work.

Collimator

In the flange connection between the previous section (the gate valve) and the next section (the shutter), a 2 3/4" solid copper gasket with a 3 mm diameter hole punched in the center is used. Normally, flanges are connected with copper ring gaskets which do not extend into the space inside the vacuum chambers. However, in this case, we want to constrict the size of the opening to help reduce the gas flow into the trap chamber and thus the pressure there.

Shutter

A simple shutter follows, which allows the atomic beam to be easily cut off. Sometimes, we need to stop the flow of atoms. The easiest way, of course, would be to simply turn the atom source off by switching off the voltage supply. While effective, turning the source back on sometimes requires time and effort. The shutter allows us to effectively switch the beam on and off rapidly with just a flip of a switch.

The shutter is powered by compressed air from a cylinder of nitrogen, under pressure of 20 lbs/in². It is simply a linear translator which moves completely in or out. A thin, 2 x 3 cm plate of aluminum is fixed into the end of the translation holder. When it is in, the atomic beam is completely blocked, and when out, the beam is completely not obstructed.

Using the gate valve also effectively cuts the atomic beam, however, because it is actuated with higher pressure, the thrust of the gate closing causes the whole system to vibrate momentarily. Using the shutter is a much gentler way of shutting off the atomic beam when desired.

Zeeman-Tuned Slower

The Current Design. Used to compensate the Doppler shift due to the velocity of the moving atoms, the Zeeman-tuned slower was first designed and demonstrated by William Phillips and Harold Metcalf in 1982. In our version, it is basically two long solenoids, one over the other on a standard 90" long vacuum pipe. Wound with 14 gauge magnet wire, each layer is connected to a separate current supply. The first is a foundational layer with a constant density of windings (6/cm) to produce a constant magnetic field. The secondary layer is wound on top of the first, but the density of windings gradually decreases. The summed effect of the two layers is a gradually decreasing magnetic field. This causes corresponding Zeeman shifts in the energy levels of the atoms travelling through the center of the pipe, which constantly compensate for the decreasing Doppler shifts as the atoms slow down. This method will be discussed in more detail in Chapter 5 .

The design of our Zeeman-tuned slower is unique. The traditional design involves different sections, each with different numbers of windings of wire. For instance, the first section may have five layers of windings, the next section, four, and so on, with the last section having one layer. This can also produce the desired magnetic field gradient. However, because the number of windings at the beginning is so thick, it may grow very hot, and the solenoid must be cooled with, for example, a water jacket. While our Slower also gets hot, it is effectively cooled using three, small fans.

To find the correct number of windings necessary to produce the desired magnetic field gradient, a simulation program was written in MathCad®. The foundational layer was treated as one long, finite solenoid. The secondary layer was treated as a string of finite solenoids, each with different lengths and number of windings. Parameters such as the initial velocity of the atoms, the distance in which the atoms must be stopped, the radius of the pipe, the current in the windings, the length of the foundational layer, the number and lengths of individual solenoid segments in the secondary winding, and the density of windings were all necessary to find the optimal parameters.

Because we used standard pipe fittings, the transition between the basic pipe which makes up the Zeeman-tuned slower to the final trap chamber section is discontinuous. The pipe itself is 2" in diameter, but the transition area is nearly 3" in diameter. Thus, extra windings over this connection region must be made to avoid a sudden gap in the magnetic field. Moreover, the transition windings are powered by a separate current supply to allow greatest flexibility in finding the optimal parameters at which to run the system.

A New Design. An improved Zeeman-tuned slower is being considered at the time of this writing. A couple undesired features of the existing design will be eliminated. The new Slower will be one layer of winding on a 3" hollow pipe, which will fit over the entire length of the atomic beam pipe. The arrangement of windings on this slower will be similar to the secondary layer of the current design, that is, a series of finite solenoids, but with different values of lengths, density of windings, and current. New calculations are being conducted to find new optimal parameters. The pipe will be large enough to fit over the transition connection regions and rest in place. The wire will be 8 gauge square magnet wire, with sides of 3.6 mm. With the new Slower, the transition region will not be a problem, since the larger pipe fits over that area.

Also, by eliminating the current design's transitional layer, much effort trying to avoid discontinuities of the magnetic field where that layer ends can be saved. The simulations found that when the transition layer ends, a residual magnetic tail extends for a certain distance. Trying to exactly match other configurations of secondary windings at this region to form the necessary slope of the magnetic field proved very difficult and time consuming. While adequate solutions were found, the results were not ideal, and inevitable experimental errors would only exacerbate the discontinuities in this region. By using just one winding, a well behaved decrease in field can be achieved without having to worry about such "trouble-spots".

Trapping Chamber

Finally, we arrive at the trapping chamber, which was custom-designed and manufactured with ten ports: seven, to allow the trapping and slowing beams to enter; two to allow fluorescence from the trapped atoms to escape the chamber and be detected by externally placed photodetectors; and one, to connect the chamber to the Zeeman-tuned slower. All ports except the last are closed using anti-reflection coated window ports. Surrounding the chamber on the outside is a 29" x 28" optical board with $\frac{1}{4}$ "-20 tapped screw holes, on which optical elements are positioned to steer the laser beams into the chamber.

End Solenoid. When the atomic beam leaves the Zeeman-tuned slower it immediately enters the first 10 cm of the trapping chamber. On the outside of this section of vacuum chamber, more magnet wire is wound, making up a final solenoid, which is powered by a separate current supply from the Zeeman-tuned slower. This "end-solenoid" is vital to make a continuous magnetic field gradient to the very end, adequately keeping in step with the slowing atoms until they enter the position dependent MOT magnetic fields.

Trapping Region. The central region of the chamber is where the trapping and slowing beams intersect. The slowing beam is reflected into chamber directly against the atomic beam direction. Two pairs of trapping beams are on the horizontal plane of the apparatus, and enter the chamber in the two, criss-crossing, 45 degree ports. One pair of trapping beams shines vertically, entering from the 6" opening at the top, and reflecting back up through the bottom.

MOT. Toward the top and bottom of the outside of the trapping region are a pair of anti-Helmholtz coils, basically two rings of wire, positioned like halos above and below the trap chamber. The same 14 gauge magnet wire as used in constructing the Zeeman-tuned slower is used to wind the anti-Helmholtz coils. The wires are wound on a custom-made, 0.1" thick, aluminum holder, to physically separate the wires from the chamber and prevent excessive conduction of heat from the wires to the chamber. In each half are 46 windings, but the sense (clockwise vs. counterclockwise) is different. To use only one current supply for both coils, an end of wire on the upper half is connected to an end on the lower half. Then, the other two ends of the wires are connected to the current supply.

When current flows through the wires, these coils provide a gradually changing magnetic field in the chamber, with a zero field in the center. The magnetic fields together with the trapping beams make up the magneto-optical trap (MOT). The

magnetic fields are needed to produce a position-dependent force, as discussed in Chapter 2. In addition, smaller rings of wire variously positioned around the trap chamber provide magnetic fields, which are used for fine-tuning where the zero-field is in the chamber. Called "tweaking coils", they allow us to move the actual ensemble of trapped atoms into the best observational position. One tweaking coil directly opposite the end of the Zeeman-tuned slower, called the "counter" coil, is particularly useful. Because of the Zeeman-tuned slower, the zero of the magnetic field is pushed away from the true center of the trap chamber. By opposing this with the counter coil, the zero can be pushed back towards center.

The fourth turbopump is connected directly to the trap chamber, bringing down the vacuum to 10^{-8} T, as measured by a nude-ion gauge. As was mentioned previously, the turbopump is connected to the same mechanical, roughing pump as the three other turbopumps in the system. Moreover, it can be isolated from the other turbopumps, so that the trapping chamber can maintain high vacuum while work is performed on the first few stages of the atomic beam line.

Detection Systems

To observe the trap, visual and electronic detectors are set up on an 24" x 24" optical board, held by Uni-Strut and joined to the optical board surrounding the trapping chamber. This "detection deck" also holds focusing lenses, beam splitters, and apertures needed to properly image the trapped atoms.

Visual Detectors

CCD Camera

The charge-coupled device (CCD) camera is commercially obtained. It is a black and white (B/W) camera with an 8-48 mm, 1:1.2 zoom lens. The focal length can be further adjusted by changing the position of the lens holder, which connects the lens and camera body. Two 12" B/W video monitors display the resulting image. (Two are set up for convenience, so we can still see the display from different positions around the room.)

IR Viewers

Because the atomic transition of interest is around 811 nm, the wavelength of the laser beam we use is in the infrared (IR). Being invisible to the naked eye, we need to use an IR viewer in order to actually see the beam during positioning of optical elements on the laser table. The principle of the viewer is straightforward: photons hitting a screen give off a position dependent electronic signal. The signal is constantly scanned and converted on a mini television screen into a visual display inside the viewer. The particular model we used must be held by one hand, thus, making one less hand available to work. Effectively, one hand was always tied behind our backs, making life even more challenging.

If the laser beam is not too intense, an IR card can be used. It is a small, plastic card, a little larger than a typical business card, coated with fluorescing material. When

IR photons impinge on the material, a bright red spot appears which clearly stands out on the orange background.

Electronic Detectors

Photodetector

A home-made photodetector is used to measure photon intensity. Designed by Kristin Corwin, a doctoral student at the University of Colorado, Boulder, it is based on a photodiode (conversion ratio $\eta = 1W / 0.5A$), and electronic circuitry involving operational amplifiers, which convert the current into a voltage and then amplify the voltage to a measurable signal. Also, a bias-voltage can be applied to conveniently position the signal on the voltage measuring device, in our case, an oscilloscope. The board was printed on a circuit board by the electronic shop, and assembled by us. (In fact, a custom in our lab is for new members, including summer intern students, to build a functional photodetector as their first project.) It is housed in a $2\frac{1}{4}'' \times 4\frac{1}{2}'' \times 1''$ metal box, and the appropriate openings were cut by the machine shop. In normal operation, two photodetectors are used, one to monitor the saturated absorption signal, and the other to measure the fluorescence of trapped atoms.

The photodetector is powered by the standard $\pm 12V$ supplied by a nuclear instrument module (NIM). A special version of the photodetector is battery powered, designed to eliminate noise inherent in the NIM power supply.

To display the photodiode output voltage, a digital oscilloscope is used. If the signal is still so small that it is masked in background noise, a lock-in amplifier is connected to improve the quality of the signal. Finally, a signal analyzer based on the Fast Fourier Transform characterizes noise in the signal, a great aid in determining and eliminating noise sources.

Faraday Cup Detector

To measure the metastable flux, that is, the number of metastable atoms produced per second per steradian, a home-made detector based on the Faraday Cup was designed and built. It is based on a very simple principle. When an excited, metastable atom collides with a metal, the excess energy can ionize an atom in the metal. As a result, a secondary electron is ejected from the metal. With a constant barrage of metastable atoms on a metal surface and the subsequent release of secondary electrons, a measurable current forms, indicating the metastable flux.

The detector itself consists of four pieces of stainless steel, a rectangular slab of Macor® ceramic, two strands of wire, a linear translator, three nine volt batteries connected in series, and a vacuum chamber electrical feedthrough.

The stainless steel pieces are affixed to the Macor® using Torr-Seal® in the following arrangement. One square piece, called the emitter, is centered on the Macor®. Enclosing it is a rectangular piece, bent around like a circle, resting on its edge. This piece is called the collector. Resting on top of the collector are two rectangular pieces with a 1 mm gap between them. The gap is centered on the emitter.

The Macor® with the metal pieces is attached to the linear translator, so that the entire assembly can be slowly moved in and out of the atomic beam. One wire connects the emitter to one pin in the electrical feedthrough, and another does the same with the collector. From the outside, the negative lead of the battery is connected to the collector pin of the electrical feedthrough. The positive lead of the battery is connected to the positive lead of a Keithley® picoammeter. The negative lead of the ammeter is grounded, as is the emitter pin of the feedthrough.

When everything is connected, the collector is negatively biased at around -27V. Electric field lines flow from the collector to the emitter, which is grounded. Thus, when metastable atoms produce secondary electrons from the collector, the electrons will leave the collector and go to the emitter, producing a current. The picoammeter in series with the collector and ground measures this current. An example of calculating the metastable flux from the measured current is given in the calculations section, Chapter 6 .

As a sidebar, the names of the emitter and collector seem to be opposite their functions. The secondary electrons seem to be "emitted" from the collector, and the emitter "collects" them. The rationale behind the names is historical. When originally designed, the emitter was to be negatively biased, and the collector positively biased. Thus, the electrons were meant to flow from emitter to collector. Furthermore, the two rectangular plates forming the 1 mm gap was meant to act as a collimator. However, with this setup, inconsistent and inaccurate reading resulted. Only when we prepared the detector in the manner described in the previous paragraph did the results make consistent sense. On the other hand, since the direction of current is defined to be opposite the direction of the actual flow of electrons, we could say that the emitter is the "source" of the current, which flows to the collector. Although not the original intention, this should help make the names of the pieces sound more sensible.

Structural Support

The entire vacuum system is firmly secured to custom built, sturdy, aluminum Uni-Strut® supports. Uni-Strut® pieces come in numerous shapes and sizes and are an adult-version of Erector Set® toys . Uni-Strut® bars are ordered in standard lengths, but are easily cut by the machine shop according to the need. Dozens of connector types to connect the bars are also available. The pieces can be put together in virtually any conceivable way to support practically anything.

Besides the atomic beam line and trapping chamber, many parts of the system are held by Uni-Strut®, including a 3' x 10' wood shelf above the laser table, to hold electronic controllers and devices. The shelf stands 5 ½' above the ground, 2 ½' above the laser table surface. The wood is treated to be fire-resistant and painted black to minimize glare. Large holes are drilled in sections to allow wires to pass through and connect to devices on the table.

A special note: the Uni-Strut® support for the first part of the atomic beam line (which includes the DSC, the skimmer chamber, the transition chamber, the gate valve, and the shutter) has four adjustable feet. The feet can be raised or lowered by turning a nut. This is an important feature when centering the atomic beam through the collimator copper gasket. The centering of the collimator will be considered in more detail in Chapter 4.

Laboratory Infrastructure

Lasers and turbopumps get hot. Gate valves need air pressure to work. And of course, nothing works without electrical power. Building 203 at Argonne National Laboratory has a dedicated water supply for cooling; the main argon-ion laser and one turbopump are cooled by it. A separate refrigerated chiller circulates a closed supply of de-ionized water to cool the Ti:Sapphire laser. Small electric fans cool the other turbopumps and the Zeeman-tuned slower. And bottles of compressed nitrogen provide the necessary air-pressure to operate the gate valve and shutter.

Electrical power is taken for granted nowadays. However, the argon-ion laser requires a unique phase arrangement, which the Laboratory generally does not support. A special transformer had to be installed to satisfy the unique requirement. Another note about electricity: the power supplies providing current for the Zeeman-tuned slower, Anti-Helmholtz Coils, and tweaking coils draw a lot of current. They should be plugged into sockets protected by fuses different from those in which the vacuum pumps are plugged. This way, if the power supplies surge and blow out a socket fuse, the pumps will not be affected and the vacuum in the apparatus remains undisturbed.

CHAPTER 4

EXPERIMENTAL PROCEDURES AND PARAMETERS

No one procedure encompasses the entire project. The basic outline is: set up the apparatus, turn everything on, and figure out why it's not working. But in the course of the countless hours of turning knobs every which way, aligning and realigning optics, attaching and reattaching vacuum chambers, an intuition about the system develops. Things which once took days to accomplish becomes second nature, easily finished in hours. Silly mistakes which once took hours to pinpoint become obvious in minutes. And soon, long past the point of wanting to give up, an atom trap appears, and all the hours of effort cumulate into one euphoric moment.

Less poetically, this chapter documents general activities performed in the course of trapping atoms, as well as invaluable tips, gained through long hours of trial and error.

Building and Optimizing the System

Of course, building the apparatus took the longest time. As mentioned, we started from ground (minus) zero, and putting the system together involved much planning, design, re-design, and re-planning. But rather than become a dizzying circle of activity, our efforts were focused and coherent. Piece by piece, day by day, the system came together. We took advantage of numerous sources for supplies, including other labs in the Physics Division, who graciously lent us parts and electronics from their own resources. Moreover, the ancillary services of the electronics, machine, and glass shops were always professional, courteous, and prompt with orders.

Metastable Atom Source

Back-Discharge

Building the metastable atom source came first. A problem immediately developed: "back-discharge." Being 7" long with a high negative voltage, much of the tungsten rod was exposed to the surrounding gas. Moreover, the end of the vacuum chamber electrical feedthrough was a 5" long length of exposed stainless steel. Thus, instead of discharging in a forward direction to the metal skimmer, the discharge would often occur off the sides of the rod. We surmised that the electric field lines bent from the metal walls of the vacuum chamber around the end of the quartz tube. Apparently, the quartz tube did not adequately fulfil one of its intended functions as an insulating agent, perhaps due to the excessive amount of exposed metal. Although the effect was a lovely display of dancing purple arcs around the rod, it did nothing to create metastable atoms in a forward direction.

After some experimenting, we decided the best solution was to insulate the exposed metal by applying a ceramic paste directly on the surface. We used a particular brand of this substance, Torr-Seal®, which is applied as a pasty liquid and dries into a hard, durable ceramic. Torr-Seal® does not release gasses, as would household glues, and thus would not be detrimental to vacuum environments. Everything except the very

tip of the tungsten rod was thus coated and insulated. Moreover, to concentrate the electric field at the tip, the rod was sanded with a Dremel® tool to a needle-point sharpness.

After these improvements, a nice forward discharge could finally be maintained.

Optimal Source Pressure and Voltage

Much time and effort went into finding the pressure and voltage for producing the best metastable flux. The pressure of the gas source chamber was the easiest to monitor, since it was at relatively high pressure, and the gauge responded more quickly to changes in the intake valve settings. Generally, higher pressures resulted in higher metastable flux. For instance, at a source pressure of 2.04 T, the measured flux current (by the Faraday Cup Detector) was 43 pA. As the pressure went down to 1.66 T, the flux current likewise diminished to 36 pA. (The voltage was held constant at -1000V in this case). However, the discharge would extinguish naturally at pressures higher than 8 T or lower than 1.5 T, depending on the voltage supplied. Higher pressures were found to result in other problems, such as fast sputter coating (to be explained below), or difficulty in maintaining low vacuum conditions in the trapping chamber itself.

The other parameter we could adjust was the source voltage applied by the voltage supply. Higher source voltage resulted in higher flux. At -1000V, the flux current was 53 pA, while at -550V, the flux current dropped to 41 pA, with an approximate linear relationship between the source voltage and flux current in between. (Here, the source pressure was held constant at 2.2 T). The problem with high voltage, however, is that it increases the velocity of the atoms coming out of the source. Using fluorescence spectroscopy, we were able to measure the velocity of the atoms coming out of the source as we changed the source voltage. At -1000V, the velocity was 658 m/s. However, at -644V, the velocity was only 390 m/s. Faster atoms require more distance to decelerate. The expected velocity is an important consideration when designing the length of the system, especially for the Zeeman slower. Thus, even though the flux is greater when the source voltage is high, we do not want to build a system which extend into the hallway! We needed to find a happy medium.

After much experimentation, we found that the optimal pressure and voltage conditions were 2 to 3 T, and 450 to 600 V. Given these settings, the current across the discharge (not to be confused with the flux current) was 1 to 2 mA. The metastable atom flux, then, is on the order of 1×10^{13} , as calculated in Chapter 6.

Sputter Coating

After approximately 50 hours of use, however, the inner surface of the quartz tube becomes noticeably darkened. The ionized gas atoms apparently sputters the glass surface with tungsten atoms. Not only does this constrict the tip opening and impede gas flow out of the tube, it also allows electric field lines to exist between the rod and the now metallic glass surface. This makes starting the discharge more difficult, and back-discharge reappears as a problem.

To remove the tungsten coating from the inner surface of the quartz tube, the chamber housing the tube must be removed from the rest of the system and then the tube itself removed from the chamber. (This is an instance when regular maintenance on the

front half of the apparatus does not have to affect the vacuum conditions in the trapping half. To work on the quartz tube, we must of course destroy the vacuum in the first few chambers. But by shutting the gate valve and closing the valves to the first three turbopumps, we can effectively isolate the trapping chamber, and keep the last turbopump and roughing pump running. Thus, the high vacuum in the trapping chamber is preserved.)

Removing Sputter Coating

By far the easiest way to clean the tube is simply to immerse the tip in a small beaker containing a base solution, such as ammonium hydroxide or potassium hydroxide. Then, set the beaker in an ultrasound vibrator. After a few minutes, all the tungsten will be dissolved, and the quartz tube will look like new.

Optimal Spacing of Tip to Skimmer

When replacing the quartz tube back inside its chamber, position it approximately 1 cm from the metal skimmer. If it is too much closer or farther, the metastable flux diminishes. For instance, if the tube opening is placed right up next to the skimmer, or if it is about 2 cm apart, the flux diminishes by roughly one-half.

Skimmer Centering

Not only should the distance between the quartz tube and skimmer be of concern, but the skimmer opening must be centered on the tube opening. This allows the atomic beam to flow unimpeded directly ahead, through the skimmer, and into the rest of the apparatus. If the tube tip and skimmer are not centered, a significant fraction of the atomic beam may be lost, and the metastable flux in the trapping region diminished.

The quartz tube is held in place by a compression port adapter, allowing it to be easily removed and inserted between two vacuum chambers. Thus, it has no permanent, fixed position. Every time the tube is removed for cleaning or other work, the tube is replaced in a slightly different position. Because of the geometry of the vacuum chamber, centering the tube itself on a fixed skimmer would not be practical. Instead, by mounting the skimmer in between two metal rings of metal, as described in the previous chapter, the position of the skimmer itself is flexible, and it can be centered on the quartz tube tip.

To accomplish this, tighten the compression port adapter ring to fix the quartz tube in place after making sure the distance between the tip and the skimmer is approximately 1 cm. Connect the discharge source chamber (DSC) and skimmer chamber, using a rubber gasket. On the side of the skimmer chamber, loosen the three screws. This frees the skimmer from between the two metal rings. Using a lens of appropriate focal length to better image the tube tip, look into the skimmer chamber at the hole in the skimmer. Move the skimmer so that the tube tip is directly centered in the skimmer opening. Shining a light into a port in the DSC helps illuminate the tube tip for

better visualization. Also, beware of the effects of parallax in finding the truly centered position.

Finally, tighten the three screws gradually to fix the skimmer in place. Excessive tightening of one screw at one time may shift the skimmer position, so tightening each screw a little bit each time around a circuit helps maintain the centered condition. Recheck that the skimmer is centered after tightening the screws.

Collimator Centering

The 3 mm hole in the center of the solid copper gasket connecting the gate valve and shutter acts as a collimator for the atomic beam. Just as centering the skimmer is important to maximize the atomic flux, making sure that the collimator is centered is also important. However, because the copper gasket is used to provide a sure vacuum seal between flanges, it is permanently fixed in place. No easy way of adjusting its position exists.

Fortunately, some freedom of motion exists for the entire last half of the apparatus. Because the Zeeman-tuned slower consists of a very long vacuum pipe, with the source chambers (DSC, skimmer, transition, gate valve, shutter) on one end and the trapping chamber on the other, either chamber can be nudged left or right with respect to the other. Furthermore, the source chambers are supported by Uni-Strut® with special, adjustable feet. Turning a nut raises or lowers the foot, and so the apparatus can also be adjusted vertically to center the collimator.

In practice, centering the collimator involves looking into the atomic beam from the window port of the trapping chamber through which the slowing beam is normally directed. Naturally, when looking in such a manner, removing the mirror that is ordinarily positioned outside the window port for the slowing beam is necessary. The purple glow of the discharge appears as a small, bright dot in the distance. Moving your head side to side as well as up and down, the dot disappears after certain points. Where it disappears indicates the edges of the collimator hole. Thus, if the dot appears in a region centered in the visual field of the chamber walls, the collimator is correctly in line with the quartz tube tip and skimmer opening. On the other hand, if the dot appears in a region too far right, left, up, or down, appropriate adjustments need to be made by moving either the source chambers or the trapping chamber. This alignment is best done by at least two people, since the apparatus weighs a lot.

Laser Beams Alignment

The only thing necessary to align the laser beams is a whole lot of patience. These tricks of the trade might also help ...

Main Beam Collimator

All the laser beams come from one main beam, the one coming from the Ti:Sapphire ring laser. If the main beam shifts in position, every subsequent beam moves. This may happen when we adjust the mirrors in the ring laser to maximize power output, or when we accidentally bump a mirror on the optics table. Thus, after every

beam is directed exactly where it is suppose to go, set two small apertures near the source of the main beam. Since two points determine a line, the apertures function as collimating reference points. Aiming the main beam through the two apertures ensures that the rest of the beams will be properly aligned.

Waxed Mirror Mounts

Use wax to stick mirrors on mirror mounts if the mirror needs to jut out beyond the border of the mount. For instance, most mirror mounts have a cavity in which the mirror is suppose to be placed. However, around the cavity are wide boarders, which make up the bulk of the face of the mount. Sometimes, we need to split a very close pair of laser beams, allowing one to continue straight ahead, while deflecting one at an angle to its original path. The boarders of the mount are so wide that they prohibit such selective reflection.

Instead of securing the mirror inside the cavity, we apply some wax onto the border close to one edge, place the entire mirror mount over a heat gun until the wax melts, and then stick the mirror on the melted wax such that one part of the mirror extends beyond the edges of the mount. The mount is allowed to cool, after which the mirror is firmly stuck. In this way, we can edge the mirror just enough into the path of one of the laser beams to deflect it, while leaving the other one undisturbed.

Using Reference Beams

The wavemeter based on Michelson's interferometer is invaluable in providing an approximation of the laser beam's wavelength. Although not calibrated accurately enough to directly use to lock the laser wavelength at the atomic resonance frequency, it is reliable to 0.1 nm. Tuning the ring laser to 811.7 nm as monitored on the wavemeter, then, brings the beam close to the atomic resonance frequency, and finding the absorption signal becomes much easier.

For the wavemeter to work, one branch of the laser beam needs to be carefully directed into the input port. The alignment is crucial. To help, a reference laser beam shines out of the port as well. By overlapping the reference beam from the wavemeter and the laser beam from the ring laser, proper alignment is achieved. Improper alignment is indicated by a flashing "Low Input" signal on the wavemeter's front panel.

To align the beams properly, position a mirror just outside of the input port in such a way that a beam can be later deflected into the port. Use another mirror to deflect the ring laser beam onto the first mirror, and adjust both mirrors so that the ring laser beam roughly enters the input port. The reference laser beam from the wavemeter will be naturally deflected back toward the second mirror. Using an IR viewer, both beams will make bright images on the surface of the mirrors. Looking at the second mirror, adjust the first mirror so that the image of the reference beam overlaps with the image of the ring laser beam. Then, looking back at the first mirror, adjust the second mirror to overlap the two laser beams. Go back to the second mirror; the images of the beams may have parted, but the separation should be less than the first time. Repeat the overlapping adjustments going back and forth between the two mirrors as often as necessary.

Eventually, both beams will overlap exactly, and the "Low Input" signal on the panel of the wavemeter will stop flashing, indicating that it is properly receiving the ring laser beam. The alignment may be so good that the "High Input" signal starts to flash. In this case, use the aperture arm on the wavemeter to attenuate the input level.

Pump and Probe Beams

Saturated absorption spectroscopy is used to better find the atomic resonance frequency. As will be discussed in Appendix 1, an additional beam is used in the saturated absorption method in contrast to a single beam in normal absorption spectroscopy. Normal absorption spectroscopy suffers from Doppler broadening, which obscures the true resonance frequency. The probe beam is the same as that used in regular absorption spectroscopy and the one we monitor via the photodetector. The pump beam travels in the opposite direction as the probe beam, and its function is simply to compete with the probe beam in exciting atoms. This way, at the true resonance frequency, the probe beam has fewer atoms to excite, and thus the absorption signal will rise a little bit at that point. This appears as a little blip in the center of the oscilloscope trace, and indicates the atomic resonance frequency much more clearly.

Ideally, the pump and probe beams exactly overlap as they counterpropagate. However, simply crossing the two beams is sufficient to produce the desired effect. This takes much less time to align. Looking at one end of the glass cell in the saturated absorption setup, adjust the mirrors to bring the two beams to the same vertical height. Of course, this height must be such that the beams enter and leave the glass cell. Turning the mirror mount tuning knobs, bring the two beams close to each other, side by side, edges touching. Know which beam is the pump or probe beam, for example, the pump beam on the right, and the probe on the left. Now, find the image of the beams on the other end of the glass cell. Adjust the mirrors so that the images of the two beams swap positions, for instance, the probe beam is now on the right, and the pump on the left. Going back and forth between the two ends of the glass cell may be needed to insure proper beam positioning.

Thus, when the images of the beams change horizontal positions at the two ends of the glass cell, the beams must cross paths somewhere in the cell. The pump beam will then effectively compete with the probe beam for atoms, and the alignment objective is achieved. Fine tuning the mirrors by maximizing the real-time trace on the oscilloscope may produce a better saturated absorption signal.

The relative intensities of the two beams are also important. The pump beam should be at least 10 times greater than the probe beam. With the attenuator in front of the saturated absorption glass cell, the intensity of the probe beam can be decreased while monitoring the response on the oscilloscope screen. Thus, maximizing the saturated absorption signal is visually direct and straightforward.

Beam Expander

The size of the laser beam when it emerges from the Ti:Sapphire laser is only 1 mm in diameter. If the beam is used at this small size, not only would the trapping region be very small, but heroic efforts would be needed to align the subsequent trapping,

slowing, and atomic beams. To make life easier, and to produce a larger trap region, the main beam is expanded to 3 cm in diameter. This virtually fills the extent of the vacuum chamber ports, enlarging the trapping region, and minimizing alignment efforts. If the beam were much bigger, glare off the sides of the chamber walls would become a limiting problem.

To expand the main laser beam to form the trapping beams, simply shine it through two lenses, the first lens having a smaller focal length than the second. The lenses are placed at a distance equal to the sum of their focal lengths apart. This is because the image of the first lens is found at the focal length of the first lens. (We consider the laser beam coming from infinity, so that the object distance of the first lens is infinite.) The image of the first lens becomes the object for the second lens, and we want the final image of the second lens to be at infinity, that is, what emerges through the beam expander should not be focused. Thus, the second lens must be placed at a distance equal to the second lens' focal length from the image of the first lens. Thus, the length between the two lenses is simply the sum of their focal lengths.

With this geometry, the ratio of the second lens' focal length to the first's is the magnification factor. So, if the second lens had a focal length of 16" and the first, 1", then the beam will be enlarged by a factor of 16.

In practice, we do not know the focal lengths of the lenses with great accuracy. Thus, simply measuring out the separation distance between the two lenses with a ruler may not be the best way to properly place them. Instead, place a card a few centimeters from the second lens and measure the diameter of the final beam's image on the card. Now, place the card at a very great distance (many meters, if possible) away, and measure the diameter of the beam's image. If the beam is the same size both near to and far from the beam expander, the lenses are positioned properly. If it is smaller at a great distance, the beam is being focused, and the lenses must be moved further away from each other. If the image is getting larger, then it is diverging, and the separation length between the mirrors is too great.

Focusing the Slowing Beam

The slowing beam is also expanded, but unlike the trapping beam, it is focused to a point near the tip of the quartz tube which makes up the metastable atom source. The focusing helps to push atoms toward the center of the atomic beamline, by providing components of force toward the center. Focusing also helps to optically pump the atoms into the proper quantum state, whereby the laser can most efficiently excite the atoms. The slowing beam's intensity is attenuated to 5 mW/cm².

To focus the slowing beam, measure the distance from a point P just outside the slowing beam's entrance window port on the trapping chamber to the quartz tube tip. Since we cannot effectively see the laser beam inside the chamber, we need to study it outside. Steer the laser beam past the vacuum chambers onto a nearby wall, for example. Place a piece of paper at the measured distance away from point P, and image the laser beam on it. Now, move the second lens of the beam expander towards and/or away from the first until the image of the beam on the paper is tightly focused. When the beam is redirected into the chamber towards the atomic source, it will be focused correctly.

Centering of Retro-Trapping Beams

The three pairs of trapping beams need to cross in the center of the trapping chamber to trap atoms there. Aligning these beams is obviously important. If one beam does not intersect the others, the scattering forces are unbalanced, and the atoms will be pushed out of the trap.

A convenient way to center the entering beams (the three beams first entering the trapping chamber) is to center their images in the entrance window ports as well as the opposite exit ports. The symmetry of the chamber geometry assures the beams will cross through the center.

The three beams then are reflected back on themselves, the so-called "retro-beams". Centering them is easily accomplished using a clever trick. Punch a pinhole in a card. Darken the area around the hole with something like black, permanent marker. Hold the card in front of the entering beam before it enters the trapping chamber in such a way as to allow the beam to pass through the pinhole. Basically, the pinhole acts like a small aperture at this point. Now, the retro-beam will be reflected back on the card as a pinhole sized image. Adjust the retro-beam's mirror so that the image is centered in the actual pinhole. Since the original beam came through the pinhole on its way to the trapping chamber, and the retro-beam is directed back in the pinhole on its way out, the two beams are truly overlapping and centered.

The trapping beams' intensities are around 10-20 mW/cm². See Table 4-1 for specific values of each beam.

Deflection Angle

Proper polarization of the laser beams is crucial for the magneto-optical trap (MOT) to work. To produce a position-dependent force, the entering beams must be circularly polarized in one direction, and the retro-beams the opposite direction. The beams are circularly polarized using quarter-wave plates set at 45° to the linear polarization of the original laser beam. When the main laser beam exits the ring laser, it is linearly polarized in the vertical direction. In order for the quarter-wave plates to definitely produce circularly polarized light, the light passing through them must be linearly polarized. Thus, the original beam's linear polarization must be preserved throughout the optical path from the ring laser to the quarter-wave plates in order for the trapping beams to be properly circularly polarized.

The vertical polarization of the main laser beam is preserved only if it is always reflected in the plane defined by both the original beam and the reflected beam, or at right angles to that plane. To better visualize this, consider that the surface of the laser table forms a horizontal plane. The main laser beam exits the laser a few centimeters above the laser table. As long as the laser beam is reflected in this plane, a few centimeters above and parallel to the surface of the laser table, the laser beam's vertical polarization is preserved. Or, a mirror may reflect the beam at 90° straight up out of the original plane, and another mirror may reflect this beam at 90° back into a plane parallel to the first, but some vertical distance above it. (We employ this strategy to form the vertical trapping beam, which must be reflected into a position as to propagate vertically through

the trapping chamber.) These beams are still linearly polarized. However, if the beam is deflected at an arbitrary angle out of the horizontal plane, then the polarization becomes arbitrary. A quarter-wave plate cannot circularly polarize a beam of arbitrary polarization.

A practical exception occurs if the pitch of the deflection out of the horizontal plane is slight. For instance, if the laser beam is originally at 5 cm above the laser table surface, and we need to reflect it to a point 6 cm above the table, as long as the distance in which this vertical change occurs is large, say 1 m, then the linear polarization of the original beam is basically preserved. It may not be perfectly linear, but it is adequate for the quarter-wave plates to fulfil its intended function. In fact the setting on a quarter-wave plate is very forgiving, allowing a +/- 10° deviation from the ideal 45°.

Proper Quarter-Wave Plate Setting

Although the quarter-wave plate does not have to be set exactly at 45°, it does need to be set in the correct direction (clockwise vs. counterclockwise) to produce the proper sense of circular polarization. Which way depends on the direction of the MOT fields. This is so important and so often the cause of failing to trap that it bears repeating. In our setup, if the MOT magnetic field in the vertical direction is away from the center of the trap, and in the horizontal direction the field is pointing in towards the trap, then all the quarter-wave plates for the beams are set with the fast-axis of polarization 45 degrees *clockwise* to the vertical. Note, though, because of the B-field direction, the quarter-wave plate in front of the top vertical beam is set at with the fast-axis 45 degrees counter-clockwise to the vertical. To positively determine the nature of the MOT field, a Gauss-meter can be used.

Operating the System to Trap Atoms

The moment has arrived. The atomic beam line is precisely centered. All the pumps on the vacuum system have been pumping down the chambers for at least several days and a vacuum of 10^{-9} exists in the trapping chamber. The optics are perfectly positioned and sparkling clean. We are eager to trap. And from here, with the system completely off, the following procedures require only 30 to 45 minutes to actually getting a trap. Of course, that's only if everything works perfectly. But even if it does not, we always eventually get our trap. Call it blind faith in our abilities, or at least in the laws of physics. Or just plain stubborn persistence. But we always get our trap.

Preparatory Activities

The first orders of business are rather mundane:

- turn on the gas supply
- turn on all the electronics (ring laser controller, oscilloscopes, wavemeter, NIM power supply, etc.)
- turn on the water cooler for the ring laser
- open the laboratory cooling water supply valves
- turn on the Argon-ion laser

Maximize Laser Outputs

For the Argon-ion laser, adjust the controls for an output of around 15 W.

For the Ti:Sapphire ring laser, place a power detector in the path of the exiting main beam. Use an attenuator (1000:1) on the detector. Adjust appropriate mirrors in the Ti:Sapphire ring laser to maximize power output (around 1 W). If the maximum power is substantially lower than this, the optical elements in the ring laser may need to be cleaned.

Check Laser Beams Alignment

Survey the laser beams. Make sure the trapping and slowing beams are centered in the trapping chamber window ports, in the photodiode of the detector in the saturated absorption setup, and in the wavemeter input port. If gross misalignment is found, adjust the very first two mirrors right after the ring laser so that the beam goes through the two collimating apertures set up for this purpose. All beams should move together and become correctly positioned if the main beam is collimated. If certain beams are still misaligned, an optical element on the table must have been accidentally bumped. Remedy this patiently.

Rough Tune the Ring Laser

On the ring laser, zero the offset frequency. Monitoring the wavelength display of the wavemeter, adjust the small etalon controller knob on the ring laser so that the wavemeter reads 811.756 nm. If adjusting the small etalon control is not enough to get this wavelength, carefully turn the large etalon knob on the ring laser to grossly change the wavelength into the desired range. Then go back to the small etalon knob to make fine adjustments.

Get the Saturated Absorption Spectrum

Above the separate vacuum chamber setup for saturated absorption spectroscopy, two pieces of electronic equipment rest on the laser table shelf. One is a signal generator. Turn it on and tune it to about 150 MHz. The other is an RF amplifier; turn this on, too. The argon in the glass cell should immediately begin to glow bright purple, indicating ionization. If not, check the position of the RF can, which should be centered over the glass tube. Also, check that the gain on the signal generator is turned up to the maximum. The pressure in the glass cell should be between 0.5 and 1 mT.

Once the discharge starts, monitor the photodetector signal on the small oscilloscope. Make sure the signal is not saturated, that is, it does not exceed about 12 V or 15 V, depending on which was selected on the NIM power supply. (A saturated signal appears flat and does not go higher than a maximum value (12 or 15 V), like when the water level in an enclosed aquarium reaches its maximum height..

Once a steady discharge is achieved, go back to the ring laser controller. Two sets of number dials are on the face. One specifies the scan range, that is, how broad is the frequency scan of the laser. The other adjusts the frequency offset, useful to center the absorption signal. Begin scanning the ring laser by turning the appropriate control knob to "Internal Frequency Scan". Enter 5 GHz (or thereabouts) for the scan range. The offset frequency should already be set at 0, from the last step. If everything is set up correctly, a saturated absorption signal should immediately become obvious on the oscilloscope. If not, widen the scan range or change the offset to find it. If either control needs excessively large values (>10 GHz) to find the signal, the rough tuning procedure may need to be attempted again.

On the oscilloscope, make sure the entire absorption spectrum is clearly visible. If the RF power is too high, if too much gas is in the cell, or if the laser beam is too intense, the bottom of the signal may disappear below the 0 voltage level. Adjust the appropriate parameters until the signal is approximately two-thirds of the range between 0 and the maximum voltage. The laser beam itself may need to be attenuated with an optical attenuator. The rotatable glass disks with gradually darkening shades is especially useful, since a continuous choice of variation of attenuation is available.

Once a good signal is found, gradually decrease the scan width to focus in on the smaller saturated absorption peak in the middle of the broader absorption dip. Changing the offset frequency will move the entire silhouette of the oscilloscope trace horizontally, thus allowing centering of the signal. Centering in this manner is crucial, since the scan range occurs symmetrically about the center of the specified frequency range. Thus, decreasing the scan range will focus in on the center of the scan. Keeping the saturated absorption peak in the center of the scan facilitates zooming in on the peak. Continue zooming in, until the scan range is approximately 0.010 GHz (10 MHz). Only the saturated absorption peak should be visible on the screen.

Finding the saturated absorption signal assures us the laser is tuned tightly on the atomic resonance frequency of the noble gas of interest. This is the same laser beam that will slow and trap the atoms in the main vacuum chambers. We're closer than ever to trapping!

Start the DC Discharge

Close the gate valve. Using the controller for the inlet gas flow valve, allow gas to flow into the discharge source chamber until the pressure is around 2.5 – 3.0 T. The pressure in the skimmer chamber should rise in step to around 0.7 mT. Turn on the Bertan® high voltage supply. Turn the voltage control knob (which changes by increments of 500 V) to 2500 or 3000 V until the discharge from the tungsten rod to metal skimmer spontaneously starts, as easily viewed through the window port. (It *should* be that easy. The original method we used for most of the experiment involved a different power supply and "tweaking" the pressure to "jump-start" the discharge. That unit provided a maximum of 1000 V. Using the Bertan® unit with its 5000 V potential requires no special tricks. Just keep turning the voltage up until the discharge begins.)

Over time, the quartz tube becomes coated with tungsten, and starting or maintaining the discharge can become more difficult, even impossible. A good cleaning

of the tube is in order at this time, as detailed in the section on "Removing Sputter Coating" above.

Final Steps

To image the trap visually, set up the CCD camera on the observation deck, so that it looks into one of the unused window ports. Make sure the focus of the lens is set at a distance equal to the distance between the lens and the center of the chamber. This can be easily done by measuring that distance and then focusing the camera onto an object outside the chamber at that distance. Then set the camera in place.

Open the gate valve. Turn on the power supplies to the Zeeman-tuned slower and the MOT field. Set the currents on these to approximately the levels specified in Table 1. Double-check that the saturated absorption peak is still centered in the oscilloscope scan.

All that's left is to look very closely at the video monitor. The trapped atoms will fluoresce as they interact with the laser and a brilliant star-like image will shine on the monitor. If the laser is scanning, the atom trap will load and dissipate as the laser frequency is swept passed the resonance frequency. The trap will flash like a renegade pulsar with a frequency equal to how fast the laser is being swept.

Once the trap is found, we can stop sweeping the laser and lock it on a single frequency. Turn off the internal frequency scan and manually adjust the frequency using the appropriate fine-tuning control, maximizing the image of the trapped atoms on the monitor.

The various tweaking coils can now be used to center the image of the atoms on the monitor. Also, making fine adjustments on the power supplies for the Zeeman-tuned slower and MOT may help maximize the brightness of the atoms.

Electronic Measurement Setup

We are ready to quantify the results using a photodetector. The trap image will be focused by a simple lens placed near the window port, through an aperture, and into the photodiode of the home-made photodetector described in Chapter 3. The aperture helps limit scattered light and thus reduces noise. In fact, black, felt paper is used to cover the detector and surrounding optics to help minimize stray light.

To receive the maximum amount of light, the image of the trap must fall directly on the photodiode, and so the photodetector must be placed where the image is focused by the lens. Conceivably, everything can be measured out on the optical board based on mathematical calculations. However, a visual method using the CCD camera is much simpler and more direct. With the lens placed at the window port, position the camera some distance away, pointing into the port. Focus the lens until the image of the trap is clear in the monitor. Still looking in the monitor and leaving the lens' focus alone, move an aperture in the line of sight of the trap image until the aperture itself is focused. Thus, the aperture is positioned on the optical board exactly where the image of the atoms is. Secure the aperture in place to the board. Then, place the photodetector right behind the aperture. Thus, it is now positioned where the trapped atoms are focused by the lens.

The signal from the photodetector is displayed on an oscilloscope. The fluorescence of the trapped atoms is registered as peaks in the oscilloscope trace. By

considering various factors such as the solid angle from the source to the photodetector, the conversion and amplification of the electronics, and the energy of the photons involved, we convert the measured voltage into the number of atoms in the trap.

General Thoughts and Words of Wisdom

Working with optics, putting together vacuum chambers, connecting miles of cables and leads requires a gentle touch, thoughtful planning, and infinite patience. Often, individual segments of the system, whether vacuum or optical, must be removed, reconsidered, and reinserted. Often, troubleshooting takes as much time, even more thought, and a good dose of humility, as the actual cause of the problem is usually, for lack of a better word, stupid. The fruit of the process, though, is more maturity and even flashes of wisdom.

Some final tidbits:

- Use only the highest grade alcohol and acetone for optics cleaning.
- Take advantage of every resource of tools, supplies, materials, knowledge.
- Safety first: wear protective gear when needed (goggles, gloves).
- Shield any exposed rotating blade, such as in a fan. Otherwise, it *will* cut you!
- Keep your head above the level of the laser beams.
- Remember to press the interlock release when the red warning light flashes.
- Torr-Seal® can be used to fix anything.
- The Dremel® tool can cut anything.
- Call equipment manufacturers for help whenever needed.

Table 4-1 summarizes the optimal system parameters for trapping.

Table 4-1
Optimum System Parameters for Trapping

<u>Parameter</u>	<u>Value</u>	
Pressure		
Discharge Source Chamber	1.93 T	
Skimmer Chamber	0.75 mT	
Transition Chamber	8.4×10^{-6} T	
Trapping Chamber	8.0×10^{-8} T	
Saturated Absorption Cell	0.5-1.0 mT	
Discharge Source		
Voltage	2000 V	
Current	2.0 mA	
Power Supplies to Coil Windings		
MOT	6.3 V	15.3 A
Zeeman-Tuned Slower (Foundation)	9.0 V	12.0 A
Zeeman-Tuned Slower (2 nd ary Layer)	10 V	22.0 A
Transition Layer	< 1 V	3.5 A
End Solenoid	~ 1 V	8.0 A
Counter Coil	< 1 V	3.98 A
Top Tweaking Coil	6.0 V	> 2 A (overscale)
Horizontal Tweaking Coil	0 V	0 A
MOT Magnetic Field		
Vertical direction	pointing away from center	
Horizontal direction	pointing toward center	
Quarter-Wave Plate Settings		
Horizontal and Slowing Beams	fast-axis 1/4 turn clockwise from vertical	
Vertical Beam	fast-axis 1/4 turn counter-clockwise from vertical	
Argon Ion Laser		
Current	35.6 A	
Power	13.87 W	
Ring Laser		
Wavelength (according to wavemeter)	811.756 nm	
Intensities of Laser Beams		
#1 Horizontal Trapping Beam	19.1 mW/cm ²	
#2 Horizontal Trapping Beam	12.7 mW/cm ²	
Vertical Trapping Beam	20.4 mW/cm ²	
Slowing Beam	5.1 mW/cm ²	

CHAPTER 5

THE ZEEMAN TUNED SLOWER

In our experiment, metastable atoms are produced from a relatively "hot" source, a discharge from a negatively charged (-500 V) tungsten rod. These atoms leave the source at about 500 m/s, as measured by fluorescence spectroscopy. By the time the atoms are trapped, their velocities are nearly zero. Thus, the atoms experience deceleration. What causes the deceleration, of course, is the longitudinal laser beam shining against the atom's direction of motion.

Basic Theory

A problem naturally arises. In order for the laser beam to decelerate an atom, the laser frequency (f_L) must be at the atomic resonance frequency (f_R). If an atom was stationary to begin with, we would simply tune the laser to exactly f_R and the atom would be in resonance. However, because an atom leaving the source has a velocity v , it sees f_L Doppler shifted by

$$+\Delta f_D = (v/c) f_L \quad (5-1)$$

To compensate, we can tune the laser to a frequency lower than f_R , so that

$$f_L = f_R - \Delta f_D. \quad (5-2)$$

Thus, the atom "thinks" the laser is really at f_R , resonates with it, and is decelerated by it. But once this happens, the atom slows down slightly, the Doppler shift decreases accordingly, and the atom no longer resonates with the laser, because f_L does not appear to equal f_R anymore. The atom is no longer affected by the laser, does not continue to decelerate, and ultimately will not be trapped.

Somehow we need to match the atom's decreasing velocity every step of the way from the source to the trap, from 500 to 0 m/s, always making f_L appear to be f_R to the atom, that is, to compensate for the changing Doppler shift. The atom is then constantly in resonance with the laser, experiences a uniform deceleration throughout its propagation, and will be trapped in the end. Two methods have been developed to do this: laser frequency chirping and Zeeman tuned slowing.

Laser frequency chirping (Phillips, 1988, p. 880) involves rapidly sweeping the longitudinal laser beam over a frequency range. Thus, many frequencies are available to the atom, as the laser is being swept (chirped) through a range of frequencies. As the atom slows down and the Doppler shift decreases, the atom needs to see a lower laser frequency for resonance. Chirping the laser, then, presents the atom with the frequencies necessary to keep the atom in resonance as its velocity decreases. The pulsed operation of this method, though, is inefficient (Barrett, 1991, p. p.3483)

Another method utilizes the Zeeman effect, the shifting of an atom's energy levels in the presence of a magnetic field B . Not only does Zeeman tuned slowing compensate for the changing Doppler shift, it also prevents a phenomenon called "optical pumping"

(Phillips, 1988, p.879). Briefly, optical pumping occurs when electrons "leak" into inaccessible states. The atom is no longer able to resonate with photons, and cooling stops. However, an applied magnetic field splits the normal energy levels, decreasing the likelihood that optical pumping will take place, and allows the atom to continue resonating with the laser. This, along with solving the problem of constantly changing Doppler shifts, makes Zeeman tuned slowing an integral part of the laser cooling process.

Mathematical Treatment

Let us explore in detail how the Zeeman tuned slower neutralizes the Doppler effect. We can design a system so that B decreases along the atom's propagation path. As B decreases, the resulting Zeeman shift Δf_Z also decreases, since

$$\begin{aligned}\Delta f_Z &= (\mu_A B) / h \\ &= (g_J J \mu_B B) / h\end{aligned}\quad (5-3)$$

μ_A = magnetic moment of the atom = $g_J J \mu_B$

g_J = g factor

J = total angular momentum

μ_B = Bohr magneton = 9.27×10^{-24} J/T

B = applied magnetic field strength

h = Plank's constant = 6.63×10^{-34} J*s

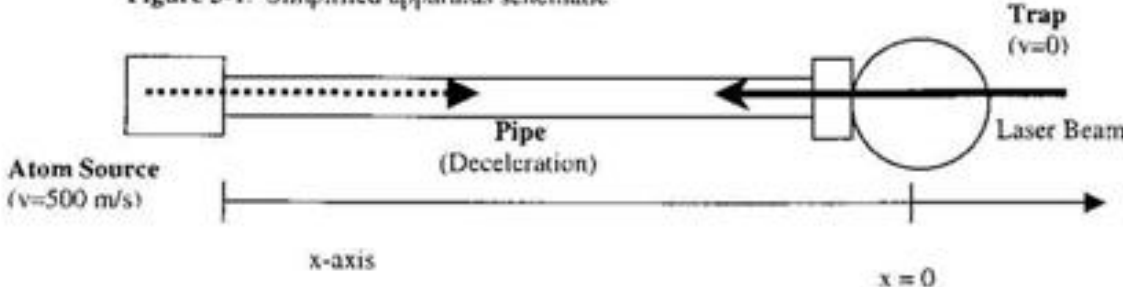
With the additional Zeeman shifting, the apparent laser frequency that the atom sees is

$$f_L = f_R - \Delta f_D + \Delta f_Z \quad (5-4)$$

Thus, if $\Delta f_Z = \Delta f_D$, that is, if the Zeeman shift exactly matches the Doppler shift, the two cancel out, and the atom always sees the laser frequency as the resonance frequency, exactly what we desire. The atom will always experience deceleration, availing itself to be trapped.

We can gain a better appreciation for the method of Zeeman tuned slowing by considering graphically the above mentioned parameters plotted as a function of the atom's position. First, consider the simplified schematic of the apparatus in Figure 5-1. An atom leaves the source at approximately 500 m/s, travels down the pipe (which we will call the x-axis), decelerates, and by the time it reaches the trap, has a final velocity close to zero. As a matter of convenience, we designate $x = 0$ as the point where the atom's velocity is zero.

Figure 5-1. Simplified apparatus schematic



If we assume the atom experiences a constant deceleration (a), then its velocity as a function of position is found from basic kinematics:

$$v(x) = (2ax)^{1/2} \quad (5-5)$$

A graph of $v(x)$ versus x is given in Figure 5-2, and a simple square root relationship can be seen.

Since the Doppler shift $\Delta f_D = (v/c) f_L$ is directly proportional to the velocity, graphing $\Delta f_D(x)$ in Figure 5-3 results in a curve identical to Figure 5-2, merely offset by some constant. Moreover, since we want the Zeeman shift Δf_Z to equal Δf_D , and since $\Delta f_Z = (\mu_A B) / h$, directly proportional to B , Figure 5-4 shows that B must fall off as the square root of position. Explicitly,

$$\begin{aligned} B &= (h \Delta f_Z) / \mu_A \\ &= (h \Delta f_D) / \mu_A \\ &= [h (v/c) f_L] / \mu_A \\ &= [h (2ax)^{1/2} f_L] / (\mu_A c) \end{aligned} \quad (5-6)$$

When B satisfies this relationship, the atom will always be in resonance with the laser and experience constant deceleration down to a final velocity of zero.

Cutoff Velocity

One of the beauties of the Zeeman tuned slowing method is that all atoms with velocities lower than a certain cutoff velocity will be slowed and brought to rest at the same final position. Consider Figure 5-5. The first curve represents how an atom (#1) with a certain velocity v_1 will slow down and come to rest at $x = 0$. However, consider another atom (#2) with a starting velocity v_2 lower than v_1 . Such an atom will not be affected by the laser at first, since the Zeeman shift (designed for the faster atom) does not cancel its Doppler shift (which is lower). Thus, #2 atom is out of resonance with the laser, and will continue travelling down the x -axis with the same velocity as it started with. (It traces out a flat, horizontal line in the graph.) However, when #2 atom reaches a certain point, it encounters a magnetic field such that the Zeeman shift induced now does cancel out the Doppler shift. That is, it has reached a position where #1 atom has slowed down to match its own speed. Now #2 atom will be affected by the laser, and will slow down in step with #1 atom. They slow down simultaneously after that point, and both come to a halt at the exact position in the end. Likewise, any other atom with a starting velocity lower than v_1 will also come to a standstill at the same position, $x = 0$.

We can also see that atoms with starting velocities higher than v_1 in Figure 5-5 will not be trapped. They will never interact with the laser, because the Zeeman shift is never large enough to cancel out the Doppler shift. Hence, v_1 is known as the *cut-off* velocity, and only atoms with velocities lower than this critical value will be trapped. From Equation 5-5, we find that the cut-off velocity is determined by "x", the stopping distance, and "a", the constant deceleration value. The stopping distance is limited by practicality.

Figure 5-2

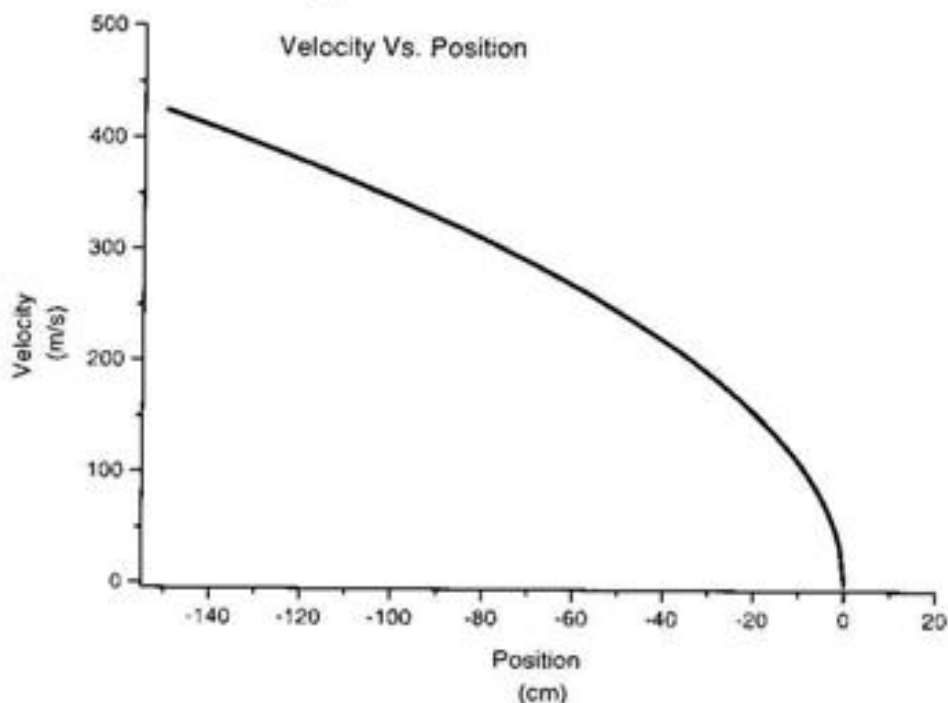


Figure 5-3

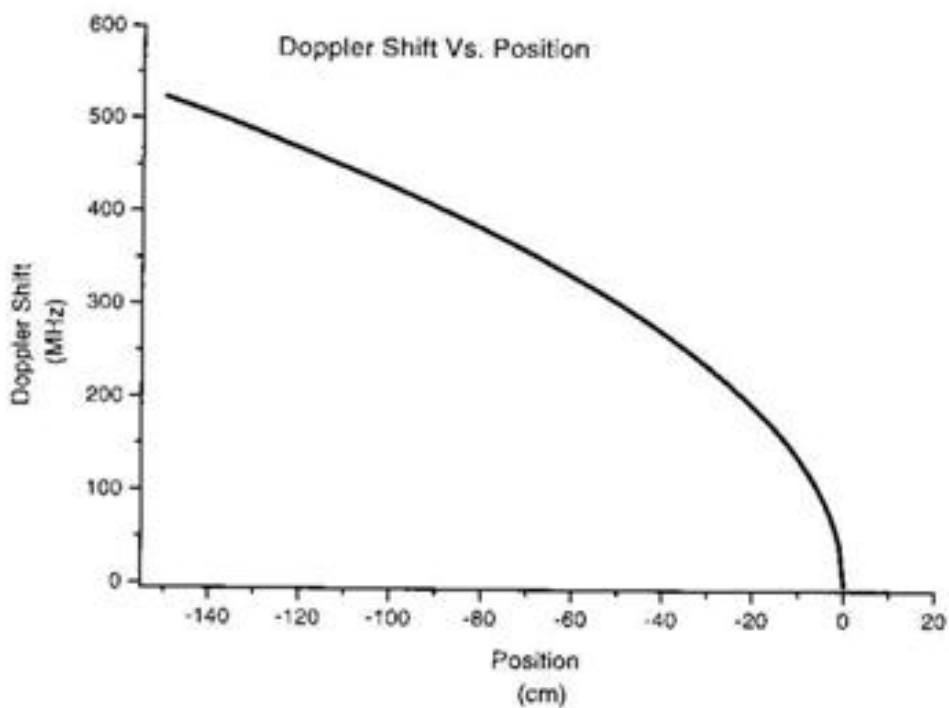


Figure 5-4

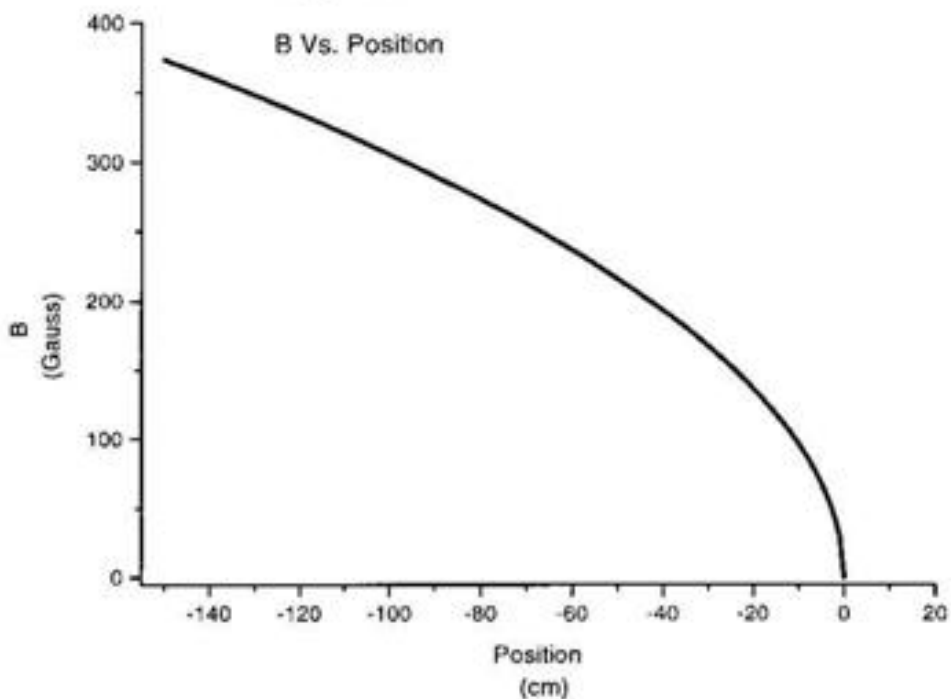
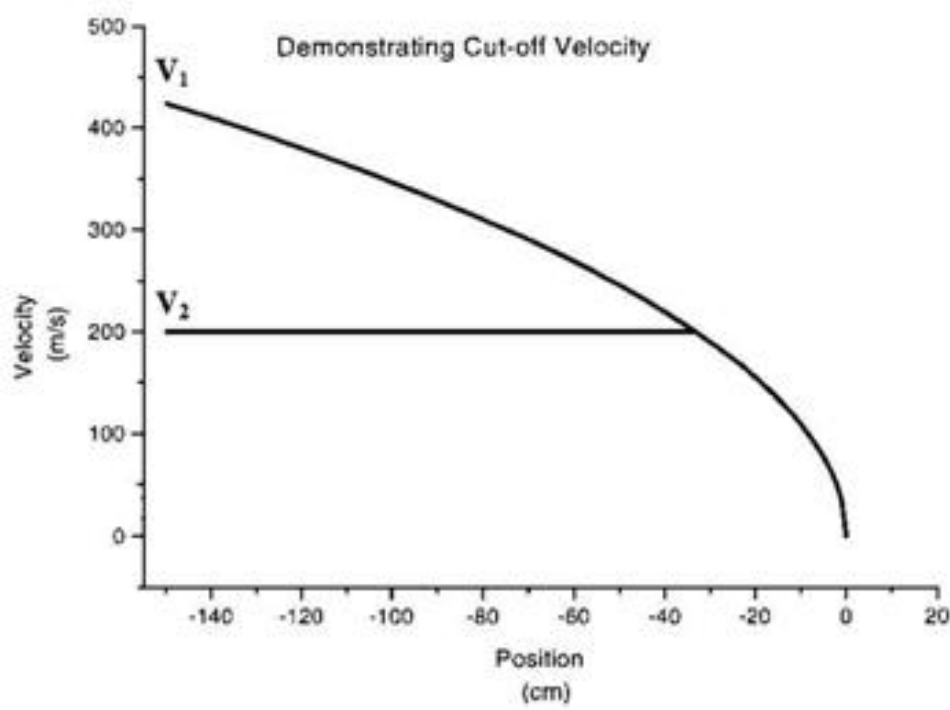


Figure 5-5



Deceleration Factor

To find the appropriate value of "a", the constant deceleration factor, we must reconsider the principles of laser cooling (Phillips, 1988, p. 239). A photon of frequency ν has momentum $h\nu/c$, which is transferred to an atom of mass M when the photon is absorbed. We can treat this as a collision, and momentum must be conserved. Thus, the atom's velocity slows down by

$$\Delta v = h\nu / Mc \quad (5-7)$$

The atom now re-emits the photon and can do so by either stimulated or spontaneous emission. In stimulated emission, the photon leaves in the same direction as it first approached the atom, and so the net momentum transferred to the atom in this mechanism is zero. However, in spontaneous emission, the photon is shot off in a random direction. Averaged over many absorption/emission cycles, the momentum changes due to spontaneous *emission* is zero. Thus, the net momentum transferred to the atom is due entirely to photon *absorption*. Since the photons are coming from only one direction, namely head-on against the atom's velocity, the cumulative effect of the momentum kicks is to slow the atom down. The faster the atom can go through the cycle of absorbing and spontaneously emitting photons, the faster it will slow down, that is, the greater the deceleration. Thus, the maximum deceleration an atom experiences during laser cooling is related to the natural lifetime of an atom's excited state, defined next.

The natural lifetime (τ_0) of an atom's excited state is simply the time needed for an atom to emit a photon spontaneously. Twice the value of τ_0 is how long it takes one complete cycle of absorption and emission of a photon between two states. We can then define $\tau = 2 \tau_0$ as the shortest time interval for this cycle.

Acceleration is simply defined as

$$a = \Delta v / \Delta t \quad (5-8)$$

Substituting Equation 7 for Δv , equating $\Delta t = \tau = 2 \tau_0$, and using $\lambda = c/\nu$, we find

$$a_{\max} = h / (2 \tau_0 M \lambda) \quad (5-9)$$

where λ is the wavelength of the atomic transition.

For krypton ($1s_5, 2p_9$), $\tau_0 = 25$ ns, $\lambda = 811$ nm, $M = 80$ amu. In this case,

$$a_{\max(Kr)} = 1.2 \times 10^5 \text{ m/s}^2 \quad (5-10)$$

This, of course, is the best deceleration we can hope to achieve. Here we assume that the atom is interacting with the photons at 100% efficiency, something which occurs only if the laser beam is infinitely intense. A more conservative value is more realistic. Specifically,

$$\tau = 2 \tau_0 [1 + (I_s/I)] \quad (5-11)$$

I_s = Saturation intensity = 2 mW/cm²

I = Actual laser intensity

(Notice that the equation properly satisfies the limiting cases. When $I = 0$, no photons exist, and τ is infinite. When I approaches infinity, the laser becomes infinitely intense, the atom attains maximum cycling efficiency, and $\tau = 2 \tau_0$.)

A realistic value of I is I_s . When $I = I_s$, $\tau = 4 \tau_o$, and it follows that

$$a_t = a_{\max} / 2 \quad (5-12)$$

Thus, for our experiment $a_t = 6 \times 10^3 \text{ m/s}^2$ is a more realistic value to use for the maximum deceleration value.

Limits of Acceleration

Another reason why we want to use a lesser deceleration value is to allow for inevitable imperfections in the actual magnetic field gradient. Ideally, we want to build a system which will provide the exact $B(x)$ vs. x curve as seen in Figure 5-4. However, the actual curve will be fluctuating about the ideal curve, as some equipment and design flaws are simply unavoidable. Assume we designed the system using a_{\max} as the deceleration value. Then, a curve similar to that depicted in Figure 5-2 shows the idealized deceleration of the atom to zero velocity, and that in Figure 5-4, pictures the idealized B gradient necessary to achieve this. If our design was indeed perfect, and Figure 5-4 was perfectly realized, then the atom will slow down exactly as portrayed in Figure 5-2. However, since such perfection is realistically unlikely, the actual B field fluctuates up and down around the ideal curve (but always hugging close to the ideal). This should translate into a velocity curve which fluctuates up and down around the ideal curve of Figure 5-2. However, a_{\max} is the maximum possible deceleration the laser can provide. Exceeding the ideal velocity curve of Figure 5-2 (as would result due to natural fluctuations in B) represents a situation where the acceleration actually exceeds a_{\max} , and the laser cannot provide enough force to keep the atom in resonance.

On the other hand, if we designed a system to provide a B field gradient associated with an acceleration well below a_{\max} , the natural fluctuations of B will translate into velocities corresponding to situations where the laser can still provide enough force to keep the atom in resonance. We are no longer "riding the edge" of the maximum deceleration. Room for error exists, since the fluctuations are well within the range of the laser's force. However, we will not be able to trap a significant portion of the atoms that are available. A lower deceleration means a lower cut-off velocity, and the faster atoms in the distribution will be lost.

In practice, a decreasing B field gradient can be designed by superposing finite solenoids of different strengths. For instance, we can start by winding a uniform solenoid as a foundational layer on the pipe. Then, in the grooves laid down by the foundational layer, we can begin to wind additional layers of wire on top. In the first 5 cm segment, we wind new wire in every groove, resulting in the greatest number of turns of wire per cm. In the next 5 cm segment, we wind a lower number of turns of wire per cm, for instance, winding every groove until the very last, which we skip. Then, in the third 5 cm segment, an even lower number, and so on. Thus, B in each 5 cm segment will become progressively weaker, and the superposition of all the fields will hopefully be more or less smoothly decreasing as dictated by Equation 5-6. A program such as MathCad is helpful in determining the specifics of the design.

Let us now consider two designs of the Zeeman slower, one which is inadequate to properly slow atoms, and another which is much better. In the inadequate slower, the

segments of differential windings are rather large, from 10 cm to over 20 cm. As a result, the B field traces out a rough curve, dropping suddenly between segments, as seen in Figure 5-6. Moreover, we can plot the acceleration corresponding to expected velocity changes versus position to examine whether it exceeds the maximum acceleration allowed by the laser. (Each point on the B field curve directly corresponds to a velocity. So, the expected B field curve is similar to the expected velocity curve. Knowing the distance between two points on the graph, then, we can calculate the expected acceleration the atoms need in order to follow the curve. If the acceleration exceeds the maximum acceleration provided by the laser, then the laser does not have enough force to slow down the atoms in the given distance, the atoms fall out of resonance from the laser forever and are no longer slowed. But if the acceleration is below the maximum, the atoms will only temporarily fall out of resonance with the laser and get back in step a little later, when the Zeeman and Doppler shifts cancel each other again. Figure 5-7 shows the expected acceleration vs. position associated with the first solenoid design. Clearly, at several points, the maximum acceleration of 1.2×10^5 m/s² is exceeded. ("Accelideal" on the vertical axis of Figure 5-7 is the acceleration used to calculate the graph, which is one-half of the maximum acceleration) Thus, this particular design is bad, and would not succeed in slowing atoms.

Now consider the results of a superior design (Figure 5-8). The segments are much smaller, about 5 cm, and the difference in the number of windings between segments is much less. Continuity of the B-field is much smoother, and the acceleration (Figure 5-9) is well below the maximum acceleration. (The end points can be ignored due to the finite nature of the solenoid. Also, because of program limitations, not all the individual segments are represented in the graph.)

Finally, Figures 5-10 and 5-11 show actual data taken from the Zeeman slower, designed for this project. Some undesirable irregularities do exist in the field, mostly during the first third of the slower. This is likely to be caused by the small differences in number of windings necessary to produce the ideal curve. Limited by the width of the wires, determining the number of windings in the first few segments was very difficult to gauge well. Practically, the roughness of the B-field means we will only trap atoms with initial velocities of around 250 m/s rather than the expected 300 m/s.

Figure 5-6. Poor Zeeman Slower Design (B vs. Position)

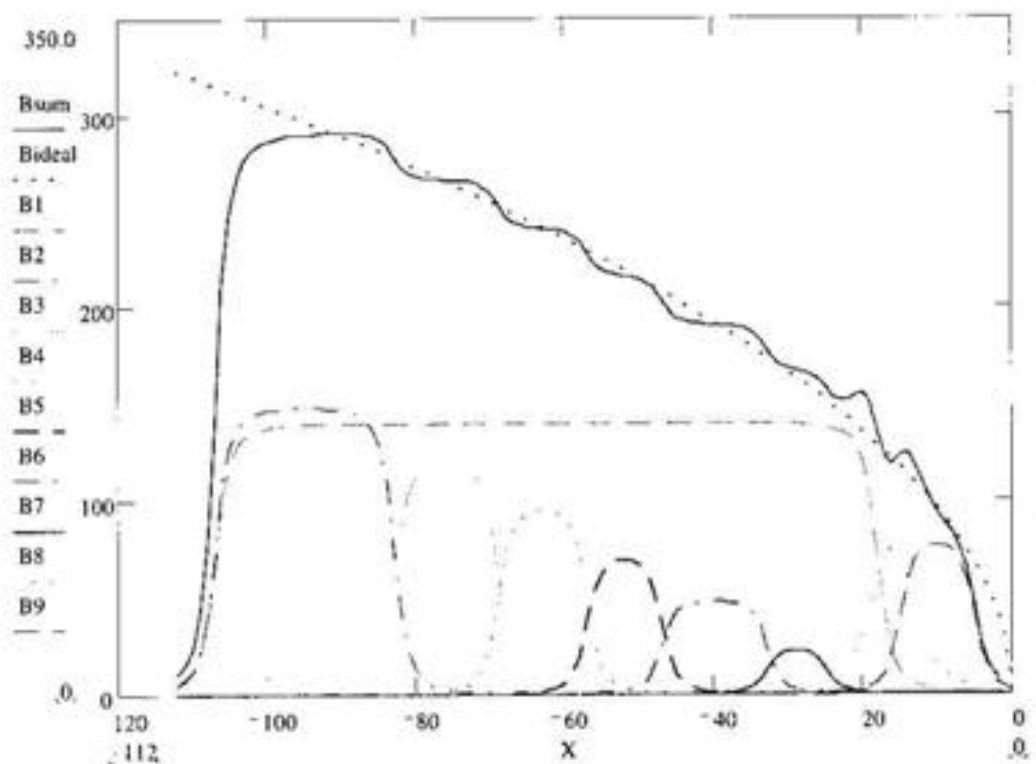


Figure 5-7 Poor Zeeman Design (Acceleration vs. Position)

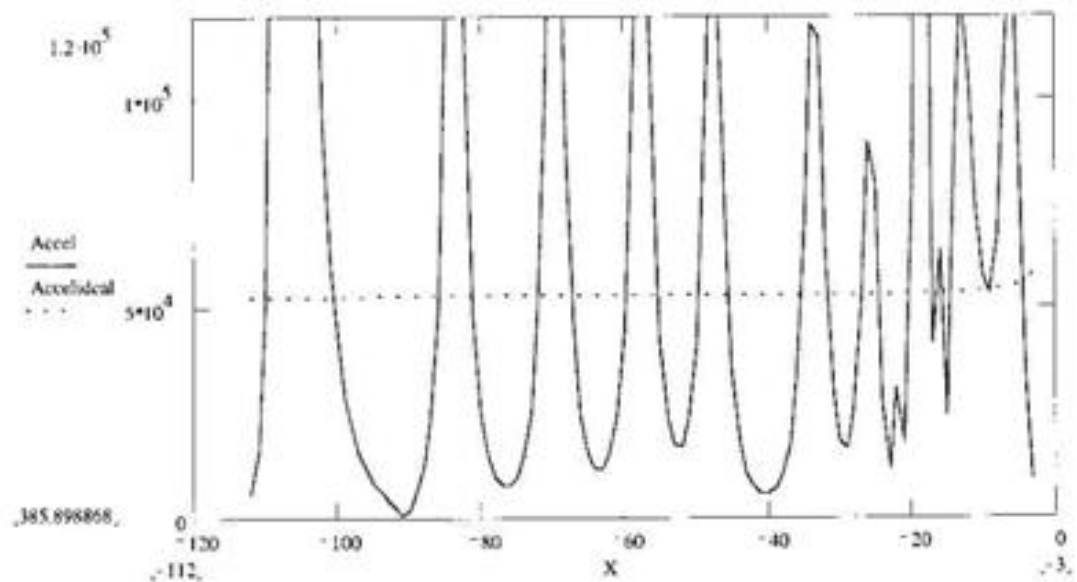


Figure 5-8 Improved Solenoid Design (B vs. Position)

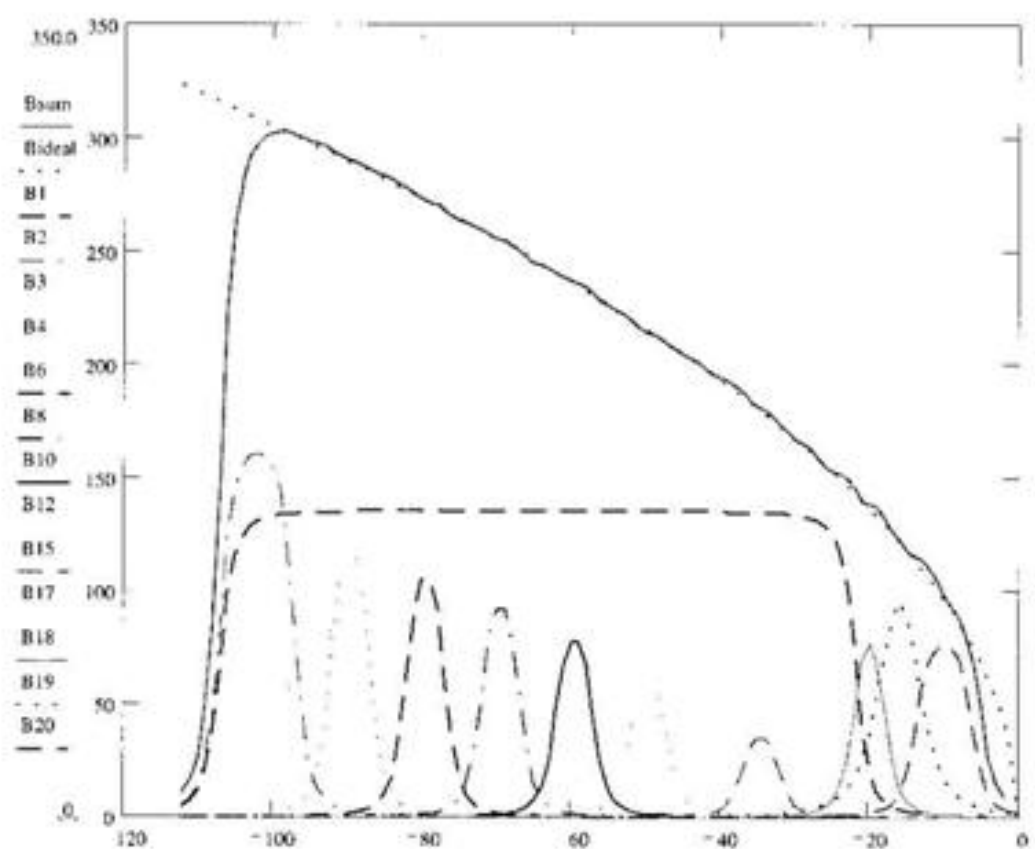


Figure 5-9 Improved Solenoid Design (Acceleration vs. Position)

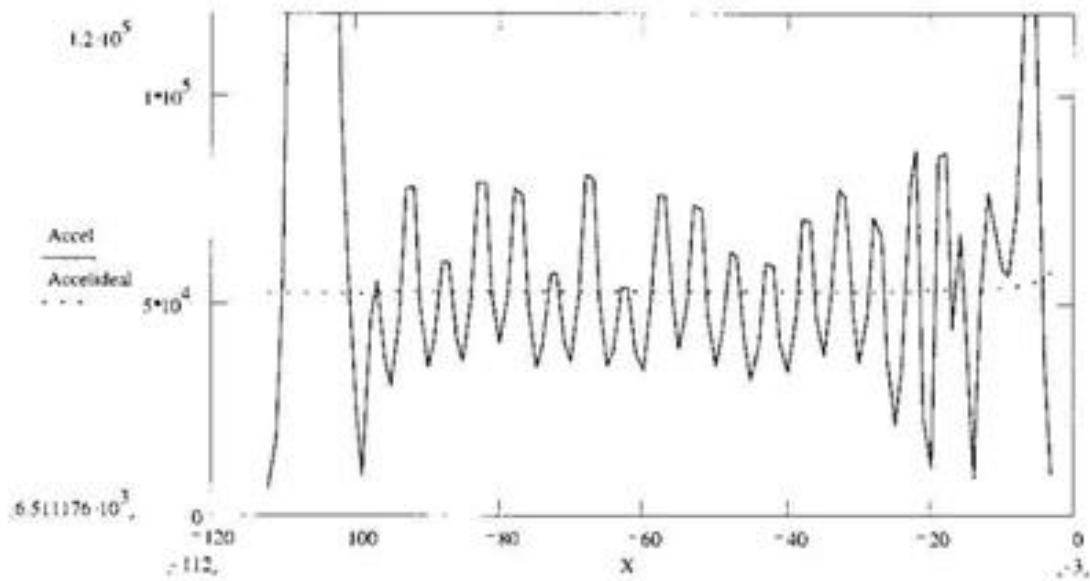


Figure 5-10 Actual Measurements from Final Zeeman Slower

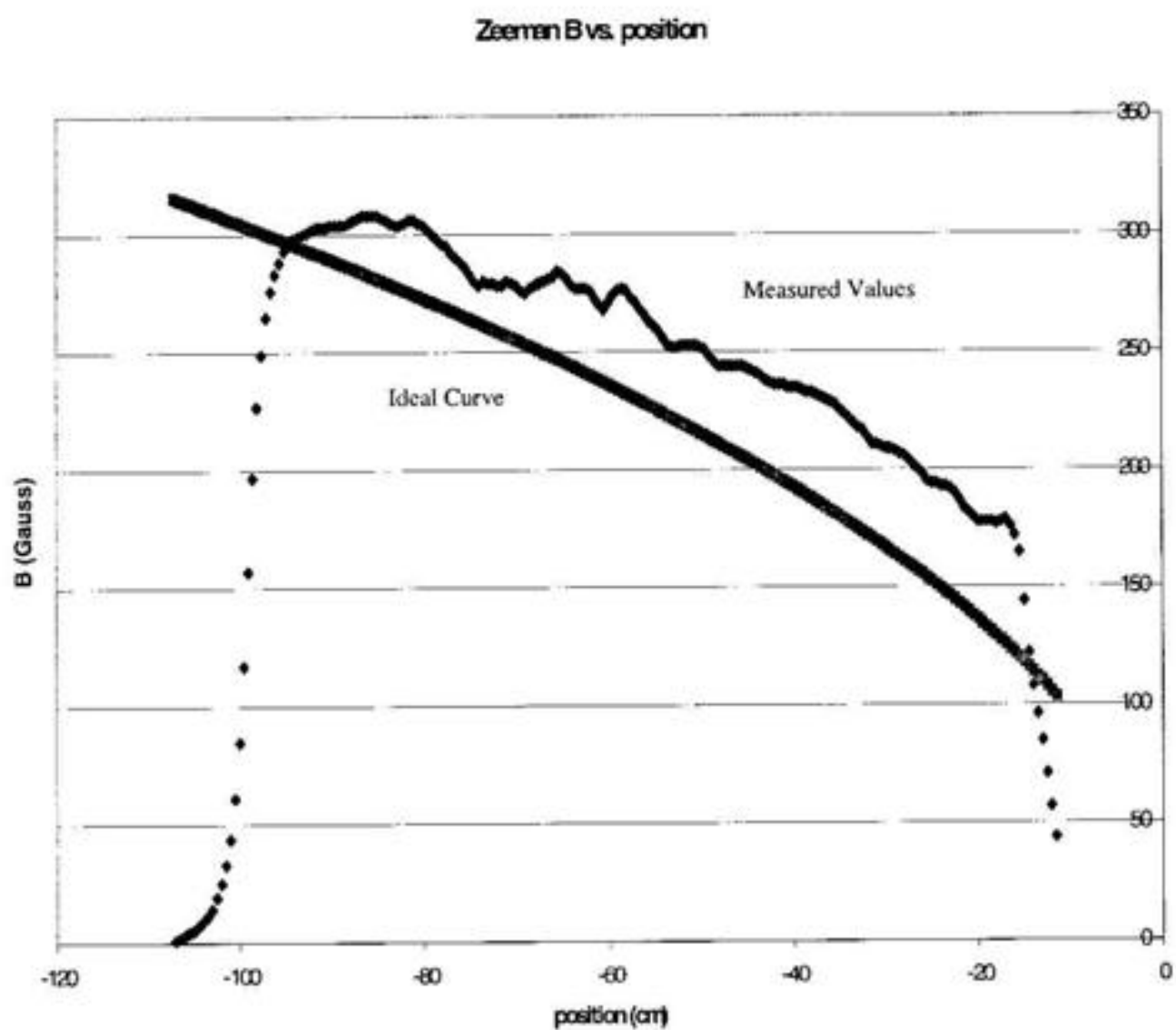
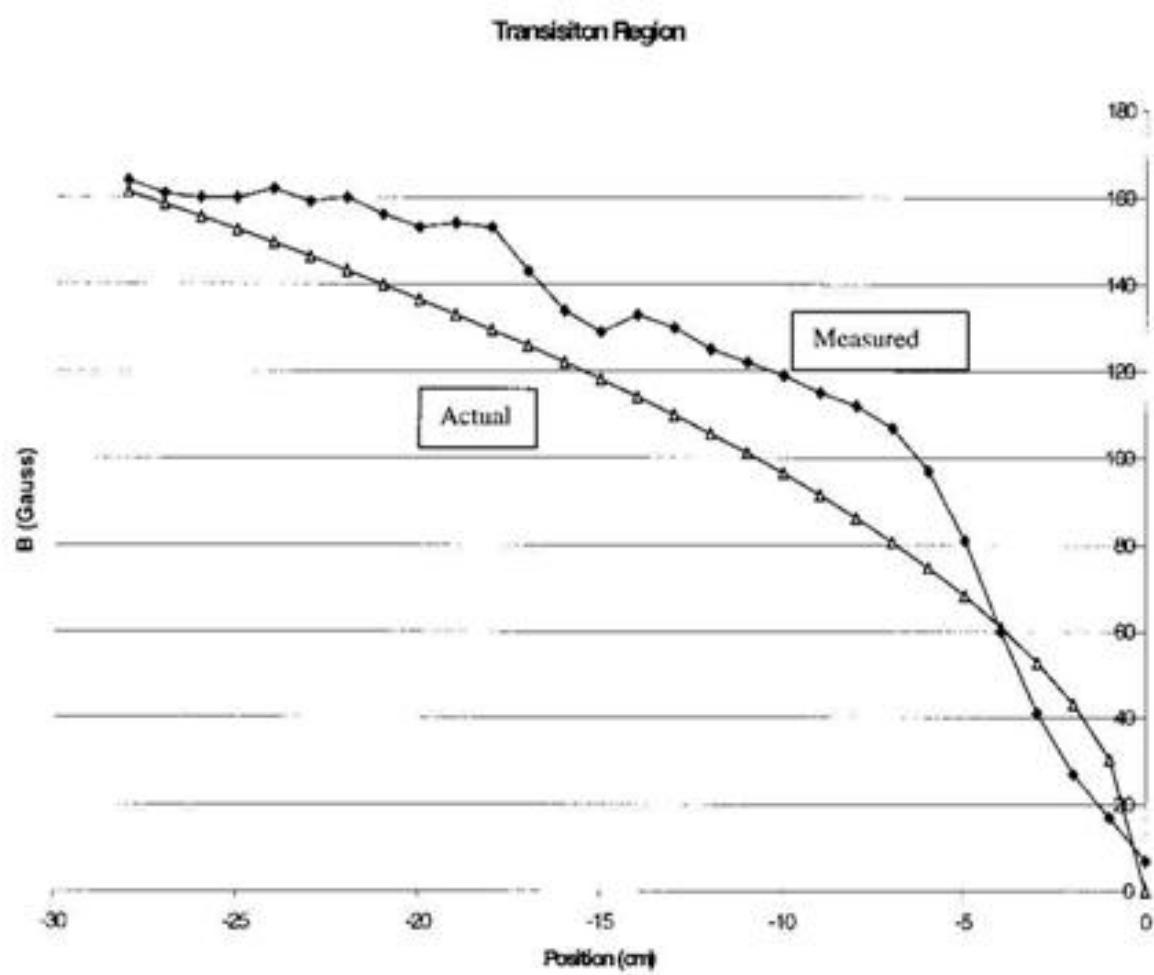


Figure 5-11 Actual Measurements of Transition Area



Here are other engineering considerations:

- The total length "x" in the equations refer to the entire length of the trap, not just the length of the Zeeman tuner slower. In our apparatus, "x" includes the length of the final, separate solenoid before the trapping chamber, as well as the extra distance to the exact center of the trapping chamber itself.
- The flange connection between the Zeeman tuner and the final solenoid should be wound too, to prevent a sudden drop of B.
- Use separate layers of wires to wind the Zeeman tuner. In case a break in the wire occurs, you'll have less to rewind!
- Tips on actually winding the pipe: The large wire spool can be mounted on a metal bar, so that the spool turns on its axis. You can then "roll" the wire onto the pipe by attaching the wire onto the pipe with tape, and slowly rolling the pipe, guiding the wire into the desired position.
- Strong adhesive tape, such as used to close packages, can be used to secure the wires temporarily, but when the wire heats up, the tape loses adhesion. A more permanent fix is obtained by using metal hose clamps. These also hold the proper segments of differential windings in place.
- Remember to use Kapton or similar insulating material between the metal pipe and wires. A layer of Kapton should be placed between the pipe and foundational layer, as well as between the wire and hose clamps.
- To test the B-field, use a Gauss meter with probe. Tape the probe to the end of a meter-stick. If that is not long enough, tape two-meter sticks together. Insert the meter-stick/probe into the pipe, and starting from the very end, gradually pull out the meter-stick in 0.5 cm or 1 cm increments, taking B-field measurements as you go.
- In our experiment, $x = 1 \text{ m}$, $a_s = 6 \times 10^4 \text{ m/s}^2$, so from Equation 5-5, the cut-off velocity is found to be 350 m/s. This represents a generous fraction of the available atoms in the Boltzmann distribution, since the most likely velocity was measured to be 500 m/s.
- For $\lambda = 811 \text{ nm}$, let us calculate some representative Doppler shifts:
$$\Delta f_D = v / \lambda = v / 811 \text{ nm}$$

 $v = 1 \text{ m/s} \quad \Delta f_D = 1.2 \text{ MHz}$
 $v = 350 \text{ m/s} \quad \Delta f_D = 430 \text{ MHz}$

- Some representative Zeeman shifts:

$$\Delta f_Z = (g_J J \mu_B B) / h$$

$$\mu_B / h = 9.27 \times 10^{-24} \text{ J T}^{-1} / 6.63 \times 10^{-34} \text{ J s} = 1.4 \text{ MHz / Gauss}$$

$$1s_5 \text{ state: } g_J = 1.506 \quad J = 2$$

$$2p_9 \text{ state: } g_J = 1.338 \quad J = 3$$

$$\begin{aligned}\Delta f_Z &= [(g_J J)_{2p9} - (g_J J)_{1s5}] (\mu_B / h) B \\ &= 1.0 \times (1.4 \text{ MHz / Gauss}) \times B\end{aligned}$$

$$1 \text{ Gauss} = 1.4 \text{ MHz}$$

$$300 \text{ Gauss} = 420 \text{ MHz}$$

Thus, a gradient from 300 to 1 Gauss within the trapping distance will slow an atom from 350 m/s to nearly at rest.

Update: New Zeeman-tuned Slower Design

Considerations for an improved design of the Zeeman-tuned slower for our project revealed valuable information. Originally in the existing slower, a 3 cm wide discontinuity of wire windings is present between the main slower and the end solenoid leading into the trapping chamber. This is because the standard way vacuum pieces are connected together is via larger diameter flange fittings. A separate "transition" layer of wires had to be wound over this region to avoid gaps in the magnetic field.

In the new design, a larger pipe will fit entirely over the flange connection region, allowing us to continually wind wire over it. No separate winding will be necessary to avoid a magnetic field drop. Not only would that save the use of one power supply, but also make the B vs. position graph easier to fit to desired values.

In the process of simulating the new design on the MathCad emulation, a significant finding occurred. Unacceptably large bumps in the B vs. position graph occurred mainly where the foundation winding ended and the secondary wire continued. Because the two wires carried different currents, inevitable roughness in the B field flared. No amount of playing with the parameters such as density of wire windings, currents, or size of individual solenoid segments adequately tamed the graph. While certain sets of parameters provided fairly decent values, they were still not close enough to ideal.

Then, in a flash of realization, we decided that since the problem was due to the foundational layer ending, getting rid of the layer altogether should solve it! A try on the simulation confirmed our conclusion. However, because the purpose of the foundational layer was to split the current load necessary to produce the value of the required B field, getting rid of one layer meant the other had to carry a much larger current. In fact, we found that 80 A of current would now be entirely on one layer (the former "secondary" layer with segments of solenoids of gradually decreasing winding densities). Because of the increased load, a wire capable of handling such a high value of current was needed, as well a power supply of producing the current. In the end, a 14-gauge square magnet wire was ordered. And to produce the high current, existing 20 A power supplies will be chained together in parallel.

CHAPTER 6

CALCULATIONS

After everything works right, meaningful data comes streaming in. Someone once said that the quality of an experiment is proportional to the ratio of how long it takes to build the apparatus to how long it takes to take the data. Or, my version of that insight is, the value of an experiment is proportional to the ratio of the number of pages in a thesis devoted to everything but the results to the number of pages in the results section. In light of this, our project is very valuable indeed! This chapter, then, presents the calculation methods appropriate to our experiment and the next chapter, the results.

Metastable Flux using the Faraday-Cup

We built a detector based on the Faraday-cup to measure the metastable flux, as described in great detail in the Chapter 3, Experimental Set-Up. The current (I) measured by the ammeter is simply

$$I = \gamma N e \quad (6-1)$$

where γ is a property of the metal ($\gamma = 1.0$ for stainless steel), N is the number of atoms per second, and e is the electron charge. We solve for N and divide by the solid angle Ω to find the flux density (F) :

$$F = N / \Omega \quad (6-2)$$

Of course, the solid angle, with units of steradians, is traditionally defined as the ratio of the detector area to the square of the distance to the source.

$$\Omega = \text{area} / R^2 \quad (6-3)$$

A numerical example follows. We measure a current of 5 nanoamps, the detector area is 10 mm^2 , and it is 100 mm from the source. Hence, the solid angle from Equation 6-3 is

$$\begin{aligned}\Omega &= 10 \text{ mm}^2 / (100 \text{ mm})^2 \\ &= 1 \times 10^{-3} \text{ sr}\end{aligned}$$

The number of atoms per second, according to Equation 6-1, is

$$\begin{aligned}N &= 5 \times 10^{-9} \text{ A} / 1.602 \times 10^{-19} \text{ C} \\ &= 3 \times 10^{10} \text{ atoms/s}\end{aligned}$$

Hence, the metastable atom flux from Equation 6-2 is

$$\begin{aligned}F &= (3 \times 10^{10} \text{ atoms/s}) / 1 \times 10^{-3} \text{ sr} \\ &= 3 \times 10^{13} \text{ atoms / (s * sr)}\end{aligned}$$

Metastable Flux using Fluorescence Spectroscopy

Another way to calculate the flux of metastable atoms is to use laser fluorescence spectroscopy. Only atoms of interest will fluoresce at a given laser wavelength, and so the strength of the fluorescence signal directly indicates the number of atoms at the interrogation site.

1. Multiplicative Factor

First, we must realize that a fluorescence signal is a composite over time. At each moment, the laser is interacting with only a fraction of the total atoms present. To account for this, we need to find the fraction of atoms represented in the peak of the signal compared to the total available, and multiply the peak signal by the inverse of that fraction. That is, if 1/10 of the atoms gave a signal of 10V, say, then, the total signal if all the atoms interacted with the laser would be 100 V.

To find the proper multiplicative factor, we divide the full-width-half-max (FWHM) by the natural linewidth (NL). The uncertainty principle dictates that a finite natural linewidth exists. That is, the energy level is not absolute – a fuzziness is associated with it. This linewidth compared to the overall width of the signal, then, gives a fair indication of the fraction of atoms represented by the peak of the fluorescence signal. The natural linewidth for the $5S[3/2]_2 - 5P[5/2]_3$ transition .

Specific numerical values will help facilitate the remaining calculations:

Say that the FWHM of our fluorescence signal is 180 MHz. The multiplicative factor to use, then, would be

$$\begin{aligned} M &= \text{FWHM} / \text{NL} \\ &= 180 \text{ MHz} / 6 \text{ MHz} \\ &= 30. \end{aligned} \tag{6-4}$$

From the oscilloscope, which displays the output of the photodetector, we find a 0.2 mV peak signal. Multiplying this by the multiplicative factor, then, the total starting signal strength is $V_1 = 30 \times 0.2 \text{ mV} = 6 \text{ mV}$. This is the final output of the photodetector, which uses operational amplifiers (op-amps) to convert a current signal from a photodiode, as well as multiply it.

2. Second Op-Amp Stage in Photodetector (Summer)

Thus, V_1 is the final result after the second op-amp. If the resistor settings were set for the highest gain ($R_1=10 \text{ k}\Omega$, $R_2=1 \text{ M}\Omega$), then the original voltage is

$$\begin{aligned} V_2 &= (R_1/R_2) \cdot V_1 \\ &= (10 \text{ k}\Omega / 1 \text{ M}\Omega) \cdot 6 \text{ mV} \\ &= 60 \mu\text{V}. \end{aligned} \tag{6-5}$$

3. First Op-Amp Stage in Photodetector (Current Converter)

V_2 is the result of a current to voltage conversion via one of three resistors, and if the highest gain is again used, then this resistor has a value $R_3=1 \text{ M}\Omega$. Thus, the original current is

$$\begin{aligned} i &= V_2 / R_3 \\ &= 60 \mu\text{V} / 1 \text{ M}\Omega \\ &= 6 \times 10^{-11} \text{ A} \end{aligned} \tag{6-6}$$

4. Total Power of Photons

The photodiode converts power from photons into a current. The conversion factor of the photodiode we use is $\eta = 0.5 \text{ A} / \text{W}$. Thus, the total power of the photons received to produce the current is

$$P = i / \eta \tag{6-7}$$

$$= 6 \times 10^{11} \text{ A} / (0.5 \text{ A/W}) \\ = 1.2 \times 10^{10} \text{ W.}$$

5. Number of Photons per Second

The energy of each photon is simply

$$\begin{aligned} E &= h\nu & (6-8) \\ &= hc/\lambda \\ &= (1240 \text{ eV} \cdot \text{nm} / 811 \text{ nm}) \cdot (1.6 \times 10^{-19} \text{ J} / 1 \text{ eV}) \\ &= 2.5 \times 10^{-19} \text{ J} / \gamma. \end{aligned}$$

Thus, the total number of photons per second entering the photodiode is

$$\begin{aligned} N_p &= P/E & (6-9) \\ &= 1.2 \times 10^{-10} \text{ W} / 2.5 \times 10^{-19} \text{ J} / \gamma \\ &= 5 \times 10^8 \gamma / \text{s} \end{aligned}$$

This is the actual number of photons received by the photodiode per second. Since the source of photons is some distance away from the detector, we need to find the number of photons emitted by the source every second per steradians. Thus, we need to calculate the solid angle to the detector.

6. Actual Number of Photons Emitted

a. Solid Angle

The interaction region is some distance away from the detector, so the solid angle must be considered. If the collection region of the detector is a circle of radius $r = 2.5$ mm, then its area $A = \pi r^2$. Also, let the distance d from the source be 120 mm. Then, by definition the solid angle is,

$$\begin{aligned} \Omega &= A/d^2 & (6-10) \\ &= \pi (2.5 \text{ mm})^2 / (120 \text{ mm})^2 \\ &= 0.001364 \text{ sr.} \end{aligned}$$

b. Number of Photons per s per sr

Having the solid angle, we can now calculate f , the number of photons per seconds per steradians.

$$\begin{aligned} f &= N_p / \Omega & (6-11) \\ &= (5 \times 10^8 \gamma / \text{s}) / 0.001364 \text{ sr} \\ &= 3.7 \times 10^{11} \gamma / (\text{s} \cdot \text{sr}) \end{aligned}$$

c. Actual Number of Photons Emitted per Second

Now, we consider f over the entire 4π steradians to find the actual number of photons emitted every second. Call this f' . Then,

$$\begin{aligned} f' &= f \cdot 4\pi \text{ sr} & (6-12) \\ &= [3.7 \times 10^{11} \gamma / (\text{s} \cdot \text{sr})] \cdot 4\pi \text{ sr} \\ &= 4.6 \times 10^{12} \gamma / \text{s} \end{aligned}$$

7. Number of Atoms Present

Now, we can calculate the actual number of atoms N_a present in the interaction region at any given time. To do this, we need to consider the rate R at which atoms scatter photons. This is dependent on several factors, including the intensity of the laser, which will be considered in detail in the next section in this chapter. For now, we take the photon scattering rate to be $1 \times 10^7 \text{ g} / (\text{atoms} \cdot \text{s})$.

$$\begin{aligned} N_a &= f^* / R \\ &= (4.6 \times 10^{12} \text{ g} / \text{s}) / 1 \times 10^7 \text{ g} / (\text{atoms} \cdot \text{s}) \\ &\approx 4.6 \times 10^5 \text{ atoms}. \end{aligned} \quad (6-13)$$

8. Metastable Flux

Finally, we can find the flux of metastable atoms produced by the discharge source. Taking the interaction region to have a volume V of 2488 mm^3 as calculated by the geometry of the situation, we find the density ρ of atoms to be,

$$\begin{aligned} \rho &= N_a / V \\ &= 4.6 \times 10^5 \text{ atoms} / 2488 \text{ mm}^3 \\ &= 185 \text{ atoms} / \text{mm}^3 \end{aligned} \quad (6-14)$$

Then, the flux is simply the density times the average velocity v of the atoms, which we take to be 530 m/s .

$$\begin{aligned} \text{Flux} &= \rho \cdot v \\ &= (185 \text{ atoms} / \text{mm}^3) \cdot 530 \times 10^3 \text{ mm/s} \\ &= 1 \times 10^8 \text{ atoms} / (\text{s} \cdot \text{mm}^2) \\ &= 1 \times 10^{14} \text{ atoms} / (\text{s} \cdot \text{m}^2) \end{aligned} \quad (6-15)$$

To express this in terms of solid angle, we recall Equation 6-10, $\Omega = A / d^2$, where A is the area under consideration, and d is the distance to the source, which is 77 cm . Since Equation 6-15 is expressed in terms of a unit area, we simply multiply the answer by d^2 to convert it to units of solid angle, sr. That is,

$$\begin{aligned} \text{Flux} &= [1 \times 10^{14} \text{ atoms} / (\text{s} \cdot \text{m}^2)] \cdot (0.77 \text{ m})^2 \\ &= 5 \times 10^{13} \text{ atoms} / (\text{s} \cdot \text{sr}) \end{aligned}$$

This is in excellent agreement with the measurement by the Faraday cup method, and supports the order of magnitude approximation that the metastable flux produced by our D.C. discharge source is $10^{13} \text{ atoms} / (\text{s} \cdot \text{sr})$.

Atomic Transition Rate

If an atom takes τ seconds to excite and de-excite, then its transition rate \mathcal{R} is defined as

$$R = 1 / \tau \quad (6-4)$$

The time τ itself depends on several factors.

$$\tau = 2 \tau_0 [1 + (I_s / I) \cdot (1 + 4 \Delta^2 / \Gamma^2)] \quad (6-5)$$

where

- τ_0 is the natural lifetime of the excited state (25 ns),
- I is the laser intensity ($\sim 110 \text{ mW/cm}^2$),
- I_s is the saturated laser intensity, (5 mW/cm^2)
- Δ is the laser detuning ($f_{\text{laser}} - f_{\text{atom}} = 10 \text{ MHz}$),
- Γ is the natural linewidth ($\Gamma = 1 / 2\pi\tau_0 = 6 \text{ MHz}$).

The laser intensity is the sum of all the slowing and trapping beams. Using the values in Chapter 4, Procedures and Parameters, we have

$$\begin{aligned} \text{Horizontal beams #1: } & (2 \times 19.1 \text{ mW/cm}^2) + \\ \text{Horizontal beams #2: } & (2 \times 12.7 \text{ mW/cm}^2) + \\ \text{Vertical beams: } & (2 \times 20.4 \text{ mW/cm}^2) + \\ \text{Slowing beam: } & (1 \times 5.1 \text{ mW/cm}^2) = \\ & I = 109.5 \text{ mW/cm}^2. \end{aligned}$$

The saturated laser intensity, I_s , involves the Hamiltonian of an oscillating electric field from the laser and the atom's dipole moment.

$$H = -E_0 \cos(\omega t) \cdot D \quad (6-6)$$

Thus, the higher the energy, the greater the probability of transition from a ground to excited state:

$$|\langle e | H | g \rangle|^2 = |\langle e | D | g \rangle|^2 \cdot E_0^2 \quad (6-7)$$

Considering some limiting cases,

if $I \gg I_s$, and the laser detuning $\Delta = \Gamma$, then $\tau = 2 \tau_0$ and $R = 1 / (2 \tau_0)$;

if $I = I_s$, and the detuning $\Delta = 0$, then $\tau = 4 \tau_0$, and $R = 1 / (4 \tau_0)$;

if $I \ll I_s$, and $\Delta = 0$, then $\tau = 2 \tau_0 - I_s/I$, and $R = I / (2 \tau_0 I_s)$.

For the present experiment, I_s is about 5 mW/cm^2 .

Using the given values in Equation 6-5, we find

$\tau = 7.7 \times 10^{-8} \text{ s}$, and

$R = 1.3 \times 10^7 \text{ photons/(s} \cdot \text{atoms)}$.

Converting Photodetector Signal Strength to Number of Atoms

The photodetector is used to estimate the number of atoms present in the trap. As described in detail in Chapter 3, Experimental Set-Up, it is based on electronic circuitry involving two op-amps, one which converts a current signal from a photodiode into a voltage signal, and the other which amplifies the new voltage signal. The result is displayed on an oscilloscope. The procedure to calculate the number of atoms from the observed signal strength is similar to part of the calculation of finding the metastable flux using fluorescence spectroscopy detailed above. In fact, the following is virtually identical to part of what was presented above, except some numbers have been changed.

In the following example, we find how many atoms would produce a signal strength of 1 V. Since all the calculations are linear, we can then simply scale up or down to correlate the actually observed signal strength into the number of atoms in the trap.

1. Second Op-Amp Stage in Photodetector (Summer)

V_1 is the final result after the second op-amp, the signal which is registered on the oscilloscope. In our example, we want $V_1 = 1 \text{ V}$. If the resistor settings were set for the highest gain ($R_1=10 \text{ k}\Omega$, $R_2=1 \text{ M}\Omega$), then the original voltage is

$$\begin{aligned} V_2 &= (R_1/R_2) \cdot V_1 \\ &= (10 \text{ k}\Omega / 1 \text{ M}\Omega) \cdot 1 \text{ V} \\ &= 0.01 \text{ V}. \end{aligned} \quad (6-8)$$

2. First Op-Amp Stage in Photodetector (Current Converter)

V_2 is the result of a current to voltage conversion via one of three resistors, and if the highest gain is again used, then this resistor has a value $R_3 = 1 \text{ M}\Omega$. Thus, the original current is

$$\begin{aligned} i &= V_2 / R_3 \\ &= 0.01 \text{ V} / 1 \text{ M}\Omega \\ &\approx 1 \times 10^{-8} \text{ A} \end{aligned} \quad (6-9)$$

3. Total Power of Photons

The photodiode converts power from photons into a current. The conversion factor of the photodiode we use is $\eta = 0.5 \text{ A/W}$. Thus, the total power of the photons received to produce the current is

$$\begin{aligned} P &= i / \eta \\ &= 1 \times 10^{-8} \text{ A} / (0.5 \text{ A/W}) \\ &= 2 \times 10^{-9} \text{ W.} \end{aligned} \quad (6-10)$$

4. Number of Photons per Second

The energy of each photon is simply

$$\begin{aligned} E &= h\nu \\ &= hc / \lambda \\ &= (1240 \text{ eV} \cdot \text{nm} / 811 \text{ nm}) \cdot (1.6 \times 10^{-19} \text{ J} / 1 \text{ eV}) \\ &= 2.5 \times 10^{-19} \text{ J} / \gamma. \end{aligned} \quad (6-11)$$

Thus, the total number of photons per second entering the photodiode is

$$\begin{aligned} N_p &= P / E \\ &= 2 \times 10^{-9} \text{ W} / 2.5 \times 10^{-19} \text{ J} / \gamma \\ &= 8 \times 10^{10} \gamma / \text{s} \end{aligned} \quad (6-12)$$

This is the actual number of photons received by the photodiode per second. Since the source of photons is some distance away from the detector, we need to find the number of photons emitted by the source every second per steradians. Thus, we need to calculate the solid angle to the detector.

5. Actual Number of Photons Emitted

a. Solid Angle

The interaction region is some distance away from the detector, so the solid angle must be considered. If the collection region of the detector is a circle of radius $r = 1.25 \text{ cm}$, then its area $A = \pi r^2$. Also, let the distance d from the source be 15 cm. Then, by definition the solid angle is,

$$\begin{aligned} \Omega &= A / d^2 \\ &= \pi (1.25 \text{ cm})^2 / (15 \text{ cm})^2 \\ &= 0.0218 \text{ sr.} \end{aligned} \quad (6-13)$$

b. Number of Photons per s per sr

Having the solid angle, we can now calculate f , the number of photons per seconds per steradians.

$$\begin{aligned}
 f &= N_p / \Omega \\
 &= (8 \times 10^{10} \gamma / s) / 0.0218 \text{ sr} \\
 &= 3.7 \times 10^{12} \gamma / (\text{s} \cdot \text{sr})
 \end{aligned} \tag{6-14}$$

c. Actual Number of Photons Emitted per Second

Now, we consider f over the entire 4π steradians to find the actual number of photons emitted every second. Call this f' . Then,

$$\begin{aligned}
 f' &= f \cdot 4\pi \text{ sr} \\
 &= [3.7 \times 10^{12} \gamma / (\text{s} \cdot \text{sr})] \cdot 4\pi \text{ sr} \\
 &= 4.6 \times 10^{13} \gamma / \text{s}
 \end{aligned} \tag{6-15}$$

6. Number of Atoms Present

Now, we can calculate the actual number of atoms N_a present in the interaction region at any given time. Again, we need to consider the rate R at which atoms scatter photons. As before, we take R to be $1 \times 10^7 \gamma / (\text{atoms} \cdot \text{s})$.

$$\begin{aligned}
 N_a &= f' / R \\
 &= (4.6 \times 10^{13} \gamma / \text{s}) / 1 \times 10^7 \gamma / (\text{atoms} \cdot \text{s}) \\
 &= 4.6 \times 10^6 \text{ atoms}.
 \end{aligned} \tag{6-16}$$

Thus, 4.6 million atoms in the trap will produce a signal strength on the oscilloscope of 1 V. If the signal were 2 V, we can conclude that 9.2 million atoms are in the trap. Or, if it were 0.5 V, then 2.3 million atoms are present. Likewise, any other observed signal can be linearly correlated with the number of atoms present.

CHAPTER 7

THE RESULTS

Finally, we present the results.

Isotope Abundance

Figure 7-1 displays two graphs, one for argon, the other for krypton. Both are oscilloscope traces of the photodetector output, where the intensity of the fluorescence is on the vertical axis, and the relative laser frequency is on the horizontal axis. For argon, three peaks are clearly distinguished, representing the three most abundant, stable isotopes. For krypton, there are five peaks. Table 7-1 summarizes the published abundance on the Chart of Nuclides associated with the specific isotope.

<u>Isotope</u>	Abundance (Chart of Nuclides)
^{36}Ar	0.3%
^{38}Ar	0.06%
^{40}Ar	99.6%
^{78}Kr	0.35%
^{80}Kr	2.25%
^{82}Kr	11.6%
^{84}Kr	57%
^{86}Kr	17.3%

Table 7-1. Summary of Ar and Kr Isotope Abundance

Isotope Frequency Shifts

In Figure 7-2, the relative frequency differences of the argon isotopes are measured. Taking ^{40}Ar as the reference, ^{36}Ar is -513 MHz, and ^{38}Ar is -247 MHz. Similarly, Figure 7-3 shows the relative frequency differences for the krypton isotopes. Table 7-2 summarizes the numerical data taken from these figures.

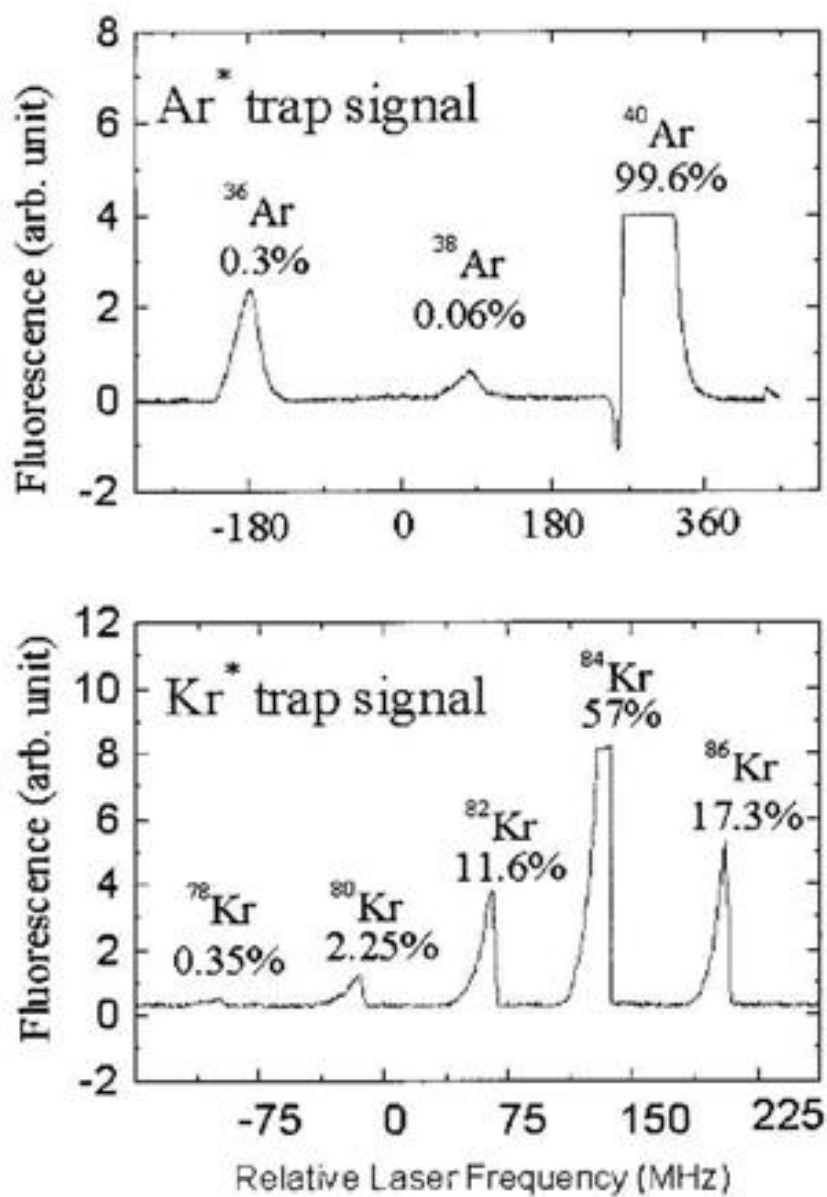


Figure 7-1. Atomic Fluorescence Intensity vs. Relative Laser Frequency

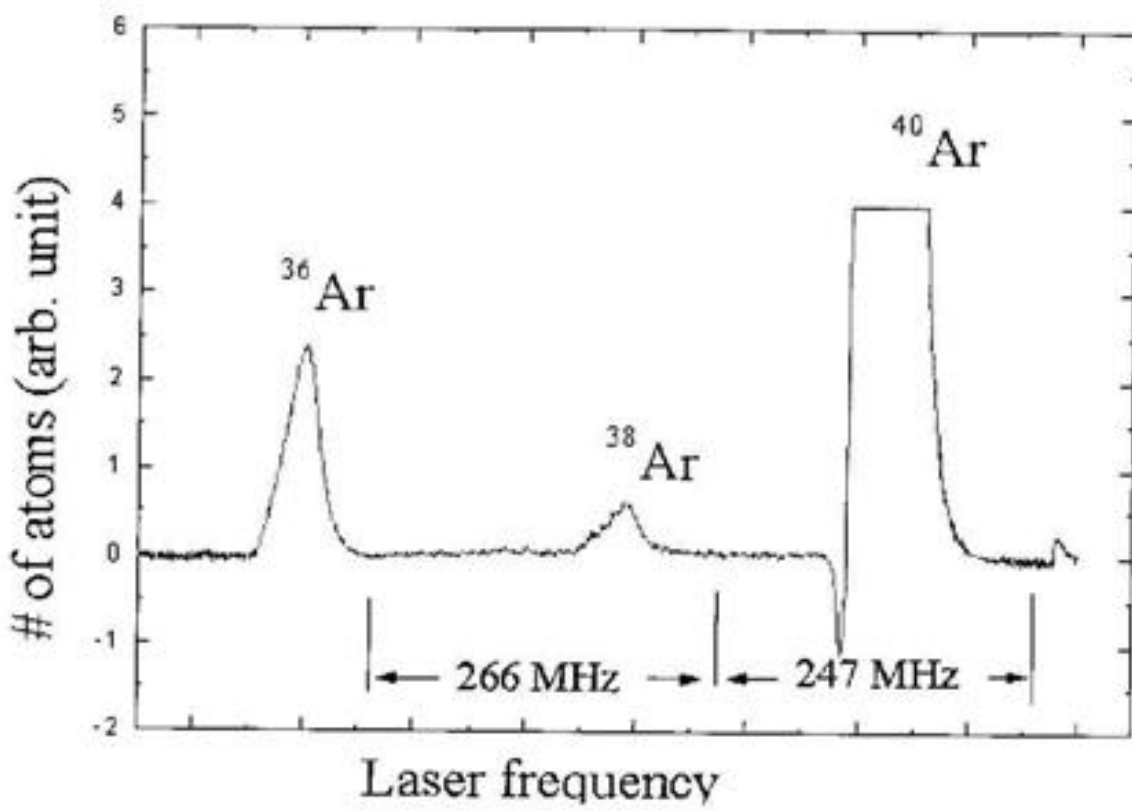


Figure 7-2. Argon Isotope Frequency Shifts

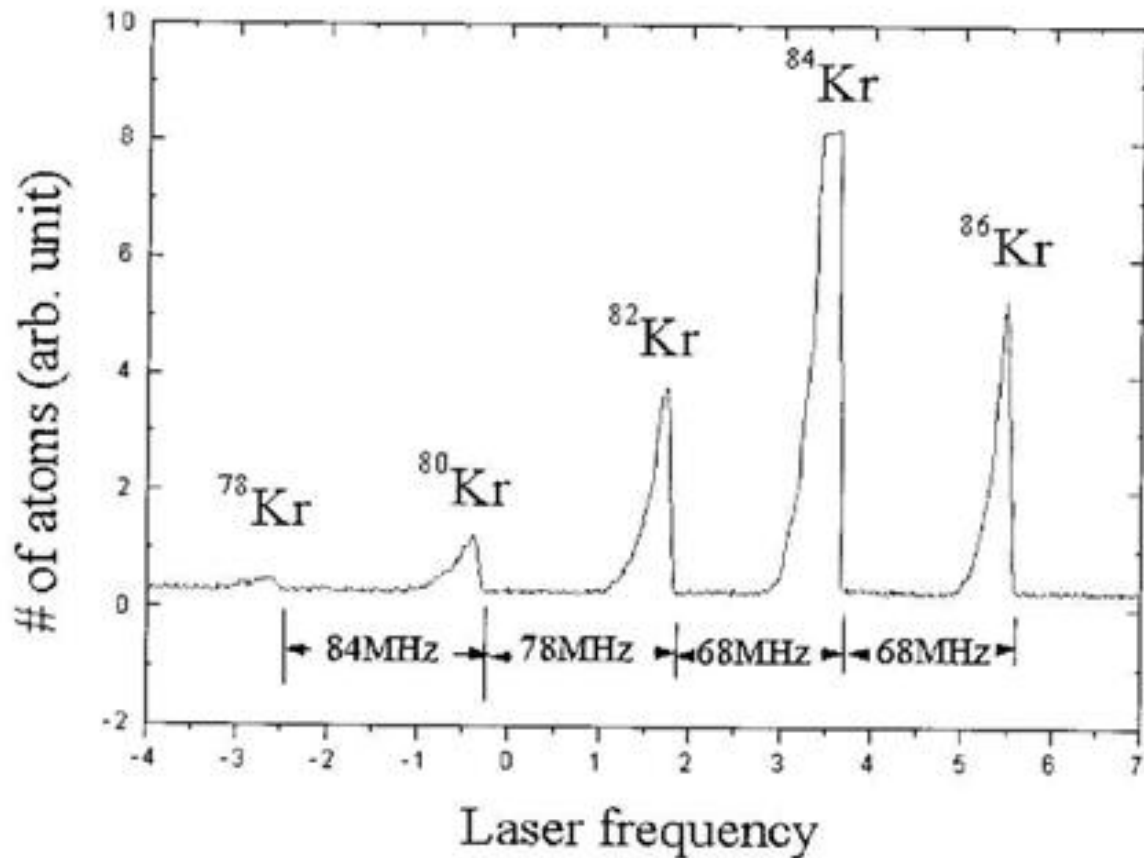


Figure 7-3. Krypton Isotope Frequency Shifts

<u>Isotope</u>	<u>Relative Frequency</u>
^{36}Ar	-513 MHz
^{38}Ar	-247 MHz
^{40}Ar	0
^{78}Kr	-230 MHz
^{80}Kr	-146 MHz
^{82}Kr	- 68 MHz
^{84}Kr	0
^{86}Kr	+ 68 MHz

Table 7-2 Relative Frequencies of Argon and Krypton Isotopes

Trap Loading Time

Figure 7-4 displays the time it takes for the atom trap to load. An electronically controlled shutter is placed in front of the slowing beam. When the shutter is closed, no trap is present, as evidenced by a low intensity reading. When it is opened, the trap begins to form, a process called "loading", and the time it takes for this to happen can be measured. We define the half time for loading ($\tau_{1/2}$) to be the time it takes for the signal to rise from the "zero" level to the maximum level.

Conclusion

This project has actually just begun. We have built most of the apparatus for laser trapping and cooling and demonstrated that it can selectively trap the various isotopes of two noble gas atoms, argon and krypton. Improvements to the system are now being undertaken, with the goal of improving the efficiency of producing metastable atoms. An alternative way to produce metastable atoms is being explored, that of using radio frequency excitations, not the currently used D.C. discharge. This method promises to improve the vacuum throughout the system, as it will not require high vacuum conditions in the source chamber. Initial data shows that the metastable flux using the R.F. discharge will be comparable with and even better than the current method.

A very important milestone will be the detection of single atoms, as evidenced by quantized signal outputs from a photomultiplier tube. This will demonstrate the sensitivity of the instrument, making fine quantitative work possible for the intended applications of trace analysis of noble gas atoms.

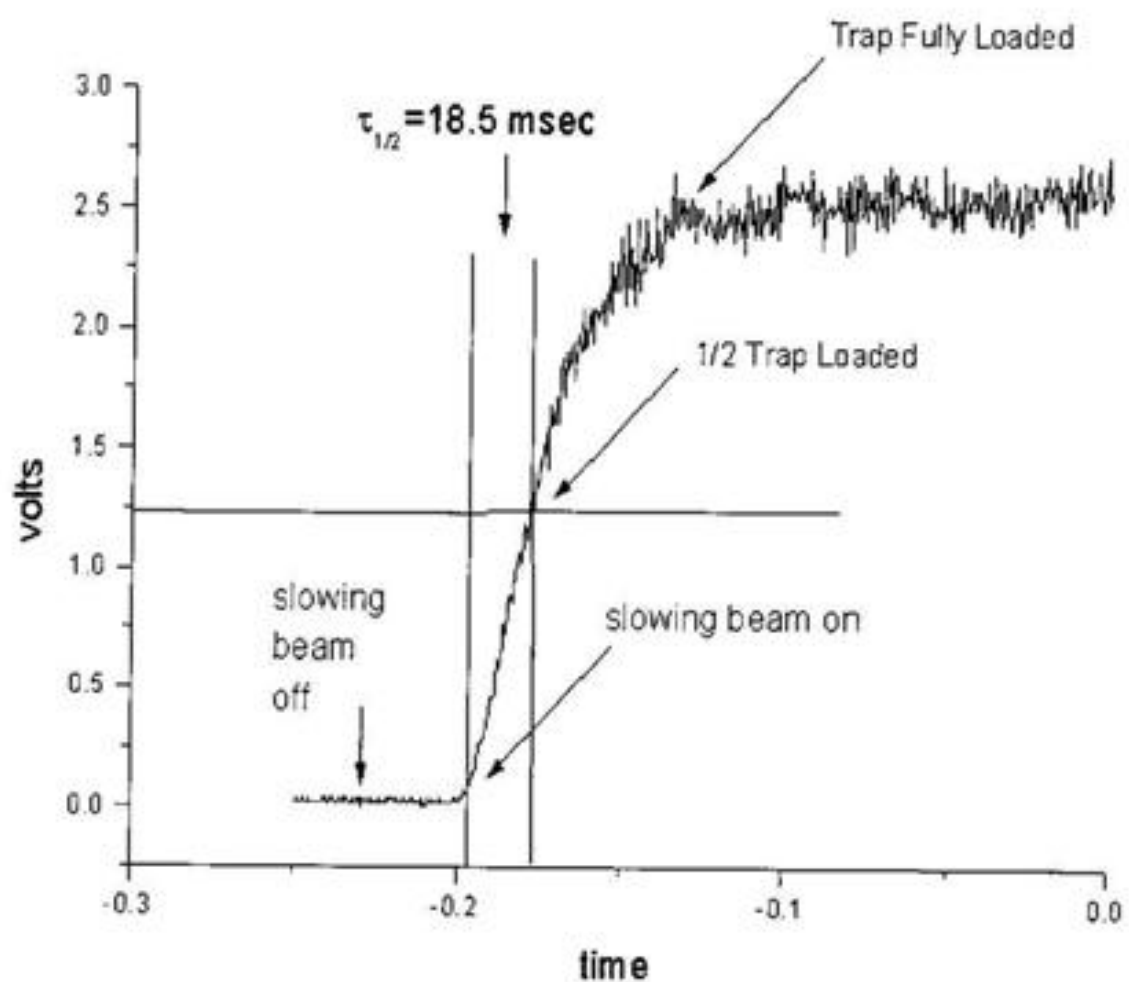


Figure 7-4. Trap Loading Time

References

- Alley, R.B., Bender M.L. (1998). Greenland Ice Cores: Frozen in Time. Scientific American, February, 80-85.
- Anderson, M.H., Ensher, J.R., Matthews, M.R., Wieman, C.E., Cornell, E.A. (1995). Observation of Bose-Einstein Condensation in a Dilute Atomic Vapor. Science, 269, 198-201.
- Apenko, S.M., Lozovik, Y.E. (1982). Parity Non-Conservation and Anapoles. Journal of Physics B: Atomic & Molecular Physics, 15, L57-62.
- Aseyev, S.A., Kudryavtsev, Yu A., Letokhov, V.S., Petrunin V.V. A Method of Detecting the Rare Isotopes ^{85}Kr and ^{81}Kr by Means of Collinear Laser Photoionization of Atoms in an Accelerated Beam. Journal of Physics B: Atomic, Molecular, and Optical Physics, 24, 2755-2763
- Ashkin, A. (1970). Acceleration and Trapping of Particles by Radiation Pressure. Physical Review Letters, 24, 156-159.
- Ashkin, A. (1970). Atomic-Beam Deflection by Resonance-Radiation Pressure. Physical Review Letters, 25, 1321-1324.
- Ashkin, A., Dziedzic, J.M. (1987). Optical Trapping and Manipulation of Viruses and Bacteria. Science, 235, 1517-1520.
- Ashkin, A., Dziedzic, J.M., Yamane, T. (1987). Optical Trapping and Manipulation of Single Cells Using Infrared Laser Beams. Nature, 330, 769-771.
- Ashkin, A., Schutze, K., Kziedzic, J.M., Euteneuer, U., Schliwa, M. (1990). Force Generation of Organelle Transport Measured in vivo by an Infrared Laser Trap. Nature, 348, 346-348.
- Ashkin, A. (1992). Forces of a Single-Beam Gradient Laser Trap on a Dielectric Sphere in the Ray Optics Regime. Biophysical Journal, 61, 569-582.
- Aspect, A., Arimondo, E., Kaiser, R., Vansteenkiste, N., Cohen-Tannoudji, C. (1988). Laser Cooling below the One-Photon Recoil Energy by Velocity-Selective Coherent Population Trapping. Physical Review Letters, 61, 826-829.
- Ballou, J.E., Buschbom, R.L., Dagle, G.E., DeFord, H.S., Tolley, H.D. (1985) Toxicology of ^{85}Kr : Effects of Whole-Body Immersion Exposure on Newborn Rats. Health Physics, 48, 453-464.

- Barr, S.M., Segre, G. (1993). Spontaneous CP Violation and Supersymmetry. Physical Review D, 48, 302-306.
- Barrett, TE; Dapone-Schwartz, SW; Ray, MD; Lafyatis, GP; (1991) Slowing Atoms with σ^- Polarized Light. Physical Review Letters, 67, 3483-3486.
- Baur, G., Boero, G., Brauksiepe, S., et al. (1996). Production of Antihydrogen. Physics Letters B, 368, 251-258.
- Berns, M.W. (1998) Laser Scissors and Tweezers. Scientific American, April, 62-67.
- Blanford, G., Christian, D.C., Gollwitzer, K., Mandelkern, M., Munger, C.T., Schultz, J., Zioulas, G. (1998). Physical Review Letters, 80, 3037-3040.
- Block, S.M., Goldstein, L.S.B., Schnapp, B.J. (1990) Bead Movement by Single Kinesin Molecules Studied with Optical Tweezers. Nature, 348, 348-352.
- Cannon, B.D., Whitaker, T.J. (1985) A New Laser Concept for Isotopically Selective Analysis of Noble Gases. Applied Physics B, 38, 57-64.
- Casella, R.C. (1968). Time Reversal and the K^0 Meson Decays. Physical Review Letters, 21, 1128-1131.
- Cornell, E.A., Wieman, C.E. (1998). The Bose-Einstein Condensate. Scientific American, March, 40-45
- Christenson, J.H., Cronin, J.W., Fitch, V.L., Turlay, R. (1964). Evidence for the 2π Decay of the K_2^0 Meson. Physical Review Letters, 13, 138-140.
- Chu, S. (1985). Three-Dimensional Viscous Confinement and Cooling of Atoms by Resonance Radiation Pressure. Physical Review Letters, 55, 48-51.
- Chu, S. (1991). Laser Manipulation of Atoms and Particles. Science, 253, 861-865.
- Chu, S. (1992). Laser Trapping of Neutral Particles. Scientific American, February, 71-76.
- Fernandez, S.J., Anderson, M.D., Motes, B.G., Chapman, T.C., Emel, W.A., Tkachyk, J.W. (1984) High Precision ^{85}Kr Monitor. IEEE Transaction on Nuclear Science, NS-31, 682-685.
- Gabrielse, G., Fei, X., Helmerson, K., Rolston, S.L., Tjoelker, R., Trainor, T.A., Kalinowsky, H., Hass, J., Kells, W. (1986). First Capture of Antiprotons in a Penning Trap: A Kiloelectronvolt Source. Physical Review Letters, 57, 2504-2507.

- Gabrielse, G., Fei, X., Orozco, L.A., Tjoelker, R.L., Haas, J., Kalinowsky, H., Trainor, T.A., Kells, W. (1990). Thousandfold Improvement in the Measured Antiproton Mass. Physical Review Letters, 65, 1317-1320.
- Goles, R.W., Brauer, F.P. (1981) An Automated Krypton-85 g-Ray Stack Monitor. IEEE Transaction on Nuclear Science, NS-28, 740-744
- Grossman, R. F., Holloway, R. W. (1985) Concentrations of Krypton-85 near the Nevada Test Site. Environmental Science and Technology, 19, 1128-1131.
- Haarsma, L.H., Abdullah, K., Gabrielse, G. (1995). Extremely Cold Positrons Accumulated Electronically in Ultrahigh Vacuum. Physical Review Letters, 75, 806-809.
- Hall, J.L., Zhu, M., Buch, P. (1989). Prospects for Using Laser-Prepared Atomic Fountains for Optical Frequency Standards Applications. Journal of the Optical Society of America, 6, 2194-2205.
- Hansch, T.W., Schawlow, A.L. (1975). Cooling of Gases by Laser Radiation. Optics Communications, 13, 68-69.
- Howett, D., O'Colmain, M. (1998) Measurement of Krypton-85 in Air at Clonskeagh, Dublin 1993-1997. Journal of Radiological Protection, 18, 15-21.
- Lawall, J., Kulin, S., Saubamea, B., Bigelow, N., Leduc, M., Cohen-Tannoudji, C. (1995). Three-Dimensional Laser Cooling of Helium Beyond the Single-Photon Recoil Limit. Physical Review Letters, 75, 4194-4197.
- Lee, T.D., Yang, C.N. (1956) Question of Parity Conservation in Weak Interaction. Physical Review, 104, 254-258.
- Lett, P.D., Watts, R.N., Westbrook, C.I., Phillips, W.D., Gould P.L., Metcalf, H.J. (1988). Observation of Atoms Laser Cooled below the Doppler Limit. Physical Review Letters, 61, 169-172.
- Lett, P.D., Gould, P.L., Phillips, W.D. (1988). Prospects for Electromagnetic Manipulation and Trapping of Antihydrogen. Hyperfine Interactions, 44, 335-348.
- Levi, B.G. (1997). Work on Atom Trapping and Cooling Gets a Warm Reception in Stockholm. Physics Today, 50, 17-19.
- Lu, Z.-T., Bowers, C.J., Freedman, S.J., Fujikawa, B.K., Mortara, J.L., Shang, S.-Q., Coulter, K.P., Young, L. (1994). Laser Trapping of short-Lived Radioactive Isotopes. Physical Review Letters, 72, 3791-3794.
- Lu, Z.-T. (1994). Laser Trapping of ^{21}Na Atoms. Ph.D. Thesis, Lawrence Berkeley Laboratory, University of California, Berkeley.

- Ludin, A.I., Lehmann, B.E., (1995) High-Resolution Diode-Laser Spectroscopy on a Fast Beam of Metastable Atoms for Detecting Very Rare Krypton Isotopes. Applied Physics B, 61, 461-465.
- Maxwell, J.C. (1892). A Treatise on Electricity and Magnetism, Vol. II, 3rd Ed. Oxford University Press, London.
- Monroe, C., Swann, W., Robinson, H., Wieman, C. (1990). Very Cold Trapped Atoms in a Vapor Cell. Physical Review Letters, 65, 1571-1572.
- Murgatroyd, J. L. Leak-Rate Determination Using Krypton 85.(1972) IEEE Transactions on Instrumentation and Measurement, IM-21, 41-48.
- Neuhauser, W., Hohenstatt, M., Toschek, P.E., Dehmelt, H. (1978). Optical-Sideband Cooling of Visible Atom Cloud Confined in Parabolic Well. Physical Review Letters, 41, 233-236.
- Neuhauser, W., Hohenstatt, M., Toschek, P.E., Dehmelt, H. (1980). Localized visible Ba⁺ Mono-Ion Oscillator. Physical Review A, 22, 1137-1140.
- Nichols, E.F., Hull, G.F. (1901). A Preliminary Communication on the Pressure of Heat and Light Radiation. The Physical Review, 13, 307-320.
- Perkins, T.T., Quake, S.R., Smith, D.E., Chu, S. (1994) Relaxation of a Single DNA Molecule Observed by Optical Microscopy. Science, 264, 822-826.
- Phillips, WD; Gould, PL; Lett, PD. (1988) Cooling, Stopping, and Trapping Atoms. Science, 239, 877-883.
- Raab, E.L., Prentiss, M., Cable A., Chu, S., Pritchard, D.E. (1987). Trapping of Neutral Sodium Atoms with Radiation Pressure. Physical Review Letters, 59, 2631-2634.
- Ramsey, N.F. (1949). A New Molecular Beam Resonance Method. Physical Review, 76, 996.
- Ramsey, N.F. (1950). A Molecular Beam Resonance Method with Separated Oscillating Fields. Physical Review, 78, 695-699.
- Ramsey, N.F. (1951). Phase Shifts in the Molecular Beam Method of Separated Oscillating Fields. Physical Review, 84, 506-507.
- Ramsey, N.F. (1972). History of Atomic and Molecular Standards of Frequency and Time. IEEE Transactions on Instrumentation and Measurement, 21, 90-99.

- Reichel, J., Bardou, F., Ben Dahan, M., Peik, E., Rand, S., Salomon, C., Cohen-Tannoudji, C. (1995). Raman Cooling of Cesium below 3 nK: New Approach Inspired by Levy Flight Statistics. Physical Review Letters, 75, 4575-4578.
- Schwarzschild, B. (1997) Optical Frequency Measurement is Getting a Lot More Precise. Physics Today, 50, 19-21.
- Udem, Th., Huber, A., Gross, B., Reichert, J., Prevedelli, M., Weitz, M., Hansch, T.W. (1997). Phase-Coherent Measurement of the Hydrogen 1S-2S Transition Frequency with an Optical Frequency Interval Divider Chain. Physical Review Letters, 79, 2646-2649.
- Waldschmidt, M. (1973) Die Krypton-85-Methode zur Ermittlung von Leckleitwerten. Vacuum, 23, 435-440.
- Walz, J., Ross, S.B., Zimmermann, C., Ricci, L., Prevedelli, M., Hansch, T.W. (1995). Combined Trap with the Potential for Antihydrogen Production. Physical Review Letters, 75, 3257-3260.
- Wang, M.D., Yin, H., Landick, R., Gelles, J., Block, S.M. (1997). Stretching DNA with Optical Tweezers. Biophysical Journal, 72, 1335-1346.
- Wineland, D.J., Dehmelt, H. (1975). Proposed $10^{14} \Delta v < v$ Laser Fluorescence Spectroscopy on Tl^+ Mono-Ion Oscillator III. Bulletin of the American Physical Society, April 1975.
- Wineland, D.J., Drullinger, R.E., Walls, F.L. (1978). Radiation-Pressure Cooling of Bound Resonant Absorbers. Physical Review Letters, 40, 1639-1642.
- Wineland, D.J., Itano, W.M. (1987). Laser Cooling. Physics Today, 40, 34-40. {section on early history of laser trapping and cooling with following references: Einstein, A. (1917). Phys. Z. 18, 121; Frisch, O. (1933). Phys. 86, 42; Kastler, A. (1950). Phys. Radium 11, 255; Letokhov, V.S. (1968). JETP Lett. 7, 272}
- Wu, C.S., Ambler, E., Hayward, R.W., Hoppes, D.D., Hudson, R.P. (1957). Experimental Test of Parity Conservation in Beta Decay. Physical Review, 105, 1413-1415.

Appendix I

Analysis of a 3.8 kHz Frequency Noise In New Focus Vortex Diode Lasers

ABSTRACT

This appendix describes the discovery of a 3.8 kHz frequency fluctuation in two New Focus "Vortex" Model 6000 tunable diode lasers used in Dr. Z.T. Lu's lab at Argonne National Laboratory. This 3.8 kHz frequency noise originally made it impossible to measure the line width of a saturated absorption signal for metastable argon atoms. Moreover, because the saturated absorption signal would ultimately be a part of the servo system used to lock the laser frequency at a specific value, eliminating or significantly reducing this frequency noise is crucial to the success of trapping noble gas atoms. Analysis showed that the noise most likely arises from the circuit design of the laser controller, and is substantially amplified when an external device or resistive plug is attached to the "Frequency Modulation" (FM) input port. A temporary solution to the problem is found by adding a 660 k Ω resistor in series with the BNC cable connected to the FM port.

INTRODUCTION -

A Primer on Saturated Absorption Spectroscopy

The basic experimental set-up used in our lab to measure absorption spectroscopy is given in Figure 1. The glass cell contains argon gas at approximately 0.7 Torr. The gas is excited by a radio-frequency (RF) oscillator and amplifier. Collisions between free electrons and neutral argon atoms produce meta-stable argon atoms, which have a resonance transition at 811.75 nm.

The laser controller is attached to a function generator, and by adjusting the voltage offset, amplitude, and frequency of a triangle wave from the function generator, I can continuously change (sweep) the frequency of the laser beam between two desired

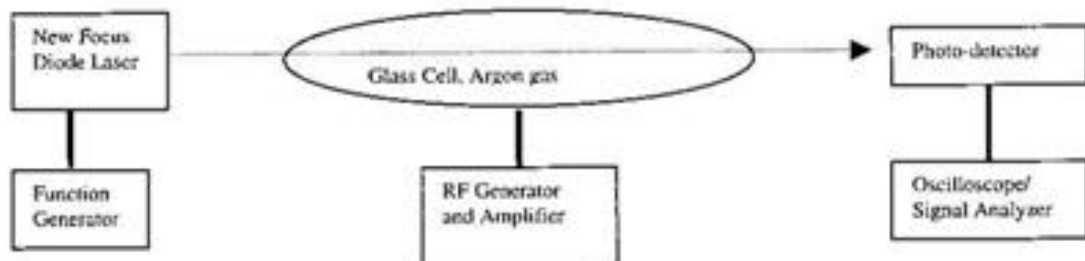


Figure 1. Laser Absorption Spectroscopy Basic Set-Up

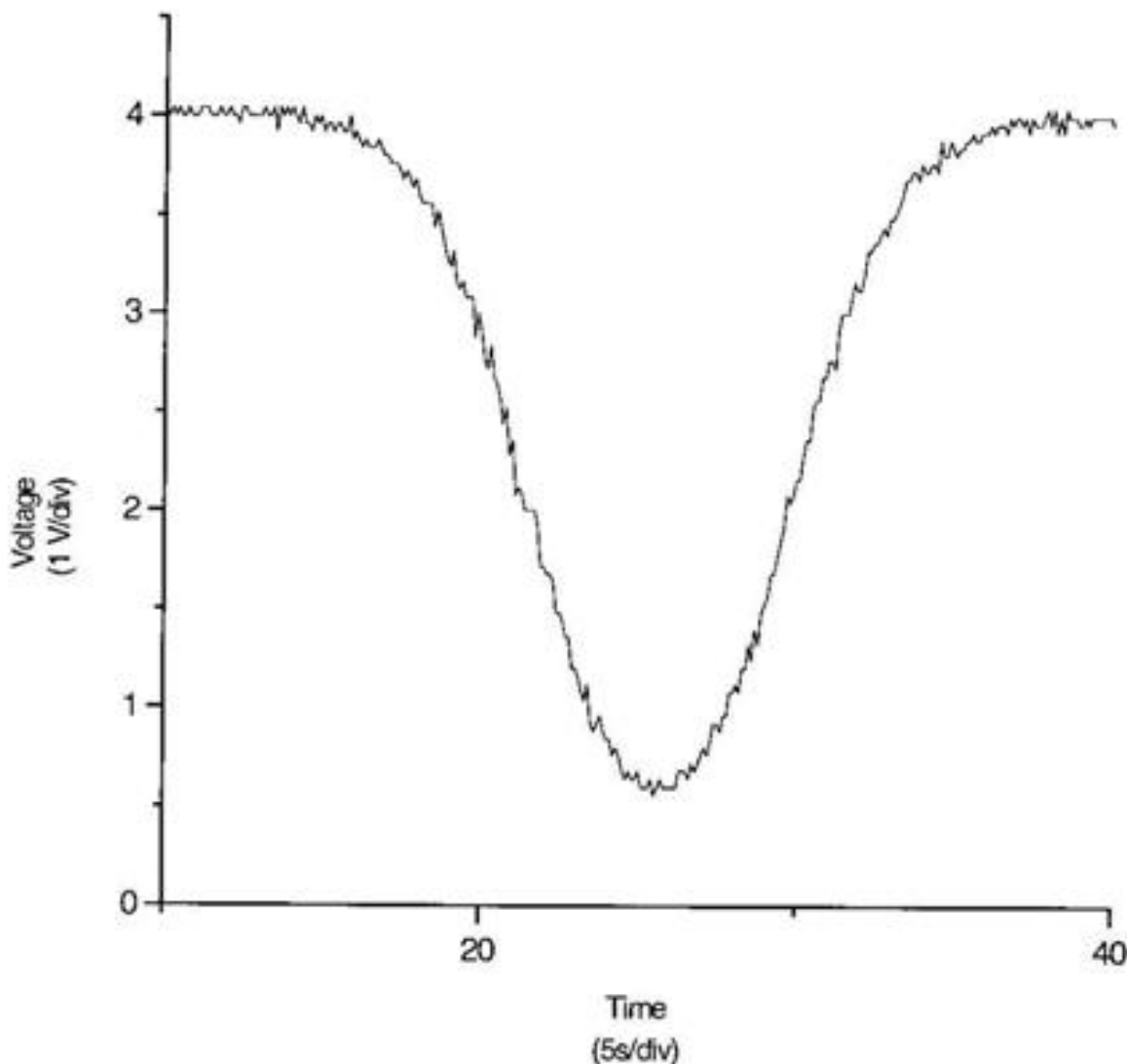
values. In practice, the laser frequency sweep is centered on the resonance transition of the meta-stable argon atoms. For instance, the sweep may start at 810 nm, increase gradually toward 811.75 nm, increase even more to, say, 813 nm, and then reverse, passing 811.75 nm again on the way back to 810 nm. Thus, in every cycle, I pass through the resonant frequency twice. Moreover, by controlling the frequency of the function generator (not to be confused with the frequency of the laser itself), I can control how fast the sweep occurs. I can even stop it at a specific frequency, called "parking" the laser, to examine the behavior of the signal at that point. This will be an important technique in evaluating the nature of the noise, to be discussed shortly.

At the other end of the glass tube, a photo-detector detects the intensity of the laser beam that emerges from the tube. As the frequency of the laser beam approaches the resonance frequency of the meta-stable argon atoms, the atoms begin to absorb the light, and the photodiode registers a decreasing intensity. At the resonance frequency, an intensity minimum is observed. Then, the intensity gradually rises back to a maximum as

the laser frequency is tuned further away from resonance. The resulting graph is an absorption spectrum of the atom (Figure 2a).

(The time axis of Figure 2a is customarily converted into a frequency axis, as will be explained later. Thus, Figure 2b represents the absorption spectrum with the frequency axis in place of the time axis.)

Figure 2a. *Absorption Spectrum of Metastable Argon Gas*



The intensity of light detected by the photo-detector diminishes as the laser frequency approaches resonance. At resonance, a signal minimum is observed.

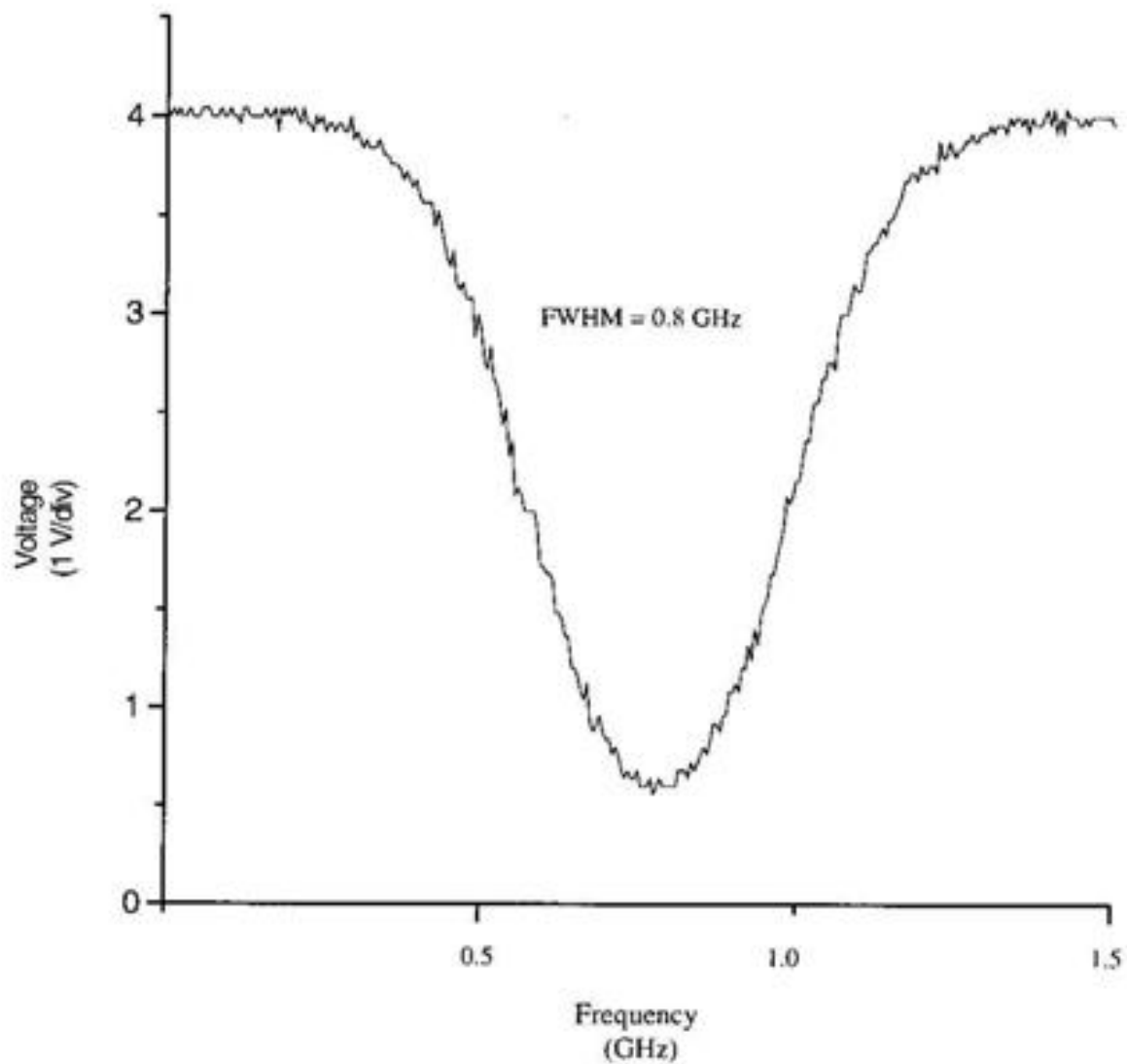


Figure 2b. Absorption Spectrum of Metastable Argon Gas

Because the laser frequency is being swept through time, the Time Axis of the previous graph is replaced by the Frequency Axis of this graph. The Full-Width-Half-Max is approximately 0.8 GHz.

An undesirable feature of the absorption spectrum is how broad it appears. This "Doppler broadening" exists because the atoms in the gas tube are travelling at different velocities. If we take the one-dimensional case and consider only the component of the velocity in the direction of the laser beam, the Boltzmann distribution (Figure 3) shows that most of the atoms will have a velocity of zero. (The atoms may have velocity components in the other two directions, but since these components are orthogonal to the laser beam, they can be ignored.) These "resting" atoms will be excited when the laser is tuned on the actual resonance frequency (as measured in the laboratory reference frame).

However, other atoms have non-zero velocities, and the velocity distribution is in fact Gaussian. Atoms moving toward or away from the laser beam at velocity $+/- v$ will observe a higher or lower laser frequency than an atom not moving toward the beam. The frequency shift is the familiar Doppler shift, $+/- \beta f$, where $\beta = v/c$, where f is the laser frequency. Thus, because the laser frequency *appears* to be at resonance in the atomic reference frame, these atoms can be excited even when the laser frequency is not at resonance in the laboratory reference frame.

The Boltzmann distribution can be interpreted as the proportion of atoms having a certain velocity. Thus, most atoms have a velocity (in one dimension) of zero, fewer atoms have moderate velocities, and very few have high velocities. As the laser is scanned from frequencies smaller than the resonance frequency, through resonance, and then past it, the beam will excite different populations of atoms depending on their velocity. The atoms with the highest velocities toward the beam will be the first ones to be excited, since their motion results in a large Doppler shift and the laser frequency shifts into resonance. But relatively few of these fast moving atoms exist, so only a little light is absorbed, and the photo-detector registers a small decrease in intensity. As the frequency scan continues, the slower (and more numerous) moving atoms will be excited. At resonance, most of the atoms are excited, since most are at rest with respect to the beam. Past resonance, the reverse process occurs, as fewer and fewer atoms have greater and greater velocities away from the laser beam. Thus, the Gaussian curve of the velocity distribution translates into the (inverted) curve of the absorption spectrum.

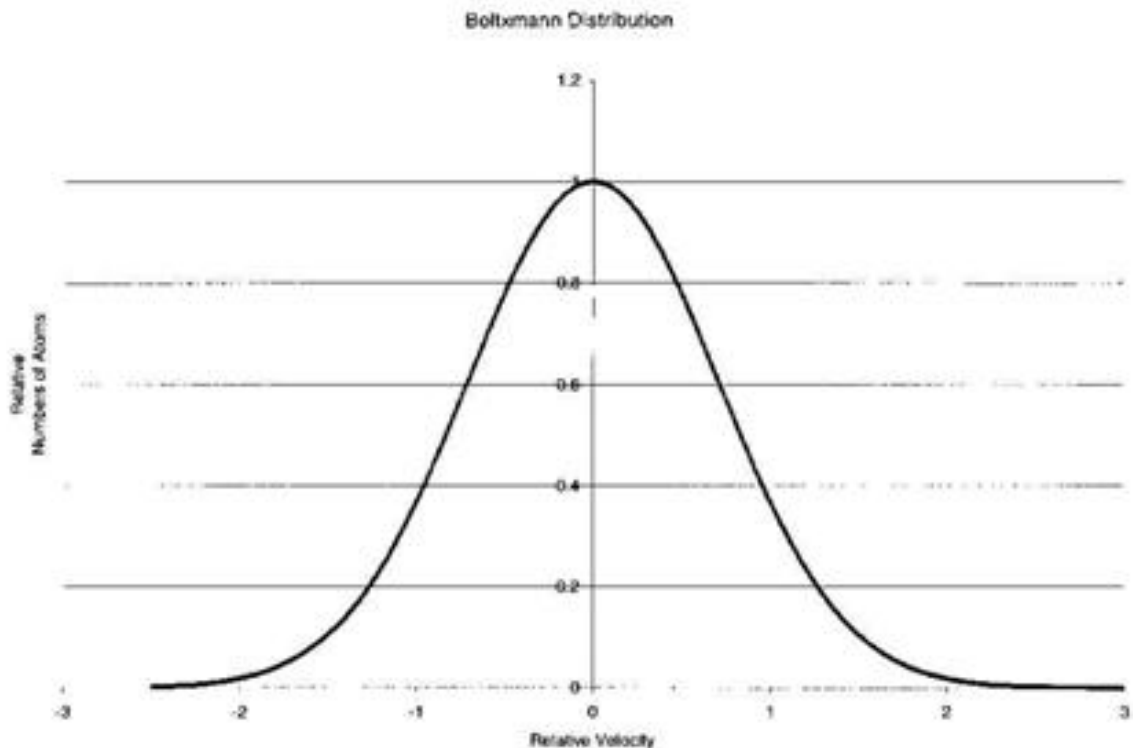


Figure 3. *The Boltzmann Distribution is Gaussian.*

In order to trap atoms, the laser must be locked to a frequency close to the true resonance frequency. Doppler broadening hides this point. The width of the absorption curve is very wide, and the true center, which corresponds to the resonant transition, is not well defined. Thus, the normal absorption spectrum does not offer sufficient precision for laser frequency locking. One way to significantly decrease Doppler broadening is *saturated absorption spectroscopy*. As seen in Figure 4, the only difference between normal absorption and saturated absorption spectroscopy is a counter-propagating laser beam in the latter method. The original beam, which is monitored by the photo-detector, is called the "probe" beam, while the counter-propagating beam is labeled the "pump" beam. When the laser is not at the resonance frequency, the two

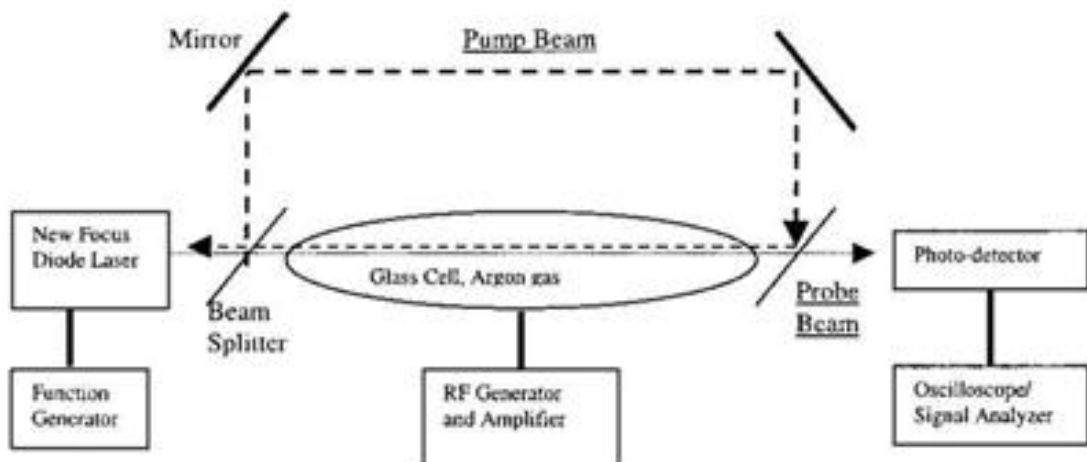


Figure 4. *Laser Saturated Absorption Spectroscopy Set-Up*

beams excite atoms at opposite ends of the velocity distribution. Only at resonance do the beams compete for the same atoms, and so the photo-detector signal rises at this point. Let me explain the rationale of this method in more detail.

Consider atoms moving toward the probe beam at velocity $+v$. Suppose the velocity is such that the laser frequency (f) is Doppler shifted $f + \beta f$ into resonance. At the same time, these atoms are moving away from the pump beam at velocity $-v$. With respect to the pump beam, the Doppler shift is $f - \beta f$ away from resonance. Thus, these atoms are excited by the probe beam, but effectively don't even know the pump beam is present. On the other side of the velocity distribution are atoms moving toward the pump beam at velocity $+v$. The situation is now the opposite of the first case. These atoms will be Doppler shifted into resonance by the pump beam, but completely ignore the probe beam. Thus, each beam addresses atoms on opposite sides of the velocity distribution. Neither beam talks to the same atoms, when the laser frequencies are not at resonance.

The situation is very different at resonance. Atoms with zero velocity experience no frequency shift, and will be excited by both probe and pump beams simultaneously at the true resonance frequency. The beams start to compete for atoms to excite. This results in the pump beam reducing the available number of atoms that can be excited by the probe beam. Fewer available atoms for the probe beam to excite means less light is absorbed, which translates into an increase in the intensity of light detected by the photo-detector centered at the true resonance frequency (Figure 5). The stronger the pump

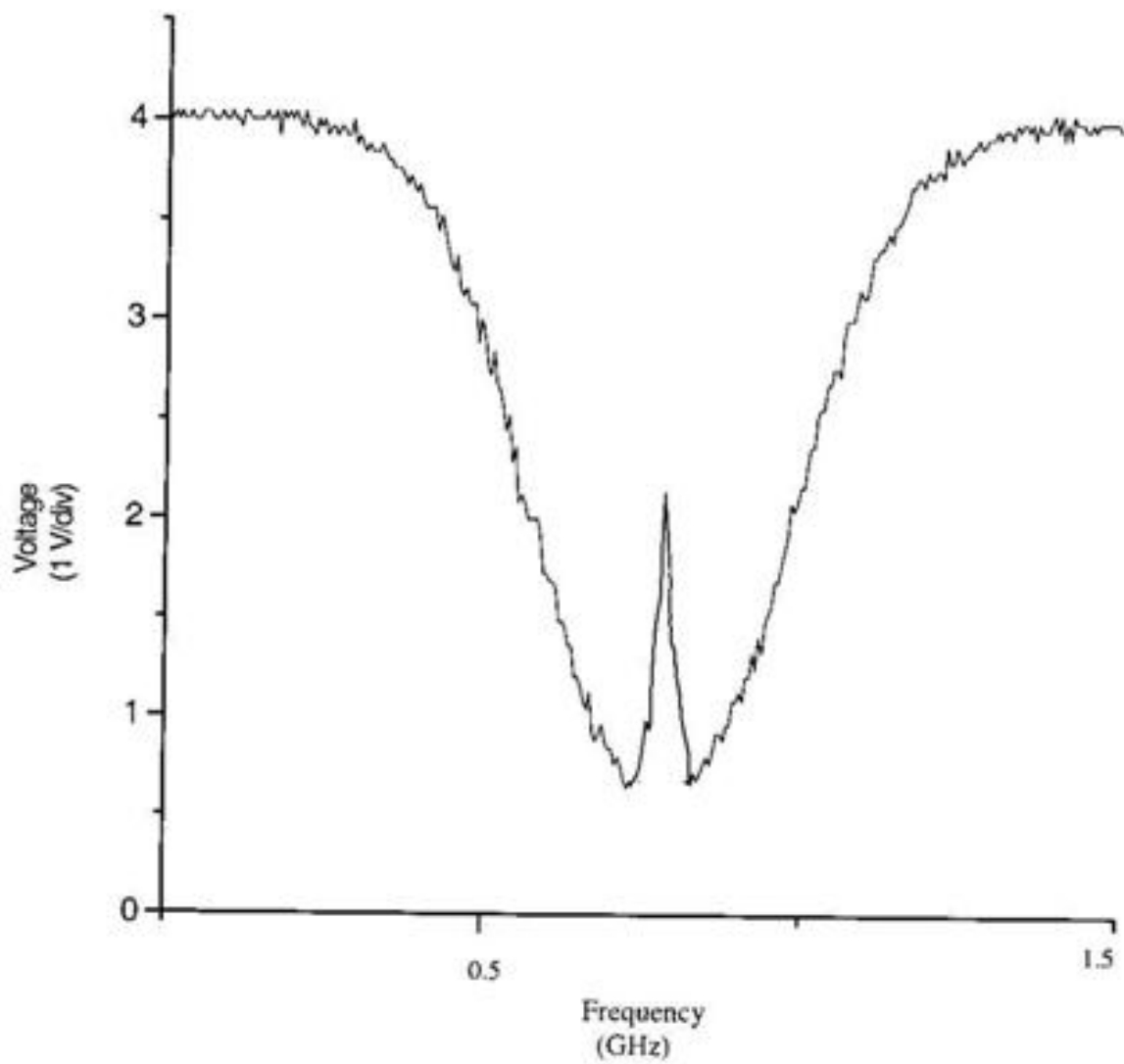


Figure 5. Ideal Saturated Absorption Signal

The increased intensity of light received by the photo-detector is due to a decreased number of available atoms to excite, which in turn, is due to the presence of the second "pump" beam.

beam, the fewer atoms are available for the probe beam at resonance, and hence, the stronger the saturated absorption signal.

A Little Bit About Noise

Noise can be categorized three ways. First, *background noise* consists of scattered light, room lights, or other sources independent of the source of the true signal from the laser. Next, *shot noise* arises from fluctuations in the electrical current associated with the discreteness of the electron charge, and is present in the photo-detector current. Finally, *technical noise* is due to fluctuations in such things as laser power and frequency. Technical noise is also present in the photo-detector.

The "Signal-to-Noise Ratio" (SNR) conveniently describes the quality of a signal. Ideally, the signal is much greater than noise, and so a high SNR is desirable. When the noise is comparable or greater than the signal ($\text{SNR} \leq 1$), it makes measurements difficult or impossible. The most practical way of getting a better signal involves trying to minimize background and technical noise, since we have more control over these sources of noise.

Noise can also be characterized as fluctuations in either the *amplitude* or *frequency* of a signal. Amplitude noise in Figure 6 is a fluctuation of the actual strength of the signal in voltage, while frequency noise in Figure 7 occurs when the signal fluctuates back and forth in time. A simple and clever way to distinguish between the

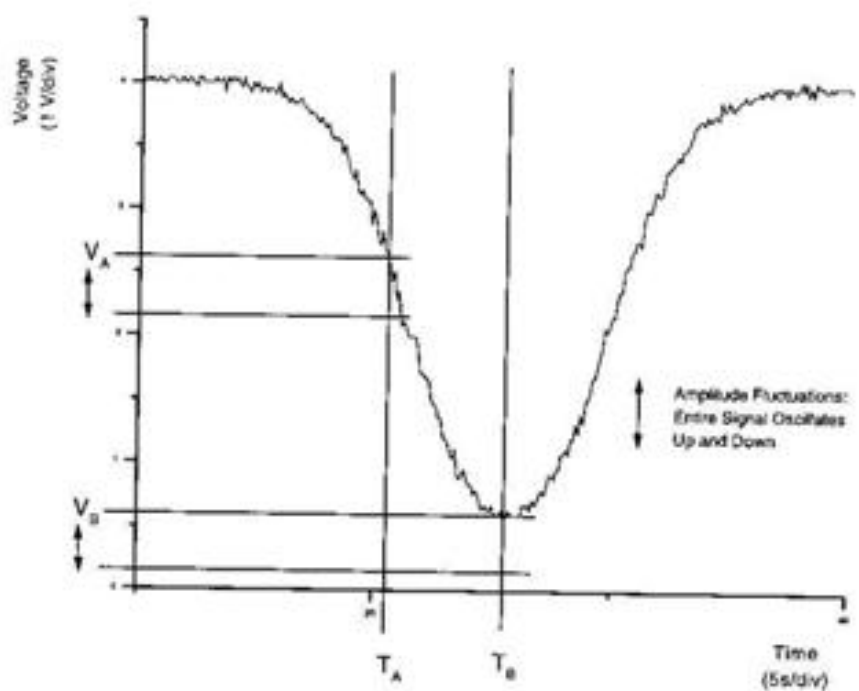


Figure 6. Amplitude Noise

Voltages corresponding to points T_A and T_B change with similar magnitudes as the signal fluctuates due to amplitude noise.

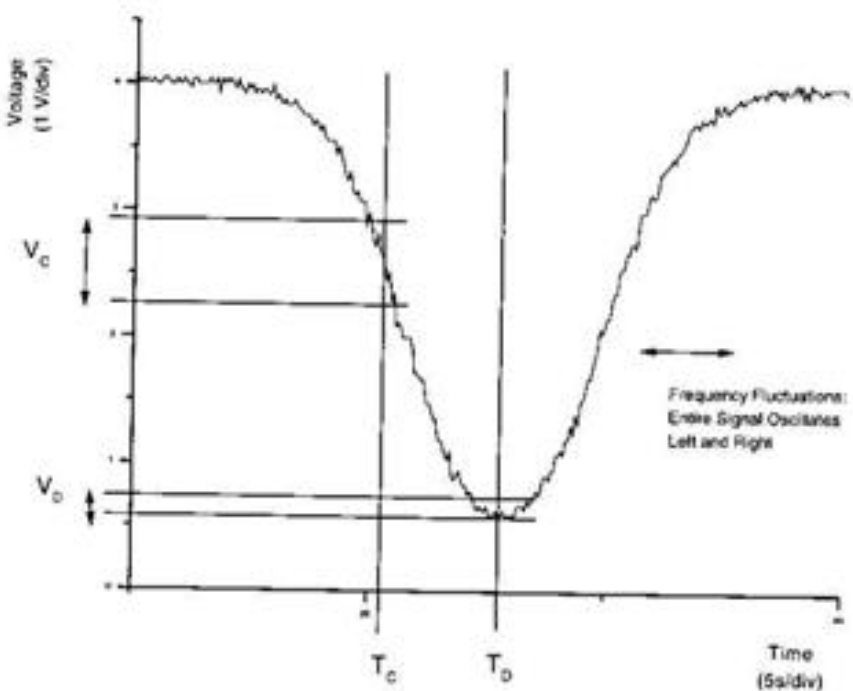


Figure 7. Frequency Noise

Voltages corresponding to points T_C and T_D change with different magnitudes as the signal fluctuates due to frequency noise.

two exists. Consider points T_A and T_B along the time axis in Figure 6. They correspond to amplitudes V_A and V_B along the voltage axis. In this case, as the signal fluctuates in voltage, V_A and V_B change by similar amounts. Now consider points T_C in Figure 7. As the signal fluctuates back and forth along the time axis, the voltage corresponding to that point (V_C) fluctuates rather significantly, since the slope of the signal is relatively steep there. However, the voltage V_D corresponding to a point near the peak of the signal T_D does not nearly change as much, since the slope of the signal at this point is both comparatively less and changing signs. Thus, amplitude and frequency noise can be distinguished by comparing the behavior of the signal at its peak versus at a point between maximum and minimum. If the noise diminishes at the peak, it is frequency noise. If not, it is amplitude noise.

In practice, how do you "Consider points T_A and T_B (or T_C and T_D) along the time axis?" The time axis of the absorption spectrum actually corresponds to the frequency of the laser. The laser frequency is changing continuously in time to produce the absorption signal. So, here, the "time axis" really is the "laser frequency axis". If one stops the laser at a specific frequency, it is equivalent to looking at a specific point on the time axis of the absorption signal. Thus, by stopping the frequency sweeping and manually parking the laser frequency at the desired point of the absorption signal, I can analyze the resulting signal using a Fast Fourier Transform Signal Analyzer for changes in the strength of the fluctuation. Again, if a substantial decrease in noise is found at the peak of the absorption signal, it is a frequency noise, not an amplitude noise.

DISCOVERY OF THE 3.8kHz FREQUENCY NOISE

The first laser used in the saturated absorption set-up described above is a New Focus "Vortex" Model 6000 tunable diode laser (Serial #607) with a center wavelength of 811.75 nm. I obtained a very noisy signal. Furthermore, the strength of the saturated absorption signal was extremely low, even though the pump beam was 20 times more powerful than the probe beam. Saturated absorption depends on the time when both beams excite the same population of atoms, that is, when the laser frequency is at the resonance transition of the atom. If the laser frequency were unstable, this amount of time is significantly reduced. As a result, the saturated absorption signal would be diminished. Thus, from the outset, a good candidate for the noise was frequency fluctuations from the laser itself. As we ruled out other possibilities of the noise, this was indeed the problem.

To pinpoint the source of the noise, Dr. Lu and I began a process of elimination. First, we switched off all room lights. This did not affect the signal noise whatsoever. Next, we considered the RF generator, which excites the argon gas. However, if we turned off the generator, we would not be able to generate the absorption signal. We needed another way to examine the signal, or a similar signal. Fortunately, we had a Fabry-Perot cavity set-up and immediately proceeded to examine its signal.

(In a Fabry-Perot cavity (Figure 8), two mirrors, which are 99% reflecting, face each other. At a special resonance condition,

$$f = (n c) / (2 d),$$

f = the frequency of light

n = an integer

c = speed of light

d = length of the cavity

almost complete transmission of the light occurs. This behavior can be understood using electromagnetic boundary conditions, or by quantum tunneling. Thus, by either sweeping the laser frequency or changing the cavity length, the resonance condition can be met and a signal received by the photo-detector. For consecutive integers, the frequency difference is simply

$$\Delta f = [(n+1) - n] c / (2 d)$$
$$= c / (2 d).$$

This is a constant, which is characteristic of the cavity, as it depends only on the length of the cavity. It is called the *free spectral range*. In our case, the free spectral range is 7.5 GHz.

In practice, as the resonance conditions are met, pulses of light are transmitted, and hence, signals generated by the photo-detector with periodic regularity (Figure 9). I can then measure the time difference between two signals. Knowing that the same difference corresponds exactly to the free spectral range, I can convert the time scale into a frequency scale. This conversion can be used to find the line width of the absorption spectrum.)

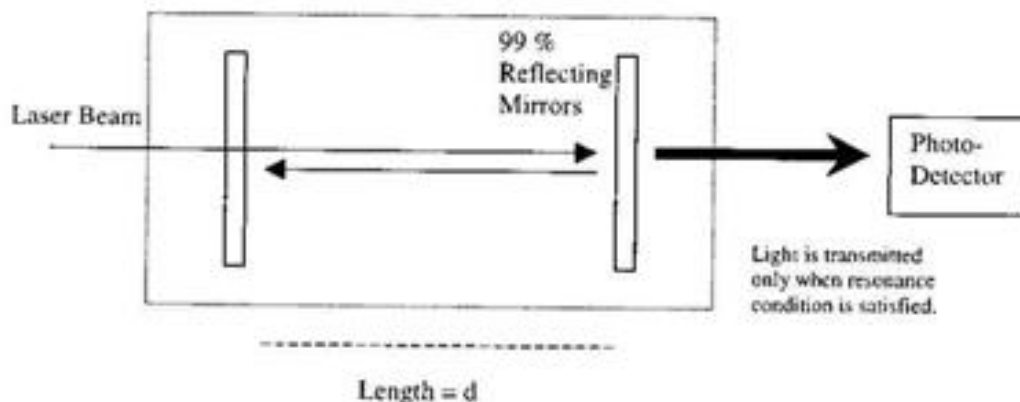


Figure 8. Fabry-Perot Cavity

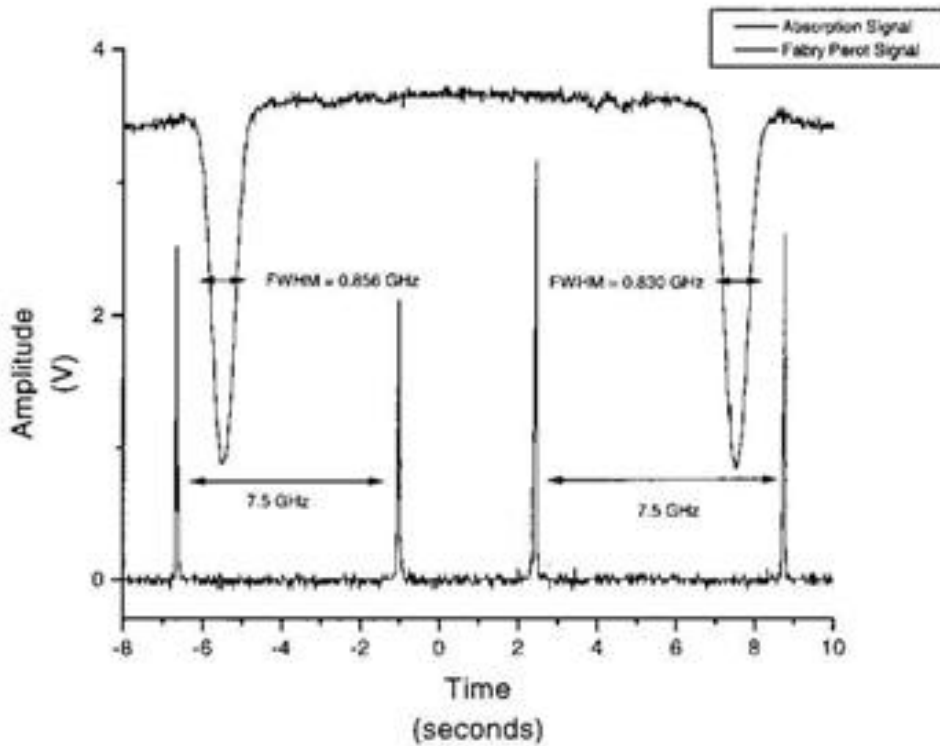


Figure 9. *Absorption Signal with Fabry-Perot Signal*

Knowing that the time difference between two Fabry-Perot signals corresponds to the free spectral range, the time scale can be converted into a frequency scale. The full-width-half-max (FWHM), or line width, of the absorption signal can then be determined.

With the Fabry-Perot, we were able to turn off the RF generator. The signal showed the same noise, and we concluded the RF generator was not the problem. Figure 10 is an oscilloscope scan of the Fabry-Perot signal. The noise dies down at the peak of the signal, which suggests it is a frequency noise. Furthermore, by measuring the frequency of the amplitude shifts, we found that the frequency of the noise was roughly 3.8 kHz.

At this point, I called New Focus for technical support. They suggested that a misalignment of the mirrors in the Fabry-Perot may be causing the noise. I ruled out this hypothesis by simply going back to the argon absorption spectrum (now assured that the RF generator was not causing the noise) and measuring the noise using a Fast Fourier

Transform (FFT) Signal Analyzer (Stanford Research SR780). The FFT clearly showed the presence of a 3.8 kHz signal. Also, 60 Hz, 180 Hz, 300 Hz, and other odd multiples of 60 Hz noise was evident.

To fully characterize the noise, I had to determine not only how *fast* the signal was shifting (the *frequency* of the noise), but also by *how much* (the *range* of the noise). This is straightforward with the Signal Analyzer. The Fourier Transform converts the range of the noise in the true signal into the amplitude of the FFT signal. That is, the strength of the FFT signal at a certain frequency corresponds to the *range* of the frequency noise. To convert the FFT signal strength (Volts) into frequency (Hz), I determined the slope of the absorption signal to find a direct relationship between the two. Thus, the noise is fully characterized as having a frequency of 3.8 kHz and a range of 40 MHz. The FFT graph is presented in Figure 11.

I reproduced the noise on the other New Focus Vortex Laser (Serial #605) in our lab. The only difference between the lasers is the center wavelength: #607 = 811.75 nm, and #605 = 811.51 nm. I found that the second laser (#605) also suffered from a 3.8 kHz frequency noise, but a range of 80 MHz, twice as great as the first laser (#607). Moreover, noise at odd multiples of 60 Hz was likewise present.

At this point, all the evidence suggested that the problem was in the circuit design of the laser controller itself. Technical Support at New Focus suggested that I try putting a $50\ \Omega$ BNC plug on the "Frequency Modulation" (FM) port at the back of the laser controller. (This port is where the BNC cable from the frequency generator is attached to the laser controller.) The rationale was the port may be receiving and amplifying stray RF frequencies from sources outside the laboratory. I tried this but found that the noise still persisted. However, I did notice that the amplitude of the noise decreased by about half. Then I tried something which led to a

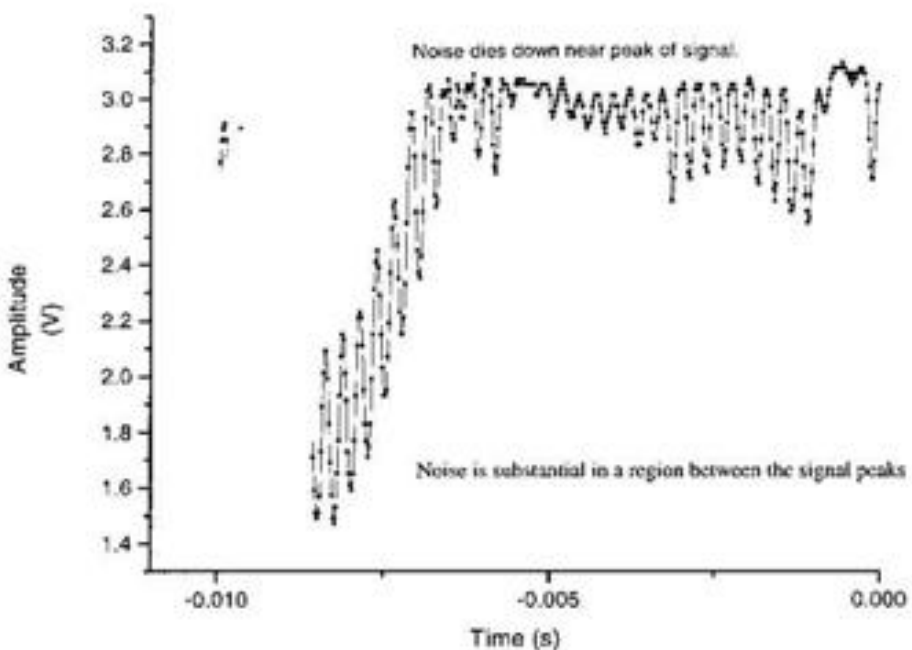
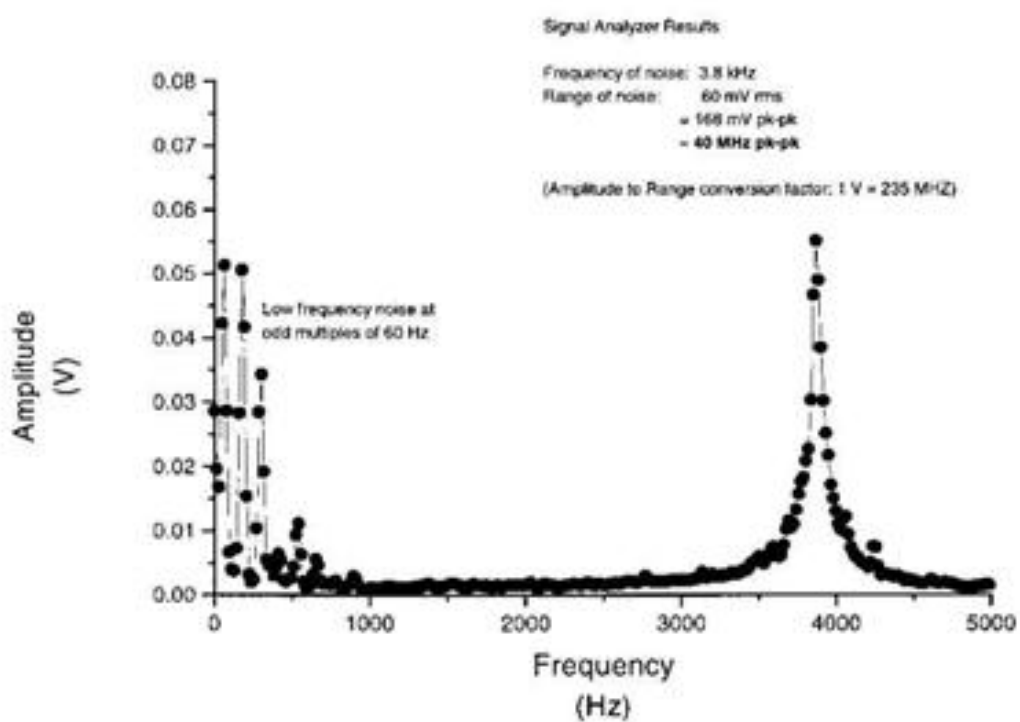


Figure 10. Oscilloscope Scan of Fabry-Perot Signal

Figure 11. FFT Output of Noise



BREAKTHROUGH

I removed the 50Ω plug and found that the noise virtually disappeared! To re-describe the situation, when the FM port was connected to the function generator, the 3.8 kHz noise was present at full strength (40 MHz). When a 50Ω plug is attached to the port, the noise is still present at 3.8 kHz, but its amplitude is now roughly 20 MHz. Then, when nothing whatsoever is plugged into the port, the noise drops down to less than 1 MHz. It is still present, but now extremely small. Likewise, the noise at multiples of 60 Hz behaved identically; their amplitudes decreased just as the 3.8 kHz signal.

When I reported this discovery to New Focus' Tech Support, they suggested I re-program the laser controller so that the gain of the FM input was LOW, instead of the default, HIGH. Doing so would result in a reduction of gain of the incoming signal by a factor of 25, and hopefully the noise would likewise diminish. However, as shown in Figures 12 and 13, this did not help much. The noise still makes the absorption signal unusable.

Dr. Lu offered better advice. He suggested I increase the resistance across the BNC plug. Thus, I examined the response of the range of the noise to increasing resistance connected across the FM port. The result for one laser is shown in Figure 14. Clearly, increasing the resistance helped decrease the noise range to an acceptable (but certainly not ideal) level. A drawback to this solution is that the range of the laser frequency would be limited proportionally. Fortunately, even this more limited range of laser frequency is still sufficient for our purposes.

Table 1 summarizes the process of characterizing the frequency noise problem.

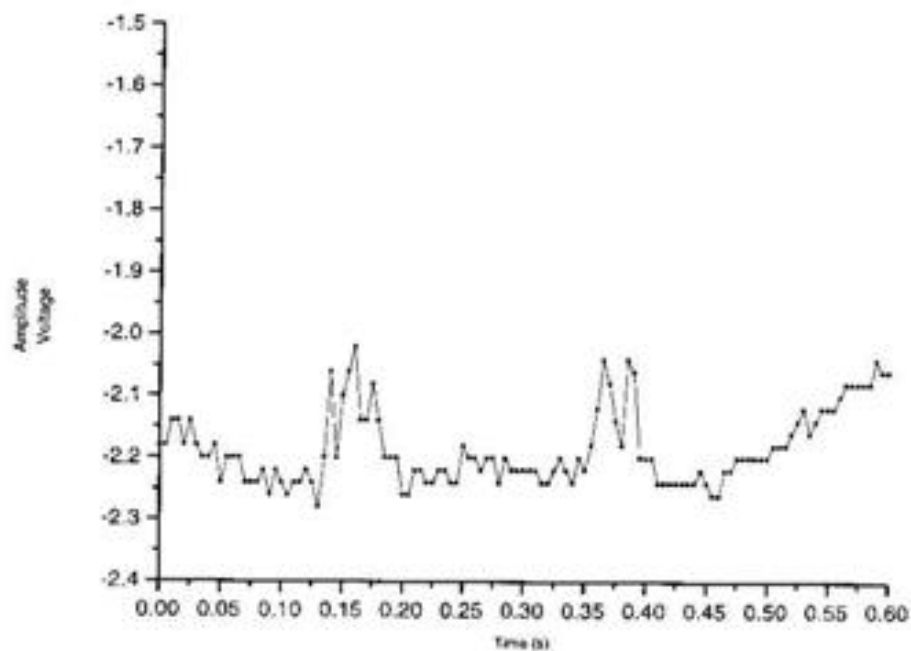


Figure 12. *Saturated Absorption Signal – FM Input at High Gain*

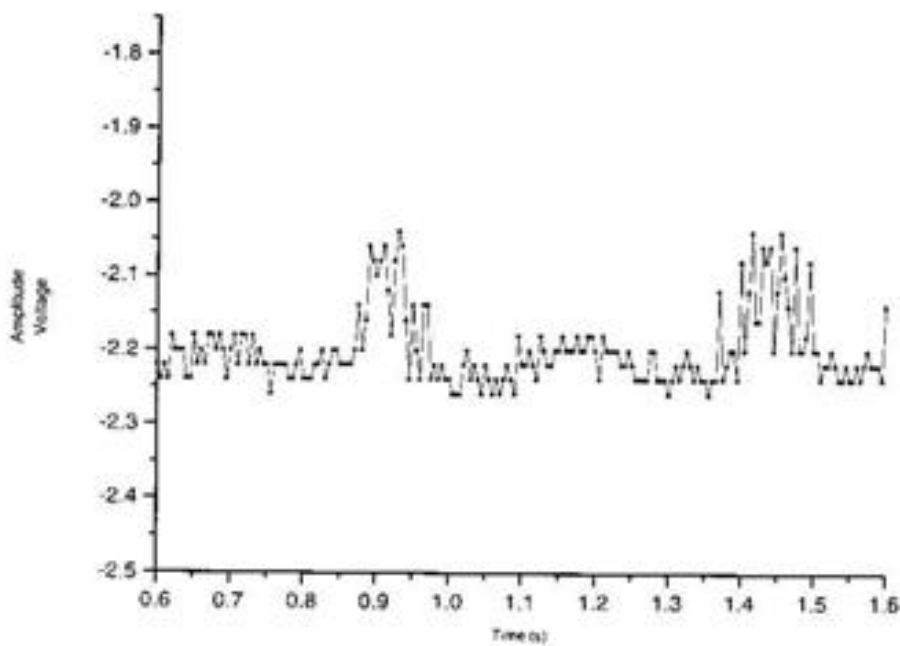


Figure 13. *Saturated Absorption Signal – FM Input at Low Gain*

Notice that the noise in both cases makes it impossible to measure the linewidth with any degree of accuracy.

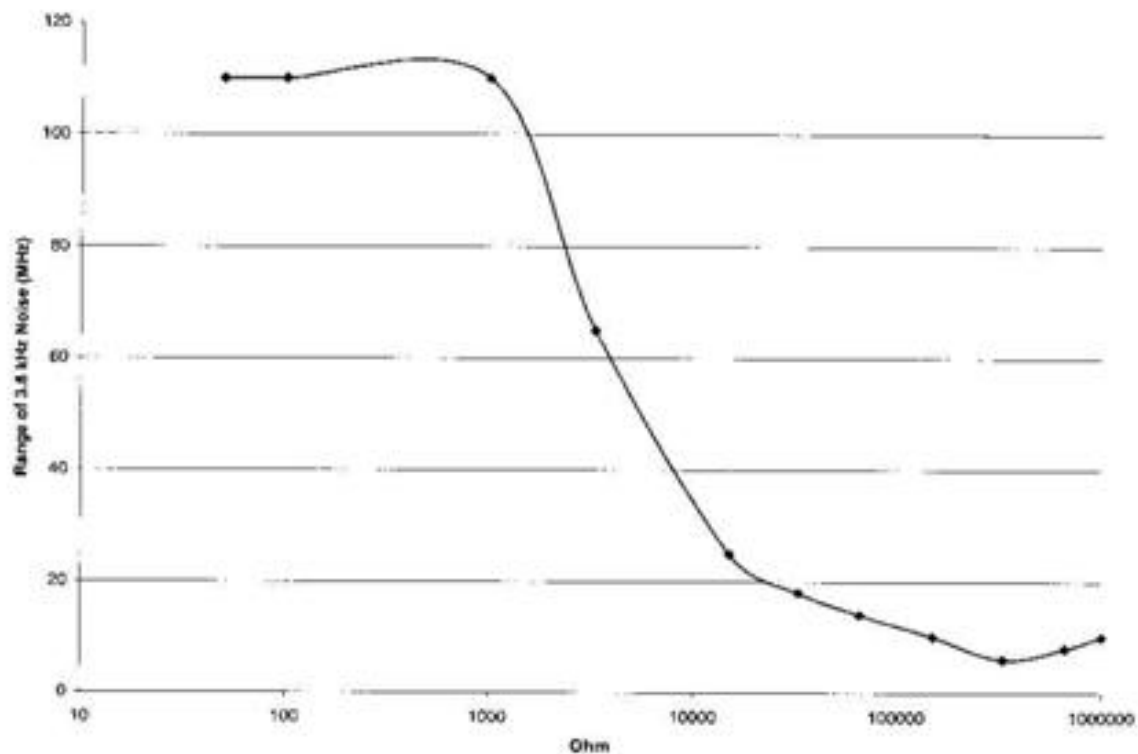


Figure 14. Response of Noise Range to Increasing Resistance

The resistance is added across the #605 laser controller FM input port.

Thus, a temporary solution to the problem is to attach a $660\text{ k}\Omega$ resistor in series with the BNC cable which connects the function generator to the laser controller. This effectively decreases the noise to around 5 MHz. With this "bandage", I was finally able to measure the line width of the saturated absorption signal (Figure 15), and found it to be roughly 10 MHz, which is acceptable. Hopefully, now that New Focus is aware of this problem, more permanent solutions can be found.

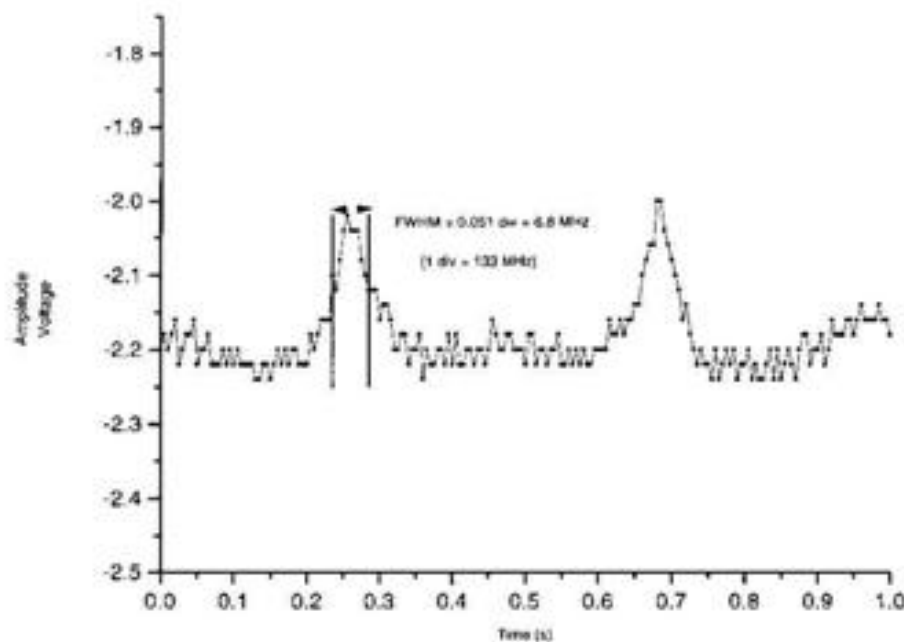


Figure 15. Final Saturated Absorption Signal

The laser frequency sweep is very close to resonance, so the wider Doppler shift features are not seen. The noise has been diminished to an acceptable level. The linewidth can finally be measured with good accuracy.

Table 1 Process of Characterizing the Problem

Action	Result on Noise	Conclusion
1. Room lights off	None	Room lights not the cause
2. RF generator off	None	RF generator not the cause
3. Examine Fabry-Perot signal	Noise diminishes at signal peak	Noise is frequency noise
4. Re-examine absorption signal	Noise persists	Fabry-Perot is not the cause
5. Attach 50 Ω plug to FM port in laser controller	Range of noise diminishes from 40 MHz to 20 MHz	Noise related to FM port
6. Remove all connections to laser controller FM port	Noise diminishes to less than 1 MHz	Noise is amplified when FM port is occupied
7. Test other laser	Same frequency of noise, but greater range	Problem is not a unique construction problem
8. Reprogram laser controller FM gain from HIGH to LOW	Noise persists	Another solution is needed
9. Increase resistance of plug in FM port	Noise diminishes substantially at large resistance	A temporary solution is found

POST SCRIPT

Confirming the 3.8 kHz frequency noise in other lasers at New Focus, the engineers there offered an explanation for where it was coming from. The culprit is the piezo in the laser head, which controls the laser frequency. For yet unknown reasons, it is resonating at 3.8 kHz.

No solution was offered for the problem, as it appears to be a serious defect in the design of the laser system.

Appendix 2
Exhaustive Equipment List

<u>Description</u>	<u>Manufacturer</u>	<u>Model</u>	<u>Serial #</u>
Argon Ion Laser	Coherent	Sabre Innova	U8502-SBR
Ti: Sapphire Ring Laser (680-1100 nm)	Coherent	899	2270
Dye Laser Controller	Coherent	899-21	2487
Power Meter	Coherent	212	3411
Wavemeter	Burleigh	WA-20VIS	E7089188
Shutter Driver	UniBlitz	D122	A697415
Chopper Controller	Standford Research Systems	SR540	5348
Analog Oscilloscope	Kikusui	C055021	45095785
Digital Oscilloscope	Tektronix	TDS210	B022006
Digital Oscilloscope	Tektronix	TDS 360	B016182
Fabry-Perot Spectrum Analyzer (FSR: 7.5 GHz)	Lansing	10.203	11767
Signal Generator (for Fabry-Perot)	EMCO	RF-1	-----
RF Power Amplifier (9.5 Watts Linear) plus RF coil can	EIN	510L	196906
Convectron Gauges	Granville-Phillips	275	-----
B/W Video Monitor		2XWG12	9703127
B/W CCD Camera		744	701365
Zoom Lens (8-48 mm, 1:12)	Computar		H6Z0812
Metal Skimmer		1.5 mm diam	
Lock-in Amplifier	Standford Research Systems	SR530	07979
FFT Signal Analyzer	Standford Research Systems	SR780	31371

Ionization Gauge (for trapping chamber)	Varian	880	565174
DC Power Supply (0-20V, 0-3A) (for transition solenoid)	BK Precision	1630	146-01200
DC Power Supply (0-20V,0-2A) Dual tracking (for top & horizontal tweaking coils)	Topward	6302A	-----
DC Power Supply (0-20V,0-10A) (for counter solenoid)	Hewlett-Packard	6286A	1141A01808
DC Power Supply (0-40V,0-10A) (for MOT coils)	TCR	60530-1-D	88F-0892
DC Power Supply (0-40V,0-10A) (for end solenoid)	Sorensen	DCR40-10A	-----
DC Power Supply (0-20V,0-20A) (for foundational solenoid)	Hewlett-Packard	6264B	8G0433
DC Power Supply (0-20V,0-20A) (for 2 nd ary solenoid)	Hewlett-Packard	6264B	2334A-06313
High Voltage Power Supply (0-5000V,0-5mA) (for source voltage)	Berian	315	159
Analog Multimeter	Simpson	260	-----
Digital Multimeter	Fluke	77	-----
Optical Power Meter	Newport	840-C	2550
Turbovac Turbopump (for trapping chamber)	Leybold	151	A971100069-85632
Turbotronik Turbopump Controller (for trapping chamber)	Leybold	NT 150/360	M971151236
Turbovac Turbopump (for transition chamber)	Leybold	360HG	A901100348-85620

Turbotronik Turbopump Controller (for transition chamber)	Leybold	NT 150/360	P1D-4389
MacroTorr Turbopump (also for transition chamber)	Varian	V-250 9699008	45856
Turbopump Controller (also for transition chamber)	Varian	V-250 969-9523	3033N
Turbovac Turbopump (for skimmer chamber)	Leybold	50	E85402-A931100481
Trubotronik Turbopump Controller (for skimmer chamber)	Leybold	10	A9202-00070-856-00-1
Roughing Pump (1/3 Hp, 1725 RPM)	GE Motors	5KCR38UN9292GX	RGL-221438
Foreline Trap	MDC	KMST-100-2	060297
Trap Valve	MDC	KAV-075	92-37129
250K Resistors (50 W)	HMITE	50J250K	-----
Input Gas Valve Servo-driven	Granville-Phillips	216	5687
Pressure/Flow Controller	Granville-Phillips	216	03235
Pressure Gauge Controller (for 2 nd ary chamber)	MDC	PGC3	D087-002
Vacuum Gauge Controller (triple display)	Granville-Phillips	316	1855
Gas Exhaust Valve	MDC	AV-075	92-37054
Convectron Gauges	Granville-Phillips	-----	-----
Linear Translator (compressed air powered) (used as shutter)	MDC	ABLM-133-2	-----
Gate Valve (compressed air powered)	MDC	GV-4000M-P-05	96-17258-G
Cooling Fans	NIDEC Alpha Boxer Leybold	TA450 BS2107FL 894 08	

IR Viewer	FJW Optical Systems, Inc.	Find-R-Scope	84499A
Laser Table	Coherent	4'x10'x3'	
Laser Table Rack	homemade	3'x10'x5 1/2'	

Main Atomic Beam Line

- 1) 1/4" Swage-Loc (gas flow input)
- 2) Gas flow valve
- 3) 2 3/4" 4-way cross (5" x 5")
- 4) Electrical feedthrough
- 5) 2 3/4" tee (5" long)
- 6) Convectron gauge
- 7) MDC Valve
- 8) 2 3/4" 5-way cross (5" x 5")
- 9) Turbopump 50
- 10) 6" 6-way cross (8 1/2" x 8 1/2")
- 11) Turbopump 360 L/s
- 12) Turbopump 250 L/s
- 13) Nude Ion-gauge
- 14) 6" tee (5" high)
- 15) Gate-valve (1/4" tubing)
- 16) 2 3/4" tee (5" long)
- 17) Shutter Valve (1/8" tubing)
- 18) Zeeman Slower
- 19) Trapping Chamber (2 3/4" windows - 7 on sides, 6" windows - top/bottom)
- 20) 6" 4-way Cross (10 1/2" down), supported on a 12"x12" aluminum plate
- 21) Turbopump 150 L/s
- 22) Nude Ion-gauge.

Total length: 6'6"

Height of beam center: 41" off floor

Peak height of Uni-Strut® off the ground

Saturated Absorption Setup

- 1) Open/Close flow valve
- 2) Granville-Phillips Variable Leak Valve #203
- 3) 2 3/4", 4 way cross (5" x 5")
- 4) 1 Convectron gauge and pressure meter
- 5) 2 3/4" to 1 1/3" reducer (3 1/2" long)
- 6) 1 1/3" tee (1 1/2" x 3")
- 7) Metal-glass connection
- 8) RF Can (1 1/2" ID, 2 1/2" OD)
- 9) Newage IndustriesVardex plastic tubing with inner metal coil support (1.000 ID x 1.319 OD)
- 10) NW 25 Kwik Flange Connector
- 11) Pexi-glass base with vibration dampening rubber "feet" (10"x12")
- 12) 1" OD glass tube

Gas Supply

- 1) AGA Compressed Nitrogen
- 2) AGA Compressed Argon
- 3) AGA Compressed Krypton
- 4) $\frac{1}{4}$ " Copper Tubing
- 5) Homemade gas valve tee

Optical Elements (mostly by Thorlabs)

<u>Item</u>	<u>Quantity</u>
1) 1" mirrors	13
2) 2" mirrors	16
3) Beam splitters	6
4) Lenses	5
5) Attenuator	2
6) Aperture	1
7) Quarter Wave Plates	7
8) Mounts, bases, stems and stem holders as necessary	

Dimensions of Apparatus

The apparatus is supported on Uni-Strut®

The optical deck surface is 3'2" off the ground

- 1) Atomic Beam Source: 30" x 30" x 38"
19" x 24" aluminum plate as a base plate
- 2) Trapping Chamber: 29" x 28" x 38"
20" x 27" optical board with $\frac{1}{4}$ "x20 tapped holes
- 3) Detection Deck: 26" x 30" x 38"
24" x 24" optical board with $\frac{1}{4}$ "x20 tapped holes